

**ADAPTIVE BEAMFORMING FOR ANTENNAS ON  
GENERAL WEDGE- AND CYLINDRICAL-SHAPED  
SURFACES**

A Dissertation  
Submitted to the Graduate Faculty  
of the  
North Dakota State University

By

Irfanullah

In Partial Fulfillment of the Requirements  
for the Degree of  
**DOCTOR OF PHILOSOPHY**

Major Department:  
Electrical and Computer Engineering

December 2013

Fargo, North Dakota

North Dakota State University  
Graduate School

---

Title

Beamforming for Antennas on General Wedge- and Cylindrical-Shaped  
Surfaces

---

By

Irfanullah

---

The Supervisory Committee certifies that this *disquisition* complies with North  
Dakota State University's regulations and meets the accepted standards for the  
degree of

DOCTOR OF PHILOSOPHY

SUPERVISORY COMMITTEE:

Dr. Benjamin D. Braaten

Chair

Dr. David A. Rogers

Dr. Daniel L. Ewert

Dr. Alan Denton

Approved:

12/12/2013

Date

Dr. Scott Smith

Department Chair

## ABSTRACT

Irfanullah, Ph.D., Department of Electrical and Computer Engineering, College of Engineering, North Dakota State University, December 2013. Adaptive Beamforming for Antennas on General Wedge- and Cylindrical-Shaped Surfaces. Major Professor: Dr. Benjamin. Davis Braaten.

Adaptive beamforming antennas capable of accommodating the growing number of wireless subscribers throughout the world has become an essential part of modern wireless systems. In this work, the beamforming of a conformal antenna on a changing conformal surface is studied by relating the varying position of each antenna element in the array to the weighting coefficients (i.e, array weights) required to give a desired antenna beamformation. In particular, the beamforming of a  $1 \times 4$  array on a changing wedge- and cylindrical-shaped surface is studied using the projection method on a wavefront of a transmitted wave in a particular direction. To validate the theory, a  $1 \times 4$  prototype antenna with individual voltage-controlled phase shifters and attenuators is used to implement the computed weights of each individual antenna element for measurements in an anechoic chamber. Overall agreement between theory, simulations and measurements is shown throughout the work. Furthermore, the effects of mutual coupling and changing conformal surfaces on the behavior of the beamforming pattern and array weights is investigated and summarized.

## **ACKNOWLEDGMENTS**

I am very grateful to take this opportunity to thank Dr. Benjamin D. Braaten, Dr. David A. Rogers, Dr. Daniel Ewert, and Dr. Alan Denton for serving on my graduate committee. I cannot thank Dr. Braaten enough for the guidance, encouragement and wisdom he gave me during my graduate studies. He has shown me the joys of teaching, rewards of research and importance of life, and for this I thank him. I would especially like to thank Dr. David A. Rogers who has been an invaluable part of my research and teaching during my graduate studies at North Dakota State University. I would like to thank Dr. Daniel Ewert and Dr. Alan Denton for serving on my graduate committee. I appreciate the comments and help you have provided as well as the willingness to serve on my committee with such short notice. Finally, I would like to thank my family for their support and understanding that I had to leave my hometown to pursue this work.

## **DEDICATION**

To my family.

## TABLE OF CONTENTS

ABSTRACT .....	iii
ACKNOWLEDGMENTS .....	iv
DEDICATION.....	v
LIST OF TABLES .....	ix
LIST OF FIGURES .....	x
1. INTRODUCTION AND PREVIOUS WORK .....	1
1.1. Background .....	1
1.1.1. Geometrical configurations of antenna arrays .....	1
1.1.2. Previous work on conformal array antennas .....	6
1.1.3. Previous work on smart antennas .....	11
2. CONDUCTED RESEARCH .....	14
2.1. Linear adaptive beamforming .....	16
3. BEAMFORMING OF A $1 \times 4$ ARRAY ON A WEDGE-SHAPED CONFORMAL SURFACE.....	23
3.1. Computing the distance to the projected element .....	25
3.2. Computing the radiation in the direction of $\theta_{SOI}$ , $\theta_{SNOI_1}$ , $\theta_{SNOI_2}$ and $\theta_{SNOI_3}$ .....	26
3.3. Computing the array weights for $N = 4$ elements .....	28
3.4. Computing the array weights for $N$ elements .....	30
4. BEAMFORMING OF A $1 \times 4$ ARRAY ON A CYLINDRICAL-SHAPED CONFORMAL SURFACE .....	32
4.1. Computing the distance to the projected element .....	32

4.2.	Computing the radiation in the direction of $\theta_{SOI}$ , $\theta_{SNOI_1}$ , $\theta_{SNOI_2}$ and $\theta_{SNOI_3}$ .....	34
4.3.	Computing the array weights for $N = 4$ elements .....	35
4.4.	Computing the array weights for $N$ elements .....	35
5.	COMPUTING THE WEIGHTING COEFFICIENTS WITH MUTUAL COUPLING.....	36
6.	DEPENDENCE OF THE ARRAY WEIGHTS ON THE CONFORMAL SURFACE GEOMETRY .....	40
7.	VALIDATION WITH ANALYTICAL, SIMULATION AND MEASUREMENT RESULTS .....	45
7.1.	The four-element beamforming array prototype. ....	45
7.2.	Beamforming results on the wedge with $\theta_b = 30^\circ$ . ....	47
7.3.	Beamforming results on the wedge with $\theta_b = 45^\circ$ . ....	48
7.4.	Beamforming results on the cylinder with $r = 10$ cm.....	48
7.5.	Discussion .....	52
8.	CONCLUSION.....	53
	BIBLIOGRAPHY .....	54
	APPENDIX A. ARRAY WEIGHTS FOR THE RESULTS IN FIGURES 27-32.....	66
	APPENDIX B. ARRAY FACTOR OF THE TWO-ELEMENT ADAPTIVE ARRAY IN FIGURE 11.....	68
	APPENDIX C. FOUR-ELEMENT LINEAR ADAPTIVE BEAMFORMING.....	69
	APPENDIX D. COMPLEX WEIGHTS FOR THE THREE-ELEMENT ARRAY ON THE WEDGE-SHAPED CONFORMAL SURFACE .....	75

APPENDIX E. COMPLEX WEIGHTS FOR THE THREE-ELEMENT ARRAY ON THE CYLINDRICAL-SHAPED CONFORMAL SURFACE	77
APPENDIX F. PATTERN 1 BEAMFORMING RESULTS WITH $\theta_B =$ $30^\circ$ .....	79
APPENDIX G. PATTERN 2 BEAMFORMING RESULTS WITH $\theta_B =$ $30^\circ$ .....	82
APPENDIX H. PATTERN 1 BEAMFORMING RESULTS WITH $\theta_B =$ $45^\circ$ .....	85
APPENDIX I. PATTERN 2 BEAMFORMING RESULTS WITH $\theta_B = 45^\circ$ . 88	
APPENDIX J. PATTERN 1 BEAMFORMING RESULTS WITH $R = 10$ CM. ....	91
APPENDIX K. PATTERN 2 BEAMFORMING RESULTS WITH $R =$ 10 CM.....	94
APPENDIX L. MEASURED ATTENUATION OF THE VOLTAGE VARIABLE ATTENUATOR. ....	97
APPENDIX M. MEASURED PHASE SHIFT OF THE ANALOG PHASE SHIFTER. ....	102

## LIST OF TABLES

<u>Table</u>	<u>Page</u>
1    Summary of the beamformation patterns 1 and 2.....	46
2    Array weights of the conformal antenna on the wedge-shaped surface with $\theta_b = 30^\circ$ without coupling using (4.17).....	66
3    Array weights of the conformal antenna on the wedge-shaped surface with $\theta_b = 30^\circ$ with coupling using (6.9). .....	66
4    Array weights of the conformal antenna on the wedge-shaped surface with $\theta_b = 45^\circ$ without coupling using (4.17).....	66
5    Array weights of the conformal antenna on the wedge-shaped surface with $\theta_b = 45^\circ$ with coupling using (6.9). .....	67
6    Array weights of the conformal antenna on the cylindrical surface with $r = 10$ cm without coupling using (4.17). .....	67
7    Array weights of the conformal antenna on the cylindrical surface with $r = 10$ cm with coupling using (6.9). .....	67
8    Measured attenuation of voltage variable attenuator. ....	97
9    Measured phase shift of analog phase shifter. ....	102

## LIST OF FIGURES

<u>Figure</u>	<u>Page</u>
1 Linear array .....	2
2 Planar array .....	3
3 Linear array bent to conform to a circular arc .....	3
4 Nonplanar array .....	4
5 SOI and SNOI in smart antenna system.....	5
6 Basic smart antenna system .....	5
7 Phase compensation of a linear array on a single curved surface shaped as a wedge.....	9
8 Analytical pattern for the 1 x 4 linear array on a wedge with $\theta_b = 45^\circ$ .....	9
9 Vision of a smart-skin antenna.....	10
10 Functional block diagram of an adaptive array system.....	12
11 The two-element adaptive array.....	15
12 Array factor of the two-element adaptive array in Figure 11. ....	15
13 N-element linear array. ....	17
14 Four element linear array combiner. ....	17
15 Beamforming results for the four-element linear array. ....	19
16 (a) Illustration of the conformal antenna on a wedge-shaped surface and (b) illustration of the conformal antenna on a cylindrical-shaped surface. ....	20
17 (a) Illustration of the 1 × 4 conformal antenna on a wedge-shaped surface with a transmitted signal of interest at angle $\theta_{SOI}$ and (b) illustration of the 1 × 4 conformal antenna on a wedge-shaped surface with a transmitted signal not of interest at angle $\theta_{SNOI}$ . ....	24

18	Illustration of the $1 \times 4$ conformal antenna on a cylindrical-shaped surface with a transmitted signal of interest (signal not of interest) at angle $\theta_{SOI(SNOI)}$ .....	33
19	N-port network illustration of the conformal array with a signal of interest at angle $\theta_{SOI}$ or $\theta_{SNOI_n}$ .....	37
20	Magnitude of the array weights for the three-element array on the wedge-shaped surface.....	43
21	Phase of the array weights for the three-element array on the wedge-shaped surface.....	43
22	Magnitude of the array weights for the three-element array on the cylindrical-shaped surface.....	44
23	Phase of the array weights for the three-element array on the cylindrical-shaped surface.....	44
24	(a) Topology of the four-element beamforming array, (b) a photograph of the power divider, voltage controlled phase shifters and voltage controlled attenuators used for measurements and (c) a photograph of the microstrip patch elements used for attachment to conformal surfaces. ....	46
25	(a) Photograph of the four-element beamforming array being measured on the wedge-shaped surface with $\theta_b = 30^\circ$ and (b) photograph of the four-element beamforming array being measured on the cylindrical shaped surface with $r = 10$ cm. ....	46
26	Picture of the four-element beamforming array in HFSS. ....	47
27	Pattern 1 beamforming results for the four-element array on the wedge-shaped surface with $\theta_b = 30^\circ$ . ....	49
28	Pattern 2 beamforming results for the four-element array on the wedge-shaped surface with $\theta_b = 30^\circ$ . ....	49
29	Pattern 1 beamforming results for the four-element array on the wedge-shaped surface with $\theta_b = 45^\circ$ . ....	50
30	Pattern 2 beamforming results for the four-element array on the wedge-shaped surface with $\theta_b = 45^\circ$ . ....	50

31	Pattern 1 beamforming results for the four-element array on the cylindrical-shaped surface with $r = 10$ cm.....	51
32	Pattern 2 beamforming results for the four-element array on the cylindrical-shaped surface with $r = 10$ cm.....	51

# CHAPTER 1. INTRODUCTION AND PREVIOUS WORK

## 1.1. Background

Usually the radiation pattern of a single radiating element is relatively wide, and each element provides low values of directivity (gain) [1]-[2]. In many applications it is necessary to design antennas with very directive characteristics (very high gains) to meet the demands of long distance communication. Several antennas can be arranged in space and interconnected to produce a directional radiation pattern. Such a configuration of multiple radiating elements is referred to as an array antenna, or simply, an array [3]. Arrays offer the unique capability of electronic scanning of the main beam. By changing the phase of the exciting currents in each element antenna of the array, the radiation pattern can be scanned through space. The array is then called a phased array [4]. Phased arrays have many applications, particularly in radar. The concept of phased arrays was proposed in 1889, but the first successful array (a two-element receiving array) did not appear until about 1906 [5]. The introduction of shortwave radio equipment in the 1920s made possible the use of reasonably sized antenna arrays, providing a convenient way to achieve a directive radiation pattern for radio communications. Around the time of World War II, array antennas operating at VHF, UHF, and later, microwave frequencies were introduced for use in radar systems. Today, arrays are used extensively.

The following section defines and briefly discusses types of antenna arrays, and particularly the concept of a phased array and adaptive antenna arrays. Discussing these topologies here will lay the foundation for the conducted research. The types of array topologies and an adaptive antenna system is described. After this, the idea of smart antennas is presented and illustrated with a functional block diagram.

### 1.1.1. Geometrical configurations of antenna arrays

Arrays are found in many geometrical configurations. The most elementary is

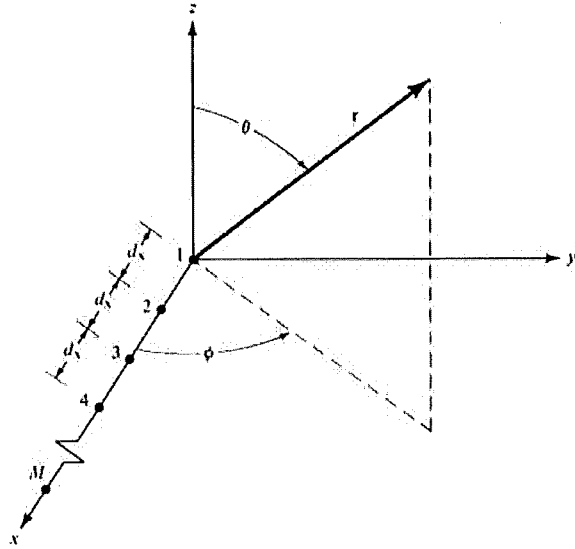


Figure 1. Linear array

a linear array in which the array element centers lie along a straight line, as shown in Figure 1. The elements in an array can form a planar array. A popular planar array is the rectangular array shown in Figure 2. Furthermore, conformal arrays are yet another class, where the array element locations conform to a nonplanar surface. This is a great advantage for arrays on the skin of a vehicle such as an airplane. Figs. 3 and 4 shows examples of conformal topologies.

An array has many advantages over a single element. For example, the narrow main beam of a parabolic reflector antenna is scanned by slewing the entire structure, whereas arrays can be phase-scanned at the speed of the control electronics without moving the antenna. In addition, it is possible to track multiple targets with a phased array. Weighting the signals before combining them enables enhanced performance features such as interference and beam steering without physically moving the aperture. It is even possible to create an antenna array that can adapt its performance to suit its environment. The price paid for these attractive features

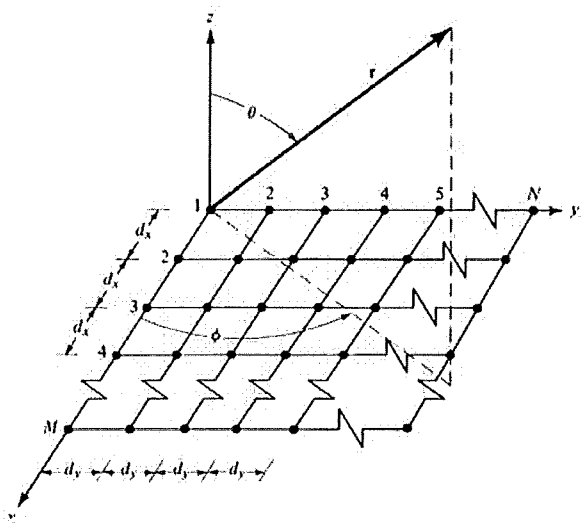


Figure 2. Planar array

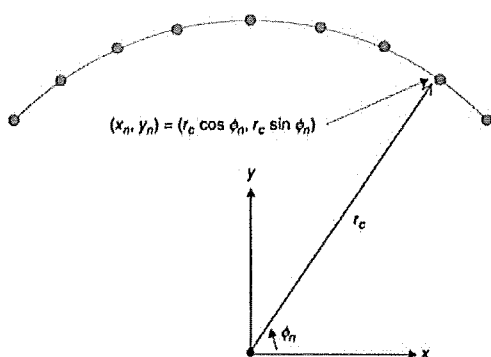


Figure 3. Linear array bent to conform to a circular arc

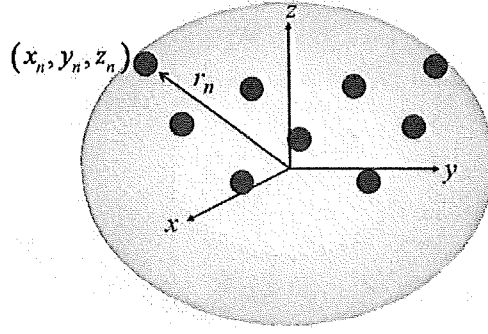


Figure 4. Nonplanar array

is increased complexity and cost.

For many years, conformal antennas have been used extensively for wireless applications that require an antenna to operate on a surface that is not flat (i.e., a singly or doubly curved surface). Wearable antennas are good examples of conformal antennas that are required to operate over a wide range of surface deformations. Another typical application could be as a base station antenna in a mobile communication system. Today, the common solution is three separate antennas each covering a 120-degree sector. Instead, one cylindrical array could be used, resulting in a much more compact installation and less cost [6].

Much attention has been paid to the design and implementation of adaptive antenna arrays (also called smart antennas), intended for use in current and future wireless communication systems. The motivation is that employment of such array

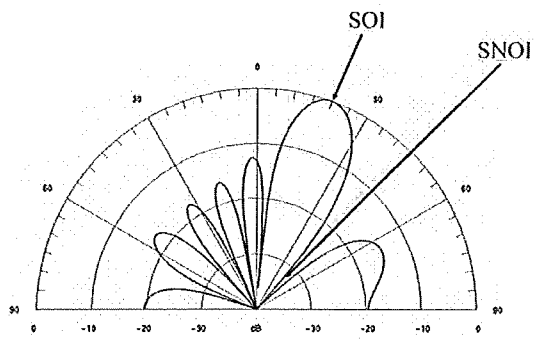


Figure 5. SOI and SNOI in smart antenna system

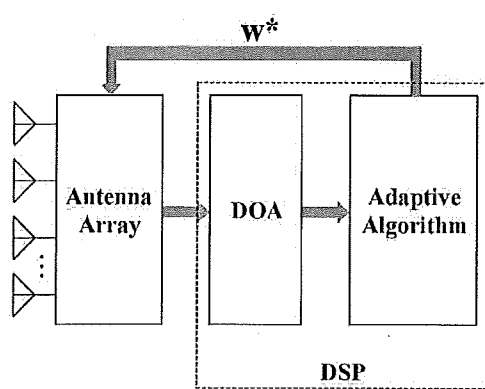


Figure 6. Basic smart antenna system

antennas can significantly increase the range and capacity of wireless systems. The main feature of smart antennas, compared with fixed-beam antennas are their abilities to form a steered beam and to track mobile users in a sector; which in many applications, has a 120 degree azimuth angular size [7].

As shown in Figs. 5 and 6 and illustrated in [8]-[10], an adaptive antenna system can tune out unwanted interferers by placing nulls toward the signal not of interest (SNOI), and concentrate on the desired user by placing the main beam toward the signal of interest (SOI). The digital signal processor (DSP) computes the direction of arrival (DOA) of the user from the time delay. The DSP also adds the strength of the signals from each antenna element together and forms a beam toward the direction as computed by the DOA.

Smart antennas integrate radio intelligence (DSP) with antenna array technology to (a) enhance communication system performance, including capacity and range and (b) improve link quality, for transmission and reception, by multipath management and mitigation of fading. These are accomplished by beam steering (placing beam maxima toward SOI) and null steering (placing beam minima, ideally nulls, toward SNOI).

### **1.1.2. Previous work on conformal array antennas**

The field of phased array antennas was a very active area of research from WW II up to about 1975 [11]. During this period, much pioneering work was done also for conformal arrays [12]. However, electronically scanned, phased array antennas did not find widespread use until the necessary means for feeding and steering the array became available. Integrated circuit (IC) technology, including monolithic microwave integrated circuits (MMIC), filled this gap, providing reliable solutions with a potential for low cost, even for very complex array antennas. An important factor was also the development of digital processors that can handle

the enormously increased rate of information provided by phased array systems. Digital processing techniques made phased array antenna systems cost effective. This being true for phased arrays in general, it also holds for conformal array antennas. However, in the area of conformal arrays, electromagnetic models and design know-how needed extra development. During the last 10 to 20 years, numerical techniques, electromagnetic analysis methods, and the understanding of antennas on curved surfaces have improved [13]-[19].

The origin of conformal arrays can be traced at least back to the 1930s when a system of dipole elements arranged on a circle, thus forming a circular array, was analyzed by Chireix [20]. Later, in the 1950s, several publications on the subject were presented; see for example [21]-[22]. The circular array was attractive because of its rotational symmetry and proper phasing can create a directional beam which can be scanned 360 degrees. The applications were in broadcasting communication and, later, navigation and direction finding. An advanced, more recent application using a large circular array, is the French RIAS experimental radar system [23]-[24].

A great deal of important conformal work was done at the U.S. Naval Electronics Laboratory Center (NELC) in San Diego. The work included development of both cylindrical and conical arrays as well as feeding systems [11]-[12]. An indication of a recent resurgence in the interest in conformal antennas is the series of conformal antenna workshops, held in Europe every second year, starting in 1999. The first was held in Karlsruhe (Germany), the second in the Hague (Netherlands), the third in Bonn (Germany), the fourth in Stockholm (Sweden), the fifth in Bristol (UK) and the seventh in Zagreb (Croatia) in 2011 [25]-[30].

More recently in [31]-[32], the effect of the radius of curvature on the radiation patterns of conformal antennas was presented. Then in 2012, Braaten [33] investigated the radiation pattern of a 1 x 4 microstrip antenna array attached to various

conformal surfaces. It was shown using measurements and analytical results that with appropriate phase compensation using the projection method [34], the radiation pattern could be recovered. The projection method presented in [33] for radiation pattern recovery on a conformal surface (wedge) is shown in Figure 7. The linear array is bent from the flat position (original reference plane) and placed on the singly curved surface shaped as a wedge with an angle  $\theta_w$ . The position of each element on the wedge is represented as a solid black dot with the outline of the surface illustrated as a black line. For this case, if each antenna element is excited with voltages that have the same phase, the E-field radiated from each element will have the same phase. However, when the fields from the elements  $A_{\pm 2}$  arrive at the new reference plane, the phase will be different than the fields radiated from elements  $A_{\pm 1}$ . This phase difference is due to the free-space propagation in the y-direction. Because these phases are not the same, the radiation may not necessarily be broadside to the array (i.e., in the z-direction with  $\phi_s = \pi/2$ ). The required phase compensation using the projection method can be computed as

$$\Delta\phi_n^w = +kL|n|\sin\theta_b \quad (1.1)$$

where  $\theta_b = (\pi - \theta_w)/2$  is the bend angle of the array. The uncorrected and corrected radiation pattern using the projection method for the conformal array in Figure 7 is shown in Figure 8.

This work was then extended further in [35]-[36] to study the effects on the radiation pattern of singly curved conformal arrays using amplitude tapering and phase tapering independently. A vision of a future smart skin conformal antenna is shown in Figure 9. This antenna constitutes a complete RF system, including not only the radiating elements but also feed networks, amplifiers, control electronics, power distribution, cooling, filters, and so on, all in a multilayer design that can be

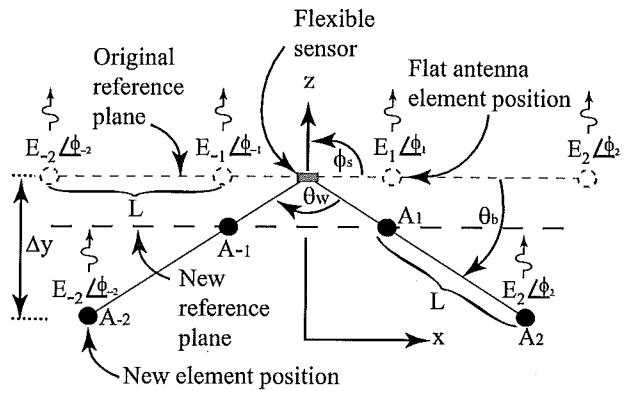


Figure 7. Phase compensation of a linear array on a single curved surface shaped as a wedge.

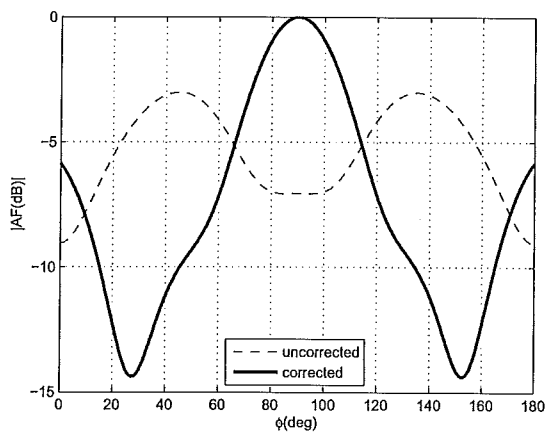


Figure 8. Analytical pattern for the  $1 \times 4$  linear array on a wedge with  $\theta_b = 45^\circ$ .

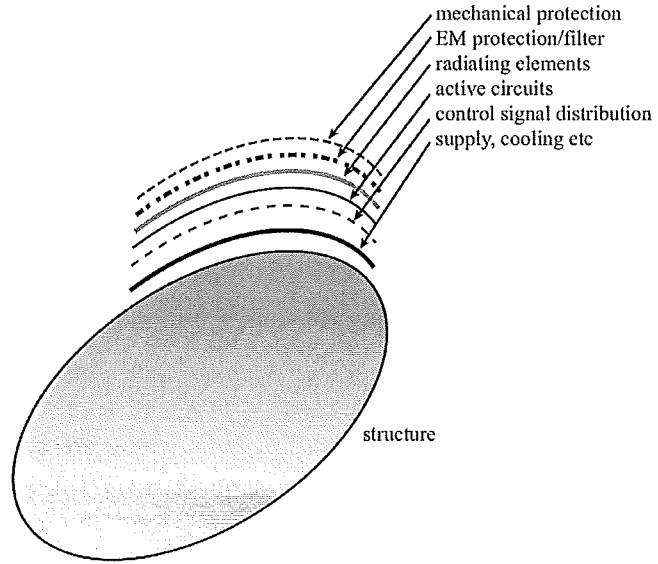


Figure 9. Vision of a smart-skin antenna.

tailored to various structural shapes [6].

The work mentioned above is just a summary of work over the past 40 years that has focused on the radiation patterns of conformal array antennas applied to various shapes (wedge, circular, cylindrical etc). Although the summary presented is not about the detailed idea of amplitude and phase tapering correction, the summary is very important because the foundations for studying the radiation pattern recovery on conformal surfaces is found throughout the work. Many other areas that involve different conformal structures, for example, conical, spherical, feed techniques [11], and microstrip patch configurations [46]-[50] exist and are not discussed here.

### 1.1.3. Previous work on smart antennas

Over the last decade, wireless technology has grown at a formidable rate, thereby creating new and improved services at lower costs. This has resulted in an increase in airtime usage and in the number of subscribers. The most practical solution to this problem is to use spatial processing. As Andrew Viterbi, founder of Qualcomm Inc., clearly stated: 'Spatial processing remains as the most promising, if not the last frontier, in the evolution of multiple access systems' [60].

Spatial processing is the central idea of adaptive antennas or smart-antenna systems. Although it might seem that adaptive antennas have been recently discovered, they date back to World War II with the conventional Bartlett beamformer [61]. It is only due to today's advancement in powerful low-cost digital signal processors, general purpose processors (and ASICs-Application-Specific Integrated Circuits), as well as innovative software-based signal-processing techniques (algorithms), that smart antenna systems have received enormous interest worldwide. In fact, many overviews and tutorials [60]-[62] have emerged, and a great deal of research is being done on the adaptive and direction-of-arrival (DOA) algorithms for smart-antenna systems [8]-[10] and [44]-[45]. As the number of users and the demand for wireless services increases at an exponential rate, the need for wider coverage area and higher transmission quality rises. Smart-antenna systems provide a solution to this problem.

In adaptive array antenna systems (also called smart antenna systems), special signal processing algorithms are applied to the digitized received signals [55]-[56]. By deriving optimum weights for the element channels, based on the received signal characteristics, the signal-to-noise-plus-interference ratio (SNIR) can be maximized. The result can be seen as creating nulls in the reception pattern in the directions of the interfering sources while preserving a high-gain beam toward the useful signal.

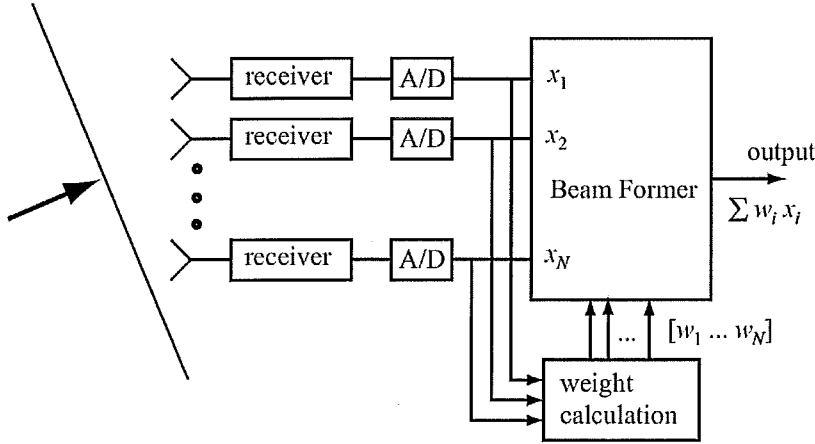


Figure 10. Functional block diagram of an adaptive array system.

A simple schematic for an adaptive beam forming system is shown in Figure 10 [9]. This figure shows that after the system downconverts the received signals to baseband and digitizes them, it locates the SOI using the DOA algorithm, and it continuously tracks the SOI and SNOIs by dynamically changing the weights (amplitudes and phases of the signals). Basically, the DOA computes the direction of arrival of all signals by computing the time delays between the antenna elements, and afterward the adaptive algorithm, using a cost function, computes the appropriate weights that result in an optimum radiation pattern. This is only necessary for DOA-based adaptive beamforming algorithms [43]. However, for reference (or training) based adaptive beamforming algorithms, it does not need the DOA information but instead uses the reference signal, or training sequence, to adjust the magnitudes and phases of each weight to match the time delays created by the impinging signals into the array. In essence, this requires solving a linear system of normal equations [43] and [56]. This linear algebra approach to compute the complex weights for linear beamforming will be explained in Chapter 2. It should be noted that all the work mentioned above was done using the planar antenna arrays for adaptive smart

antenna systems. At this point the work by [8]-[10] and [33]-[36] is the closest to the work presented here. This seems to be the first time adaptive antenna arrays (smart antennas) on conformal geometries are considered.

In this section it was shown that significant research is still being conducted on smart antenna arrays. But throughout this summary it was also shown that the case of adaptive beam forming on conformal surfaces has not been studied.

## CHAPTER 2. CONDUCTED RESEARCH

There are many properties of interest of conformal and smart antennas. These include array topologies, array factor, resonant frequency, bandwidth, gain, efficiency, far-field patterns, spacing between elements and different feed techniques. From the summary in chapter 1, it can be seen that more recent research involves adaptive beamforming for linear and planar arrays. But throughout all this research many fundamental questions have not been answered about adaptive beamforming for conformal surfaces that change shape with time.

To introduce the conducted research, the two-element adaptive linear antenna array in Figure 11 will be considered. The array factor (AF) expression for an array with  $N$  elements, like the one in Figure 4, Chapter 1 with elements distributed in three-dimensional space is given by [55]:

$$AF = \sum_{n=1}^N w_n e^{jk[x_n u + y_n v + z_n \cos \theta]} \quad (2.1)$$

Equation (2.1) assumes a spherical coordinate system where  $u = \sin \theta \cos \phi$ ,  $v = \sin \theta \sin \phi$ , and  $w_n$  are the complex excitation coefficients. Each complex weighting function is defined as  $w_n = A_n e^{j\alpha_n}$  where  $\alpha_n$  is the phase and  $A_n$  is the amplitude of the nth element. The weights for the two element adaptive array shown in Figure 11 can be computed using a linear algebra approach with two equations and two unknowns. The array factor obtained on the basis of these weights is shown in Figure 12. These complex weights were calculated to receive a desired signal (SOI) at  $\theta = 0$  (broadside) while simultaneously rejecting the interference signal (SNOI) at angle  $\theta = \pi/6$  radians from broadside. The matrix method for linear adaptive beamforming (discussed in next section) along with projection method for conformal antennas (discussed in Section 1.1.2 of chapter 1, and detailed work in [33]) will be

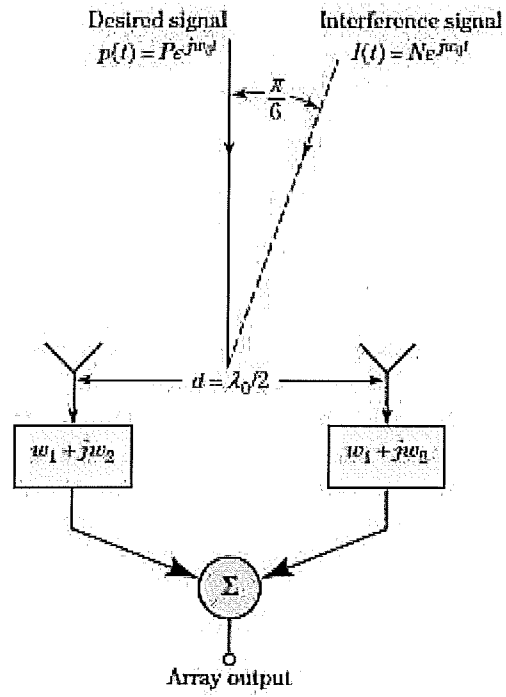


Figure 11. The two-element adaptive array.

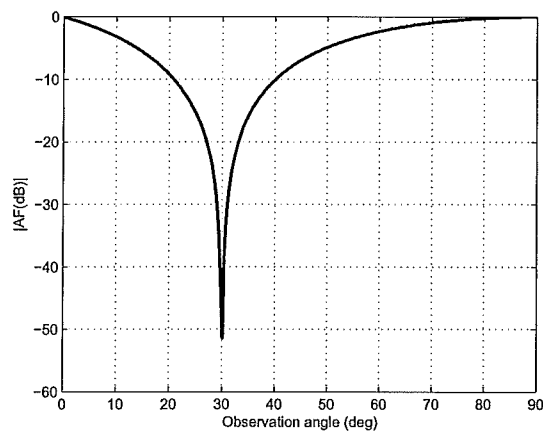


Figure 12. Array factor of the two-element adaptive array in Figure 11.

used for adaptive beamformation on conformal surfaces that change shape with time.

## 2.1. Linear adaptive beamforming

In this section, the matrix method in [71] and the projection method in [33] and [34] for linear adaptive beamforming is discussed. The array factor of a linear array of  $N$  (even) identical elements with uniform spacing positioned symmetrically along the x-axis, as shown in Figure 13, can be written as [71]:

$$(AF)_N = w_1 e^{+j(1/2)\psi_1} + w_2 e^{+j(3/2)\psi_2} + \dots + w_{N/2} e^{+j[(N-1)/2]\psi_{N/2}} \\ + w_{-1} e^{-j(1/2)\psi_1} + w_{-2} e^{-j(3/2)\psi_2} + \dots + w_{-N/2} e^{-j[(N-1)/2]\psi_{N/2}}. \quad (2.2)$$

Simplifying and normalizing, (2.2) reduces to

$$(AF)_N = \sum_{n=1}^{N/2} w_n \cos[(2n-1)\psi_n] \quad (2.3)$$

where

$$\psi_n = \frac{\pi d}{\lambda} \sin \theta. \quad (2.4)$$

The angle  $\theta$  represents the angle of the signal of interest ( $\theta_{SOI}$ ) or the angle of the signal not of interest ( $\theta_{SNOI}$ ) and  $w_n$  are the complext excitation coefficients (i.e., array weights) to be determined to give the desired SOI and SNOI radiation pattern for linear antenna array.

To compute the array weights in (2.3), consider the four-element linear array shown in Figure 14. The matrix method for linear adaptive beamforming in [71] is adopted. Assuming one SOI and three SNOIs, four equations with four unknown complex weights can be determined as follows: The output  $y(t)$  of the array in Figure 14 due to the desired signal at  $\theta_{SOI}$  is analyzed first, followed by the output due to

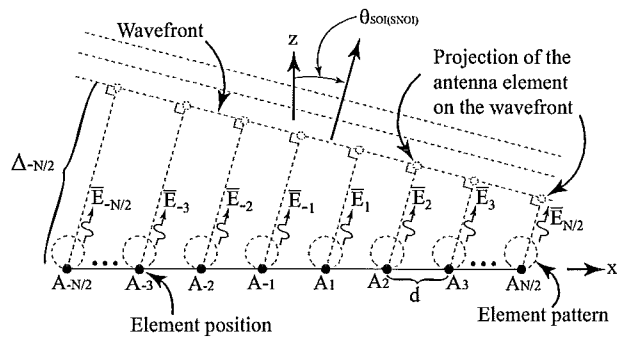


Figure 13.  $N$ -element linear array.

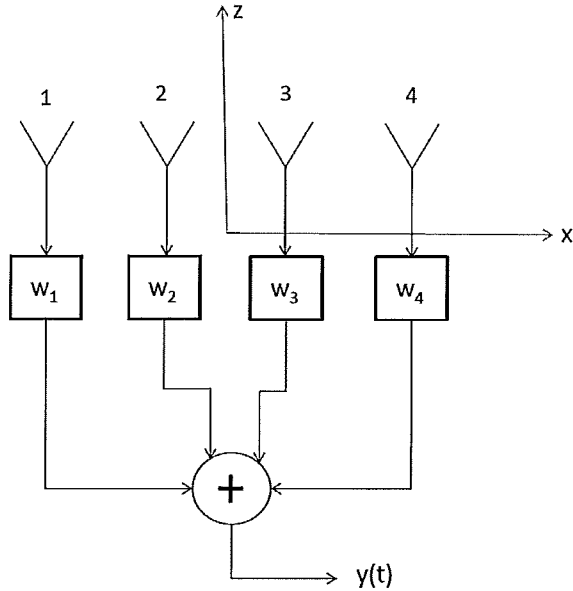


Figure 14. Four element linear array combiner.

the interferers at angles  $\theta_{SNOI_1}$ ,  $\theta_{SNOI_2}$  and  $\theta_{SNOI_3}$  respectively. Thus, the output  $y(t)$  of the array due to the desired signal at  $\theta_{SOI}$  using (2.2) can be written as

$$y(\theta_{SOI}) = w_1 e^{\pm j(3/2)\psi_1} + w_2 e^{\pm j(1/2)\psi_2} + w_3 e^{\pm j(1/2)\psi_1} + w_4 e^{\pm j(3/2)\psi_2}. \quad (2.5)$$

where the plus or minus sign is associated with phase lead or lag respectively. For the output  $y(\theta_{SOI})$  to be equal (unity) only to the desired signal, it is necessary that

$$y(\theta_{SOI}) = 1. \quad (2.6)$$

On the other hand, the outputs  $y(t)$  due to the interfering signals are given as

$$y(\theta_{SNOI_1}) = w_1 e^{\pm j(3/2)\psi_1} + w_2 e^{\pm j(1/2)\psi_2} + w_3 e^{\pm j(1/2)\psi_1} + w_4 e^{\pm j(3/2)\psi_2}, \quad (2.7)$$

$$y(\theta_{SNOI_2}) = w_1 e^{\pm j(3/2)\psi_1} + w_2 e^{\pm j(1/2)\psi_2} + w_3 e^{\pm j(1/2)\psi_1} + w_4 e^{\pm j(3/2)\psi_2}, \quad (2.8)$$

and

$$y(\theta_{SNOI_3}) = w_1 e^{\pm j(3/2)\psi_1} + w_2 e^{\pm j(1/2)\psi_2} + w_3 e^{\pm j(1/2)\psi_1} + w_4 e^{\pm j(3/2)\psi_2} \quad (2.9)$$

where  $\psi_n$  in (2.5)-(2.9) at each value,  $\theta_{SOI}$ ,  $\theta_{SNOI_1}$ ,  $\theta_{SNOI_2}$  or  $\theta_{SNOI_3}$ , can be evaluated using (2.4). For the output response  $y(t)$  to be zero (i.e., reject totally the interference), it is necessary that

$$y(\theta_{SNOI_1}) = (\theta_{SNOI_2}) = (\theta_{SNOI_3}) = 0. \quad (2.10)$$

Solving simultaneously the linear system of four complex equations (2.5), and (2.7)-(2.9), the array weights can be computed. These are the optimum weights that

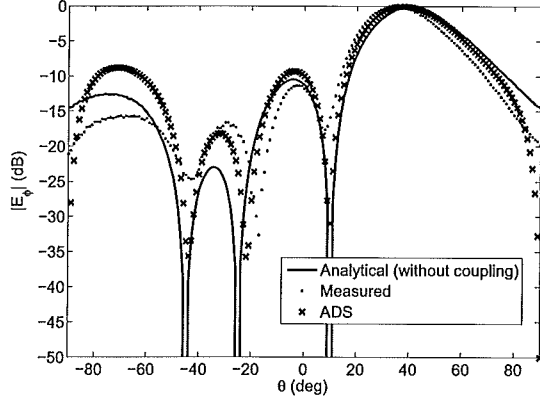
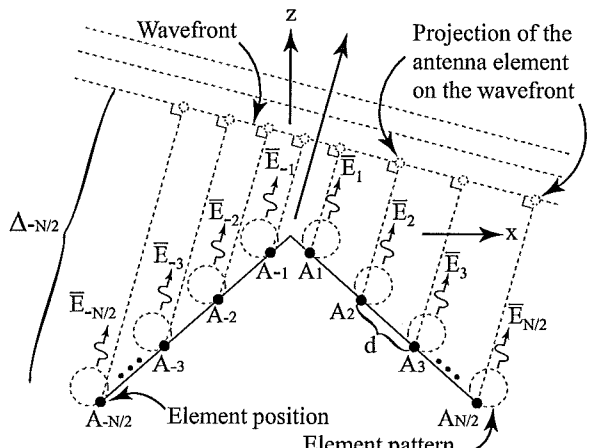


Figure 15. Beamforming results for the four-element linear array.

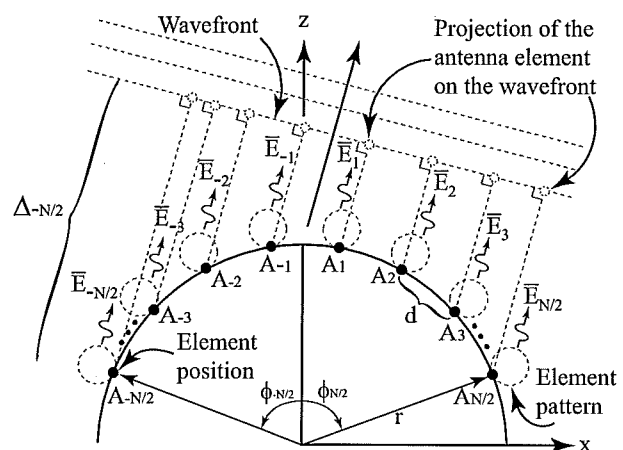
guarantee the desired SOI and SNOI radiation pattern. The previous expressions were determined for  $N = 4$  and can be generalized for more elements. It should be mentioned that similar work could be carried out for an odd value of  $N$ .

Next, the beamforming results for the four-element linear array are shown in Figure 15 for  $\theta_{SOI} = 40^\circ$ ,  $\theta_{SNOI_1} = -45^\circ$ ,  $\theta_{SNOI_2} = -25^\circ$  and  $\theta_{SNOI_3} = 10^\circ$ . Good agreement between measurements, simulations and analytical computations is shown. Details of the measurement setup will be discussed in Chapter 7.

In the area of conformal antennas, researchers have studied how the radiation pattern of a conformal antenna changes as it is deformed in various ways [81]-[55]. It has been shown that the overall gain of an antenna array can be reduced by as much as 25 dBi in a particular direction without appropriate phase and amplitude compensation [55]. To mitigate some of the unwanted affects of deformation on the overall gain of an array, several compensation techniques have been proposed [85]-[91]. In summary, it has been shown that the radiation pattern of a conformal antenna attached to a changing surface (i.e., vibrating surface) can be improved with different calibration techniques, signal processing algorithms, sensor circuitry and phase- and amplitude-adjustments. Then again, the previous work was developed under the



(a)



(b)

Figure 16. (a) Illustration of the conformal antenna on a wedge-shaped surface and (b) illustration of the conformal antenna on a cylindrical-shaped surface.

assumption that the main lobe direction of the radiation pattern was fixed, and the location of the nulls for beamforming was not defined.

Thus, the objective of this work is to study the theory of beamforming for conformal antennas attached to changing surfaces. Moreover, the changing surface affects on the radiation properties of conformal beamforming antennas will be explored. In particular, this work will focus on beamforming for the one dimensional  $1 \times N$  arrays on the wedge- and cylindrical-shaped surfaces shown in Figures 16(a) and 16(b), respectively. For both Figures 16(a) and 16(b), the location of each antenna element on the conformal surface is shown as a black dot and denoted as  $A_{\pm n}$  where  $N$  is assumed to be even and  $n = -N/2, \dots, -1, 1, \dots, N/2$ . It should be noted that similar work could be carried out for an odd value of  $N$ . Also, the wavefront is denoted as a grey dotted line and the direction of propagation is shown with a black arrow. The wavefront is shown away from the origin for illustrative purposes only.

By developing beamforming for the arrays in Figures 16(a) and 16(b), new applications for smart antennas are possible. One new area is wearable networks and, in particular, wearable antennas [92]. Wearable antennas can be attached to search and rescue personnel, military gear and clothing, and, in many of these applications, the wearable antenna can be deformed due to movement. This can make it difficult to implement a wearable smart antenna for successful wireless communications. By understanding the effects of surface deformation and combining this information with the self-adapting network developed in [85], a wearable smart antenna could be developed. Furthermore, the results presented in this paper could be used to improve the performance of existing smart antennas attached to buildings, vehicles or aircraft that are moving or vibrating.

In the conducted research, the beamforming of a conformal antenna on a changing conformal surface is studied by relating the varying position of each antenna

element in the array to the weighting coefficients (i.e, array weights) required to give a desired antenna beamformation. In particular, beamforming for a  $1 \times 4$  array on a changing wedge- and cylindrical-shaped surface is studied using the projection method on a wavefront of a transmitted wave in a particular direction. To validate the theory, a  $1 \times 4$  prototype antenna with individual voltage-controlled phase shifters and attenuators is used to implement the computed weights of each individual antenna element for measurements in an anechoic chamber. Overall agreement between theory, simulations and measurements is shown throughout the conducted research. Furthermore, the effects of mutual coupling and changing conformal surfaces on the behavior of the beamforming pattern and array weights is studied, and validated through analytical, full-wave simulations and measurements.

## CHAPTER 3. BEAMFORMING OF A $1 \times 4$ ARRAY ON A WEDGE-SHAPED CONFORMAL SURFACE

In this chapter the  $1 \times 4$  array (i.e.,  $N = 4$ ) on the wedge-shaped surface shown in Figure 17 with a bend angle of  $\theta_b$  will be considered first. The inter-element spacing along the surface of the wedge is denoted as  $d$  and the location of element  $A_{\pm n}$  is denoted as  $(x_{\pm n}, z_{\pm n})$ .

The motivation for using a beamforming antenna is the feature of being able to define a main radiation lobe in a particular direction while simultaneously defining nulls in the radiation pattern in other directions. The main lobe can then be used to communicate with a desired user in a particular direction and the nulls can be used to reduce the incoming signal from users not of interest. For this work, the angle of the signal of interest will be denoted as  $\theta_{SOI}$  and one user of interest will be assumed while the angle of the  $n^{th}$  user not of interest will be denoted as  $\theta_{SNOI_n}$ . Because a four-element array is being considered here, three nulls at  $\theta_{SNOI_1}$ ,  $\theta_{SNOI_2}$  and  $\theta_{SNOI_3}$  are defined. Now, the goal is to define appropriate array weights that can be used to drive the four elements in Figure 17 to give a main lobe at  $\theta_{SOI}$  and three nulls at  $\theta_{SNOI_1}$ ,  $\theta_{SNOI_2}$  and  $\theta_{SNOI_3}$ . Furthermore, to determine how the shape of the wedge changes the weights, they (weights) are to be determined for various bend angles  $\theta_b$  of the wedge.

To compute the surface-dependent array weights, the projection method [34] will be used along with the matrix method for computing antenna weights as defined in [71]. Since a maximum radiation in the direction of  $\theta_{SOI}$  and nulls in the directions of  $\theta_{SNOI_1}$ ,  $\theta_{SNOI_2}$  and  $\theta_{SNOI_3}$  are desired, the array will be considered as a transmitter in Figure 17. First, consider the case when the array is radiating in the direction of  $\theta_{SOI}$ , as shown in Figure 17(a). One method used to provide a field in the direction of  $\theta_{SOI}$  is to ensure that the fields radiated from elements  $A_{-2}$ ,  $A_{-1}$ ,  $A_1$  and  $A_2$  arrive

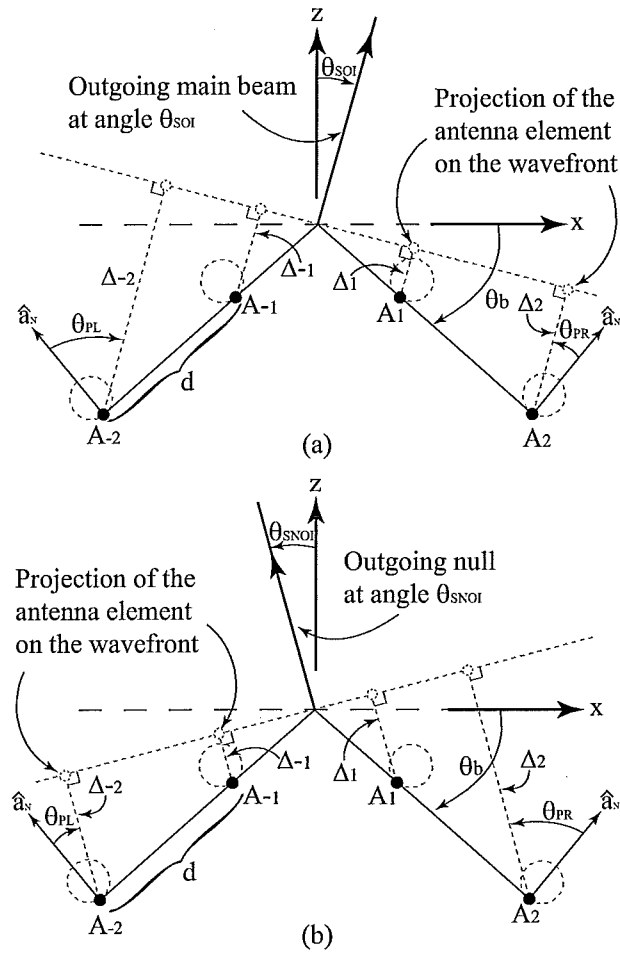


Figure 17. (a) Illustration of the  $1 \times 4$  conformal antenna on a wedge-shaped surface with a transmitted signal of interest at angle  $\theta_{SOI}$  and (b) illustration of the  $1 \times 4$  conformal antenna on a wedge-shaped surface with a transmitted signal not of interest at angle  $\theta_{SNOI}$ .

at the wavefront with the same phase. This will then result in a broad-side radiation to the wavefront. To ensure that these fields arrive with the same phase, the voltage phase driving each individual element can be adjusted with a phase shifter. The amount of phase required is equal and opposite to sign of the phase introduced by the free-space propagation from the antenna element to the wavefront. To compute this distance, the values for  $\Delta_{-2}$ ,  $\Delta_{-1}$ ,  $\Delta_1$  and  $\Delta_2$  in Figure 17(a), which denote the distance from the elements  $A_{-2}$ ,  $A_{-1}$ ,  $A_1$  and  $A_2$ , respectively, to the wavefront (or the projected elements on the wavefront), need to be computed. Furthermore, the expressions for  $A_{-2}$ ,  $A_{-1}$ ,  $A_1$  and  $A_2$  should be written in a general manner that includes the location of each antenna element on the surface and the bend angle  $\theta_b$ . A similar argument can be made for the case when the array is transmitting a null in the direction of  $\theta_{SNOI_n}$ , which is shown in Figure 17(b). For this case, the values of  $\Delta_{\pm n}$  still need to be computed.

### 3.1. Computing the distance to the projected element

For this work, the values of  $\theta_{SOI}$  and  $\theta_{SNOI_n}$  are between  $-\pi/2$  and  $\pi/2$ . Because of this, the problem will be broken down in to two cases. For the first case,  $-\theta_b \leq \theta_{SOI(SNOI_n)} \leq \theta_b$ . For these angles of  $\theta_{SOI(SNOI_n)}$  the projected elements on the wavefront are all outside of the wedge-shaped surface. For the second case,  $\theta_b \leq \theta_{SOI(SNOI_n)} \leq \pi/2$  or  $-\pi/2 \leq \theta_{SOI(SNOI_n)} \leq -\theta_b$ . For these angles of  $\theta_{SOI(SNOI_n)}$ , half of the projected elements are outside of the wedge-shaped surface and half are inside of the surface. This is because when  $\theta_{SOI(SNOI_n)} \geq \theta_b$  or  $\theta_{SOI(SNOI_n)} \leq -\theta_b$  the projected elements for  $A_1$  and  $A_2$  or  $A_{-1}$  and  $A_{-2}$ , respectively, are inside of the wedge-shaped surface in Figure 17.

*1) Case 1: computing  $\Delta_{\pm n}$  for  $-\theta_b \leq \theta_{SOI(SNOI_n)} \leq \theta_b$ :*

Using the notation in Figure 17, the distance from the antenna elements on the wedge

to the projected elements on the wavefront can be computed using:

$$\Delta_{\pm n} = d \frac{|n|}{2n} (2|n| - 1) \sin (\theta_b \mp \theta_{SOI(SNOI_n)}) \quad (3.1)$$

for  $0 \leq \theta_{SOI(SNOI_n)} \leq \theta_b$  and

$$\Delta_{\pm n} = d \frac{|n|}{2n} (2|n| - 1) \sin (\theta_b \pm |\theta_{SOI(SNOI_n)}|) \quad (3.2)$$

for  $-\theta_b \leq \theta_{SOI(SNOI_n)} \leq 0$ . Notice that the expressions in (3.1) and (3.2) are written in terms of the bend angle  $\theta_b$  of the wedge and the location of each antenna element, indicating the generality of the expressions.

*2) Case 2: computing  $\Delta_{\pm n}$  for  $\theta_b \leq \theta_{SOI(SNOI_n)} \leq \pi/2$  or  $-\pi/2 \leq \theta_{SOI(SNOI_n)} \leq -\theta_b$ :*

Next, for the remaining values of  $\theta_{SOI(SNOI_n)}$  the distance from each element in the array to the projected elements on the wavefront can be computed as:

$$\Delta_{\pm n} = d \frac{|n|}{2n} (2|n| - 1) \sin (\theta_{SOI(SNOI_n)} \mp \theta_b) \quad (3.3)$$

for  $\theta_b \leq \theta_{SOI(SNOI_n)} \leq \pi/2$  and

$$\Delta_{\pm n} = d \frac{|n|}{2n} (2|n| - 1) \sin (|\theta_{SOI(SNOI_n)}| \pm \theta_b) \quad (3.4)$$

for  $-\pi/2 \leq \theta_{SOI(SNOI_n)} \leq -\theta_b$ . Notice that (3.3) and (3.4) are also written in terms of  $\theta_b$  and the position of each antenna element in a general fashion.

### 3.2. Computing the radiation in the direction of $\theta_{SOI}$ , $\theta_{SNOI_1}$ , $\theta_{SNOI_2}$ and $\theta_{SNOI_3}$

Next, the field from the array in the direction of  $\theta_{SOI}$ ,  $\theta_{SNOI_1}$ ,  $\theta_{SNOI_2}$  and  $\theta_{SNOI_3}$  on the wedge-shaped surface can be computed using the following array factor ( $AF_w$ )

expression [55]:

$$AF_w(\theta, \phi) = \sum_{n=-2}^{-1} F_{n,L} e^{jk[ux_n + vy_n + z_n \cos \theta]} + \sum_{n=1}^2 F_{n,R} e^{jk[ux_n + vy_n + z_n \cos \theta]} \quad (3.5)$$

where

$$F_{n,L} = w_n \cos(\theta_{PL}) e^{\pm jk\Delta_{\pm n}} \quad (3.6)$$

and

$$F_{n,R} = w_n \cos(\theta_{PR}) e^{\pm jk\Delta_{\pm n}}. \quad (3.7)$$

A spherical coordinate system is assumed in (3.5) with  $u = \sin \theta \cos \phi$ ,  $v = \sin \theta \sin \phi$ ,  $\Delta_{\pm n}$  is defined in (3.1)-(3.4),  $(x_n, y_n, z_n)$  is the location of the  $n^{th}$  array element and  $w_n$  are the complex weighting functions (i.e., array weights). Furthermore, the element patterns for  $A_1$  and  $A_2$  are denoted as  $e_R(\theta) = \cos \theta_{PR}$  and the element patterns for  $A_{-1}$  and  $A_{-2}$  are denoted as  $e_L(\theta) = \cos \theta_{PL}$  where  $\theta_{PR}$  and  $\theta_{PL}$  are defined in Figure 17. To compute the complex excitation coefficients for antenna elements on the conformal wedge we determine  $\theta_{PL}$  and  $\theta_{PR}$  as shown in Figure 17. These are the offset directions of SOI and SNOIs on the conformal wedge for the left and right antenna elements of the array midpoint and must be included to compute the weighting coefficients to give the desired SOI and SNOIs radiation pattern. To compute  $\theta_{PL}$  and  $\theta_{PR}$  for  $\theta_{SOI(SNOI)} > 0$ , consider Figure 17(a). From the geometry, we can write

$$\theta_{PL} = (\theta_b + |\theta|) \quad (3.8)$$

and

$$\theta_{PR} = -(\pi/2 - |\theta| - (\pi/2 - \theta_b)) = -\theta_b + |\theta|. \quad (3.9)$$

Similary for  $\theta_{SOI(SNOI)} < 0$  in Figure 17(b) we can write

$$\theta_{PL} = \pi/2 - [(\pi/2 - \theta_b) + |\theta|] = \theta_b - |\theta| \quad (3.10)$$

and

$$\theta_{PR} = -(\theta_b + |\theta|) = -\theta_b - |\theta|. \quad (3.11)$$

### 3.3. Computing the array weights for $N = 4$ elements

The complex weighting functions (i.e., array weights) in (3.5) are of interest in this work because these are the array weights that need to be computed for the beamforming of the array. To compute these weights, the matrix method for smart antennas presented in [71] will be used. Because the array studied here has four-elements, four array weights are needed. This then requires a set of four equations with four unknowns that can be written as a square matrix. Then the array weights can be computed using a matrix solver. The sum in (3.5) has four terms for  $N = 4$  and to get four equations with four unknowns, (3.5) will be evaluated at each value of  $\theta_{SOI}$ ,  $\theta_{SNOI_1}$ ,  $\theta_{SNOI_2}$  and  $\theta_{SNOI_3}$ . This then gives the following array factor matrix

$\mathbf{AF}_w$ :

$$\mathbf{AF}_w = \begin{bmatrix} AF_w(\theta_{SOI}) \\ AF_w(\theta_{SNOI_1}) \\ AF_w(\theta_{SNOI_2}) \\ AF_w(\theta_{SNOI_3}) \end{bmatrix} \quad (3.12)$$

where  $\theta = \theta_{SOI}$ ,  $\theta_{SNOI_1}$ ,  $\theta_{SNOI_2}$  or  $\theta_{SNOI_3}$  and  $\phi = 0$ . Then, factoring out the array

weights gives

$$\mathbf{A}\mathbf{F}_w = \mathbf{A}\mathbf{W} \quad (3.13)$$

where  $\mathbf{A}$  is the array factor on the wedge in (3.5) with the weights factored out and

$$\mathbf{W} = \begin{bmatrix} w_{-2} \\ w_{-1} \\ w_1 \\ w_2 \end{bmatrix}. \quad (3.14)$$

Next, to ensure that the conformal antenna will have a main beam at the scan angle  $\theta_{SOI}$ ,  $AF_w(\theta_{SOI})$  must equal 1 in (3.12), or  $AF_w(\theta_{SOI})=1$ . Then, in order to provide nulls in the directions of  $\theta_{SNOI_1}$ ,  $\theta_{SNOI_2}$  and  $\theta_{SNOI_3}$ ,  $AF_w(\theta_{SNOI_1})=AF_w(\theta_{SNOI_2})=AF_w(\theta_{SNOI_3})=0$  in (3.12). This can be written in matrix form in the following manner:

$$\mathbf{A}\mathbf{W} = \mathbf{C} \quad (3.15)$$

where

$$\mathbf{C} = \begin{bmatrix} 1 \\ 0 \\ 0 \\ 0 \end{bmatrix} \quad (3.16)$$

and  $\mathbf{A}\mathbf{W}$  is defined in (3.13). Finally, solving for the weights in (3.15) gives

$$\mathbf{W} = \mathbf{A}^{-1}\mathbf{C}. \quad (3.17)$$

By setting the first element in (3.16) to be 1 and the rest of the elements to be 0, the array factor is forced to give nulls (or a zero field) analytically at the angles of  $\theta_{SNOI_1}$ ,  $\theta_{SNOI_2}$  and  $\theta_{SNOI_3}$ . Thus, the solution of (3.17) yields the array weights required to

give these pattern null features. Furthermore, since the values of  $\Delta_{\pm n}$  in the array factor expression in (3.12) are written in terms of the wedge angle  $\theta_b$  and the location of each antenna element, the weights computed with (3.17) are determined in a setting where the antenna, and hence the wedge, can change shape.

### 3.4. Computing the array weights for $N$ elements

The previous expressions were determined for  $N = 4$  and can be generalized for more elements. More specifically, equations (3.12)-(3.17) can be generalized in the following manner:

$$\mathbf{AF}_w = \begin{bmatrix} AF_w(\theta_{SOI}) \\ \vdots \\ AF_w(\theta_{SNOI_1}) \\ \vdots \\ AF_w(\theta_{SNOI_n}) \end{bmatrix} \quad (3.18)$$

where

$$AF_{wn}(\theta, \phi) = \sum_{n=-N/2}^{-1} F_{n,L} e^{jk[ux_n + vy_n + z_n \cos \theta]} + \sum_{n=1}^{N/2} F_{n,R} e^{jk[ux_n + vy_n + z_n \cos \theta]}, \quad (3.19)$$

and  $F_{n,L}$  and  $F_{n,R}$  are defined in (3.6) and (3.7), respectively. Then, factoring out the array weights gives

$$\mathbf{AF}_{wn} = \mathbf{A}_n \mathbf{W}_n \quad (3.20)$$

where  $\mathbf{A}$  is the array factor on the wedge in (3.19) with the weights factored out and

$$\mathbf{W}_n = \begin{bmatrix} w_{-N/2} \\ \vdots \\ w_{-1} \\ w_1 \\ \vdots \\ w_{N/2} \end{bmatrix}. \quad (3.21)$$

Finally, the coefficients in (3.16) can be generalized as

$$\mathbf{C}_n = \begin{bmatrix} c_1 \\ c_2 \\ \vdots \\ c_n \end{bmatrix} \quad (3.22)$$

and the weights can be computed using

$$\mathbf{W}_n = \mathbf{A}_n^{-1} \mathbf{C}_n. \quad (3.23)$$

Equation (3.23) can then be used to solve for the array weights that will result in a main radiation pattern in the direction of  $\theta_{SOI}$  and nulls in the directions of  $\theta_{SNOI_1}$ ,  $\theta_{SNOI_2}$ , ...  $\theta_{SNOI_{(N-1)}}$  for an  $N$ -element array on a changing wedge-shaped surface.

## CHAPTER 4. BEAMFORMING OF A $1 \times 4$ ARRAY ON A CYLINDRICAL-SHAPED CONFORMAL SURFACE

The array weights for the conformal antenna on the cylindrical shaped surface shown in Figure 18 are computed next. Again, for illustration, the derivations will be carried out for  $N = 4$  elements.

### 4.1. Computing the distance to the projected element

As with the wedge-shaped conformal surface, the distance from the elements on the cylindrical surface to the projected elements on the transmitted wavefront at angle  $\theta_{SOI(SNOI_n)}$  must be computed. Again, these distances are denoted as  $\Delta_{\pm n}$  in Figure 18. First, the distance from the point where the cylinder intersects the z-axis (denoted as point  $P$  in Figure 18) to each antenna element is computed using

$$h_{\pm n} = \sqrt{(0 - x_{\pm n})^2 + (r - z_{\pm n})^2} \quad (4.1)$$

where again  $(x_{\pm n}, z_{\pm n})$  is the location of the  $n^{th}$  element on the cylindrical surface,  $x_{\pm n} = r \cos \phi_{\pm n}$ ,  $z_n = r \sin \phi_{\pm n}$  and  $\phi_{\pm n}$  is defined in Figure 18. As with the wedge-shaped surface, the problem will be considered as two different cases. The first case is for  $\theta_{SOI(SNOI_n)} \geq 0$  and the second case is for  $\theta_{SOI(SNOI_n)} \leq 0$ . The first case is shown in Figure 18. The projected elements of  $A_{-2}$ ,  $A_{-1}$  and  $A_2$  in the direction of  $\theta_{SOI(SNOI_n)}$  are outside of the cylindrical surface and the projected element of  $A_1$  in the direction of  $\theta_{SOI(SNOI_n)}$  is inside of the cylindrical surface. Because some projected elements are outside of the cylinder and some are inside, each case will be broken into two parts. The first part will compute the distance from the elements  $A_{-1}$  and  $A_{\pm 2}$  to the projected elements on the wavefront and the second part will compute the distance from the element  $A_1$  to the projected element on the wavefront (as shown in Figure 18).

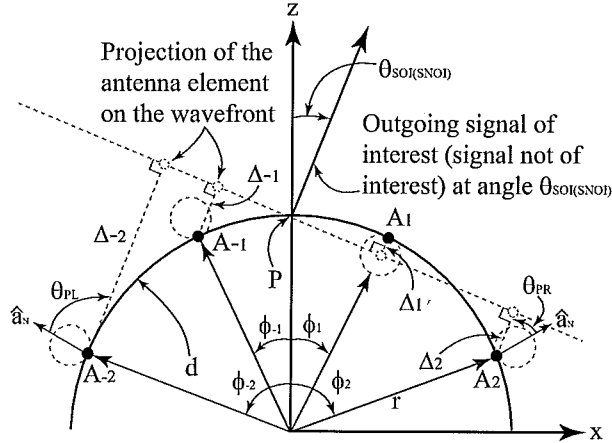


Figure 18. Illustration of the  $1 \times 4$  conformal antenna on a cylindrical-shaped surface with a transmitted signal of interest (signal not of interest) at angle  $\theta_{SOI(SNOI)}$ .

1) Case 1 with  $\theta_{SOI(SNOI_n)} \geq 0$

Next, using (4.1) the distance from the elements  $A_{-1}$  and  $A_{\pm 2}$  to the projected elements on the transmitted wavefront can be computed as:

$$\Delta_{\pm n} = h_{\pm n} \sin(\mp \theta_{SOI(SNOI_n)} + \theta_{\pm n}) \quad (4.2)$$

where  $\theta_{\pm n} = \cos^{-1} |x_{\pm n}/h_{\pm n}|$ . Then, for element  $A_1$  the distance to the projected element can be computed as:

$$\Delta_{+n} = h_{+n} \sin(\theta_{SOI(SNOI_n)} - \theta_{+n}). \quad (4.3)$$

2) Case 2 with  $\theta_{SOI(SNOI_n)} \leq 0$

Again, using (4.1) the distance from the elements  $A_1$  and  $A_{\pm 2}$  to the projected elements can be computed as:

$$\Delta_{\pm n} = h_{\pm n} \sin(\pm |\theta_{SOI(SNOI_n)}| + \theta_{\pm n}) \quad (4.4)$$

where  $\theta_{\pm n} = \cos^{-1} |x_{\pm n}/h_{\pm n}|$ . Then for element  $A_{-1}$  the distance to the projected element can be computed as:

$$\Delta_{-n} = h_{-n} \sin(|\theta_{SOI(SNOI_n)}| - \theta_{-n}). \quad (4.5)$$

A few comments can be made about (4.2)-(4.5). As with the wedge-shaped surface, these expressions have been written in a general manner in terms of antenna position on the cylindrical surface and the radius of curvature. Also, special care should be taken when implementing these equations if  $|\theta_{SOI(SNOI_n)}| \leq \theta_{\pm 1}$ . This is because for these angles all of the projected elements on the wavefront will be outside of the cylindrical surface. In this case, the distance to the wavefront can be computed using (4.2) or (4.4) (depending on whether  $\theta_{SOI(SNOI_n)} \leq 0$  or  $\theta_{SOI(SNOI_n)} \geq 0$ ) and the computations of (4.3) and (4.5) are not required.

#### 4.2. Computing the radiation in the direction of $\theta_{SOI}$ , $\theta_{SNOI_1}$ , $\theta_{SNOI_2}$ and $\theta_{SNOI_3}$

Next, the field from the array in the direction of  $\theta_{SOI}$ ,  $\theta_{SNOI_1}$ ,  $\theta_{SNOI_2}$  and  $\theta_{SNOI_3}$  on the cylindrical-shaped surface can be computed using (3.5) (with updated distances computed using (4.2)-(4.5)). As mentioned in Section 3.2, Chapter 3, to obtain the correct SOI and SNOIs radiation pattern for conformal antennas array, we need to determine  $\theta_{PL}$  and  $\theta_{PR}$ . To compute  $\theta_{PL}$  and  $\theta_{PR}$  for  $\theta_{SOI(SNOI)} < 0$ , consider Figure 18. From the geometry, we can write

$$\theta_{PL} = \pi/2 - \phi_n - |\theta| \quad (4.6)$$

and

$$\theta_{PR} = -(\pi/2 - \phi_n + |\theta|). \quad (4.7)$$

Similary for  $\theta_{SOI(SNOI)} > 0$  in Figure 18 we can write

$$\theta_{PL} = \pi/2 - \phi_n + |\theta| \quad (4.8)$$

and

$$\theta_{PR} = -(\pi/2 - \phi_n - |\theta|) = -\pi/2 + (\phi_n + |\theta|). \quad (4.9)$$

#### 4.3. Computing the array weights for $N = 4$ elements

Next, as with the conformal antenna on the wedge-shaped surface, the array weights can be computed using (3.17). For the computations of these array weights on the cylinder, the distance from the elements to the wavefront should be computed using (4.2)-(4.5).

#### 4.4. Computing the array weights for $N$ elements

Finally, (3.23) can be used (with updated distances computed using (4.2)-(4.5)) to compute the array weights for  $1 \times N$  array on a cylindrical surface with radius  $r$ . As with the wedge-shaped surface, the expressions to compute the array weights have been written in a general manner that includes element spacing and the radius of the cylinder. This makes the technique presented here useful for an array attached to a changing cylindrical surface.

## CHAPTER 5. COMPUTING THE WEIGHTING COEFFICIENTS WITH MUTUAL COUPLING

For the previous derivations of (3.17) and (3.23), it was assumed that there was no mutual coupling between the elements. To model the mutual coupling, the work presented in [93] was considered. More specifically, the work in [93] proposed a model for the mutual coupling in adaptive arrays and demonstrated that the mutual coupling between the elements of an adaptive array can cause a significant degradation in the signal-to-interference-plus-noise ratio (SINR). The methods in [93] will be adopted here to model the mutual coupling effects on the radiation pattern of the conformal beamforming array.

The coupling between the antenna elements can be modeled as an  $N+1$  port network, as shown in Figure 19. The antenna elements in the array are all terminated with  $Z_L$  and denoted as ports 1, 2, ...  $N$ . The antenna port being driven by a voltage source  $V_s$  is denoted as  $N+1$ . The port being driven with  $V_s$  is the representation of the transmitted (or incoming) signals at angles  $\theta_{SOI}$  or  $\theta_{SNOI_n}$ . Then, using the Kirchhoff relations for the  $N+1$  terminal network, the voltage at the terminated port  $n$  can be written as:

$$V_{Tn} = I_1 Z_{n,1} + I_2 Z_{n,2} + \dots + I_n Z_{n,m} + \dots + I_s Z_{n,s} \quad (5.1)$$

where  $Z_{n,m}$  is the mutual impedance between the  $n^{th}$  and  $m^{th}$  port,  $I_n$  is the current going through the terminating resistor on the  $n^{th}$  port,  $Z_{nn}$  is the self-impedance of the  $n^{th}$  port and  $Z_{n,s}$  represents the mutual coupling term between the driven element with  $V_s$  and the  $n^{th}$  antenna element.

Furthermore, the current at the  $n^{th}$  port can be written in terms of the terminal

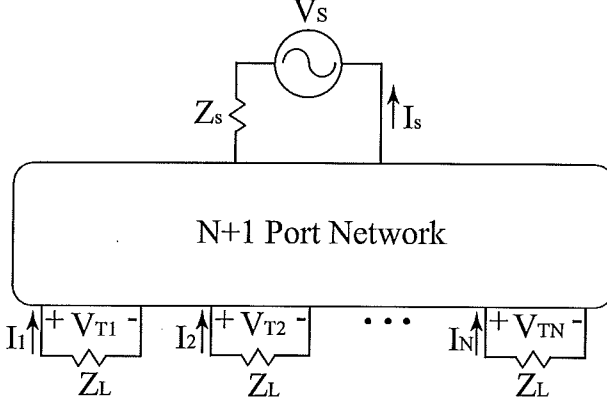


Figure 19. N-port network illustration of the conformal array with a signal of interest at angle  $\theta_{SOI}$  or  $\theta_{SNOI_n}$ .

voltage and load impedance in the following manner:

$$I_n = \frac{-V_{Tn}}{Z_L}. \quad (5.2)$$

Then, making use of the open-circuit condition and removing the terminating impedances results in  $I_1 = I_2 = \dots = I_N = 0$ . This then simplifies (5.1) to  $V_{Tn} = I_s Z_{n,s}$ . Under these conditions, (5.1) represents the open circuit voltages at the  $n^{th}$  port caused by the mutual coupling between the driven element and the  $n^{th}$  port, and can be computed as  $V_{Tn} = I_s Z_{n,s} = V_{OCn}$ . Next, substituting (5.2) into (5.1), making use of the open-circuit condition and writing (5.1) in matrix form results in the following:

$$\mathbf{Z}_c \mathbf{V}_T = \mathbf{V}_{OC}. \quad (5.3)$$

where

$$\mathbf{Z}_c = \begin{bmatrix} 1 + \frac{Z_{1,1}}{Z_L} & \frac{Z_{1,2}}{Z_L} & \dots & \frac{Z_{1,N}}{Z_L} \\ \frac{Z_{2,1}}{Z_L} & 1 + \frac{Z_{2,2}}{Z_L} & \dots & \frac{Z_{2,N}}{Z_L} \\ \vdots & \vdots & \ddots & \vdots \\ \frac{Z_{N,1}}{Z_L} & \frac{Z_{N,2}}{Z_L} & \dots & 1 + \frac{Z_{N,N}}{Z_L} \end{bmatrix}, \quad (5.4)$$

$$\mathbf{V}_T = \begin{bmatrix} V_{T1} \\ V_{T2} \\ \vdots \\ V_{Tn} \end{bmatrix} \quad (5.5)$$

and

$$\mathbf{V}_{OC} = \begin{bmatrix} V_{OC1} \\ V_{OC2} \\ \vdots \\ V_{OCn} \end{bmatrix}. \quad (5.6)$$

The normalized impedance matrix  $\mathbf{Z}_c$  includes self- and mutual-terms, and can be determined from a 3D full wave simulator such as HFSS [94]. The open circuit voltage column matrix  $\mathbf{V}_{OC}$  represents the array weights (i.e., the complex voltages used to drive the beamforming conformal antenna) without including mutual coupling. This then results in  $\mathbf{V}_{OC} = \mathbf{W}_n$  where  $\mathbf{W}_n$  is given in (3.21). The terminal voltage column matrix  $\mathbf{V}_T$  represents the array weights that include the mutual coupling and can be computed from (5.3) as follows:

$$\mathbf{V}_T = \mathbf{Z}_c^{-1} \mathbf{V}_{OC}. \quad (5.7)$$

Next, to write the array weights with mutual coupling in terms of the array factor expressions in (3.20), (3.20) is equated to (3.22), and  $\mathbf{V}_{OC} = \mathbf{W}_n$  is substituted into the equality. This results in the following expression:

$$\mathbf{A}_n \mathbf{V}_{OC} = \mathbf{C}_n. \quad (5.8)$$

Then, solving for  $\mathbf{V}_{OC}$  in (5.7), substituting into (5.8) and reorganizing gives:

$$\mathbf{V}_T = \mathbf{Z}_c^{-1} \mathbf{A}_n^{-1} \mathbf{C}_n = \mathbf{W}_n^c \quad (5.9)$$

where  $\mathbf{W}_n^c$  represents the new array weights with the coupling included in the computations. In the next section, validation of  $\mathbf{W}_n$  and  $\mathbf{W}_n^c$  for various values of  $\theta_{SOI}$  and  $\theta_{SNOI_n}$  will be presented followed by the characteristics of the array weights for various conformal surfaces.

## CHAPTER 6. DEPENDENCE OF THE ARRAY WEIGHTS ON THE CONFORMAL SURFACE GEOMETRY

In this chapter, the array weights for a three-element array were computed analytically using (3.23). This was done to show how the array weights are dependent on  $\theta_b$  and the radius of curvature  $r$ . It should be mentioned that  $N = 3$  was chosen because the problem becomes much more complex for  $N > 3$  and requires a numerical analysis of the matrices in (3.23). Assuming one SOI and two SNOIs, we can write the following three equations with three unknown array weights:

$$w_{-1}F_{-1,L}(\theta_{SOI}) + w_0 + w_{+1}F_{1,R}(\theta_{SOI}) = 1, \quad (6.1)$$

$$w_{-1}F_{-1,L}(\theta_{SNOI_1}) + w_0 + w_{+1}F_{1,R}(\theta_{SNOI_1}) = 0, \quad (6.2)$$

and

$$w_{-1}F_{-1,L}(\theta_{SNOI_2}) + w_0 + w_{+1}F_{1,R}(\theta_{SNOI_2}) = 0. \quad (6.3)$$

Subtracting (6.2) and (6.3) from (6.1) we obtain

$$w_{-1}[F_{-1,L}(\theta_{SOI}) - F_{-1,L}(\theta_{SNOI_1})] + w_{+1}[F_{1,R}(\theta_{SOI}) - F_{1,R}(\theta_{SNOI_1})] = 1, \quad (6.4)$$

$$w_{-1}[F_{-1,L}(\theta_{SOI}) - F_{-1,L}(\theta_{SNOI_2})] + w_{+1}[F_{1,R}(\theta_{SOI}) - F_{1,R}(\theta_{SNOI_2})] = 1, \quad (6.5)$$

Next subtracting (6.3) from (6.2) we obtain

$$w_{-1}[F_{-1,L}(\theta_{SONI_1}) - F_{-1,L}(\theta_{SNOI_2})] + w_{+1}[F_{1,R}(\theta_{SNOI_1}) - F_{1,R}(\theta_{SNOI_2})] = 0. \quad (6.6)$$

Equation (6.6) can be written as:

$$w_{-1} = -w_{+1} \frac{F_{1,R}(\theta_{SNOI_2}) - F_{1,R}(\theta_{SNOI_1})}{F_{-1,L}(\theta_{SONI_2}) - F_{-1,L}(\theta_{SNOI_1})}, \quad (6.7)$$

or

$$w_{-1} = -w_{+1}D \quad (6.8)$$

where

$$D = \frac{F_{1,R}(\theta_{SNOI_2}) - F_{1,R}(\theta_{SNOI_1})}{F_{-1,L}(\theta_{SNOI_2}) - F_{-1,L}(\theta_{SNOI_1})}. \quad (6.9)$$

Next, substituting (6.8) into (6.4) we get

$$w_{+1}[F_{1,R}(\theta_{SOI}) - F_{1,R}(\theta_{SNOI_1})] = 1 + w_{+1}D[F_{-1,L}(\theta_{SOI}) - F_{-1,L}(\theta_{SNOI_1})], \quad (6.10)$$

or

$$w_{+1}[F_{1,R}(\theta_{SOI}) - F_{1,R}(\theta_{SNOI_1})] - D[F_{-1,L}(\theta_{SOI}) - F_{-1,L}(\theta_{SNOI_1})] = 1., \quad (6.11)$$

Now, from (6.11) we can calculate  $w_{+1}$  as follows:

$$w_{+1} = \frac{1}{[F_{1,R}(\theta_{SOI}) - F_{1,R}(\theta_{SNOI_1})] - D[F_{-1,L}(\theta_{SOI}) - F_{-1,L}(\theta_{SNOI_1})]} \quad (6.12)$$

or

$$w_{+1} = \frac{1}{F_{1,R}^{\Delta} - DF_{-1,L}^{\Delta}}. \quad (6.13)$$

Equation (6.13) can be used to calculate  $w_{-1}$  from (6.8). Finally using (6.8) and

(6.13) in (6.1), we can calculate the array weight  $w_0$  as follows:

$$w_0 = 1 - w_{+1}[F_{1,R}(\theta_{SOI}) - DF_{-1,L}(\theta_{SOI})], \quad (6.14)$$

where

$$D = \frac{F_{1,R}(\theta_{SNOI_2}) - F_{1,R}(\theta_{SNOI_1})}{F_{-1,L}(\theta_{SNOI_2}) - F_{-1,L}(\theta_{SNOI_1})}. \quad (6.15)$$

Also,  $F_{1,R}^\Delta = F_{1,R}(\theta_{SOI}) - F_{1,R}(\theta_{SNOI_1})$ ,  $F_{-1,L}^\Delta = F_{-1,L}(\theta_{SOI}) - F_{-1,L}(\theta_{SNOI_1})$  and  $F_{n,L}$  and  $F_{n,R}$  are defined in (3.6) and (3.7), respectively, with the weights factored out.

For a small value of  $N$ , the results in (6.8), (6.13) and (6.14) show that the expression for the array weights can be quite complicated. Then again, it does also show the dependence of each weight on the angle  $\theta_{SOI(SNOI_n)}$  and the location of each antenna element on the array.

To illustrate the behavior of the weights computed using (6.8), (6.13) and (6.14) for various surfaces, the three element array was considered on a wedge-shaped surface for various values of  $\theta_b$ . For these computations the values of  $\theta_{SOI}$  and  $\theta_{SNOI_n}$  were  $\theta_{SOI} = 40^\circ$ ,  $\theta_{SNOI_1} = -45^\circ$  and  $\theta_{SNOI_2} = 10^\circ$ . The amplitude and phase of the array weights computed using (6.8), (6.13) and (6.14) are shown in Figs. 20 and 21, respectively for wedge-shaped conformal surface. Similarly the amplitude and phase of the array weights for various values of radius of curvature on a cylindrical surface are shown in Figs. 22 and 23, respectively. The results show that for a fixed beamformation there is a strong relationship between the array weights and the conformal surface.

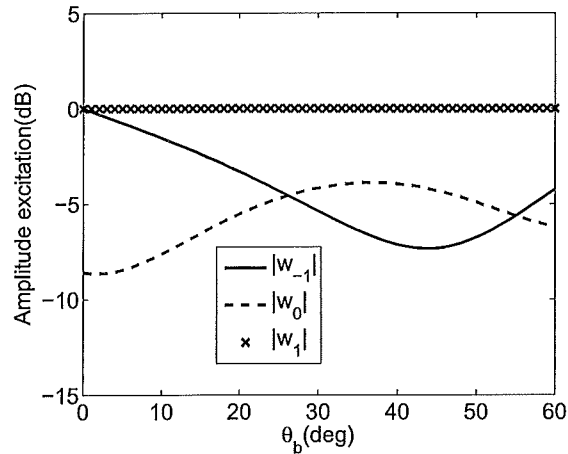


Figure 20. Magnitude of the array weights for the three-element array on the wedge-shaped surface.

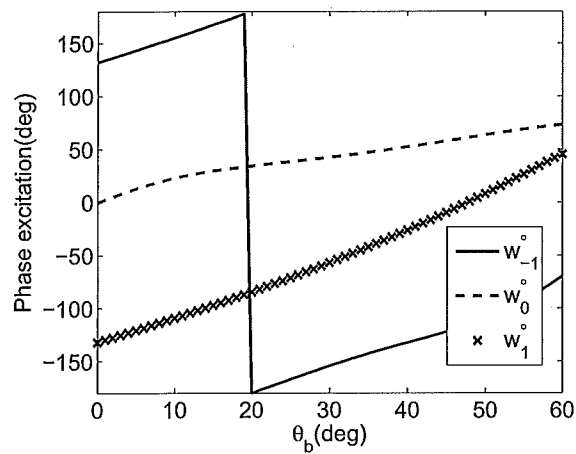


Figure 21. Phase of the array weights for the three-element array on the wedge-shaped surface.

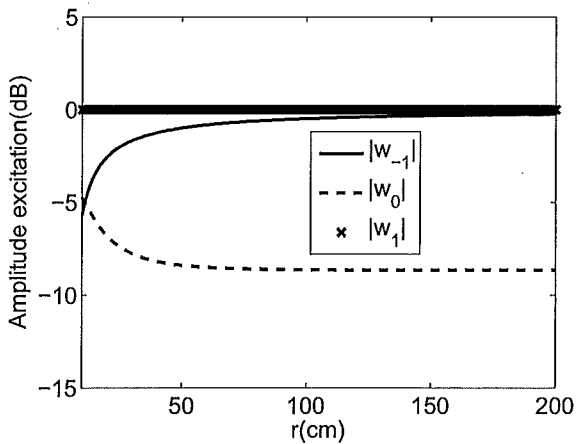


Figure 22. Magnitude of the array weights for the three-element array on the cylindrical-shaped surface.

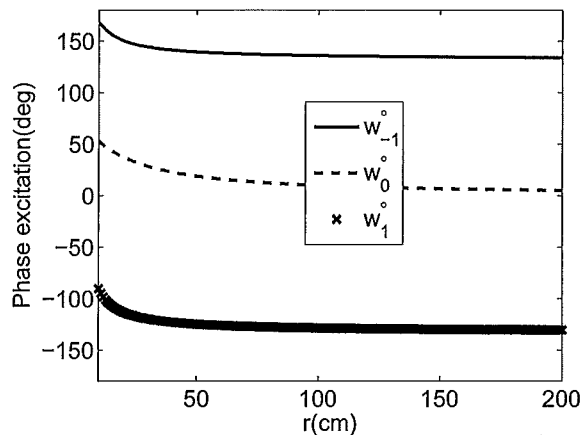


Figure 23. Phase of the array weights for the three-element array on the cylindrical-shaped surface.

## CHAPTER 7. VALIDATION WITH ANALYTICAL, SIMULATION AND MEASUREMENT RESULTS

In this chapter, a beamforming array is used to validate the previously derived array weight expressions using simulations and measurements. More specifically the array weights are computed using (3.23) and (5.9) for the four-element array on the wedge- and cylindrical-shaped surface shown in Figs. 17 and 18. Two different beamformation patterns were considered and each pattern was evaluated on three different conformal surfaces. The characteristics of each beamformation pattern, denoted as pattern 1 and pattern 2, are summarized in Table 1. Furthermore, the three conformal surfaces considered were the wedge-shaped surface with  $\theta_b = 30^\circ$  and  $\theta_b = 45^\circ$  and a cylindrical surface with  $r = 10$  cm.

### 7.1. The four-element beamforming array prototype.

For measurement purposes, the four-element beamforming array shown in Figure 24(a) was manufactured. The array consisted of connectorized voltage-controlled phase shifters, voltage-controlled attenuators, a four-way power divider, an amplifier and four microstrip patches designed to operate at 2.47 GHz. A picture of the attenuators, phase shifters and power divider of the manufactured array is shown in Figure 24(b) and a picture of the four microstrip patches is shown in Figure 24(c). Four individual microstrip patches were used for the convenience of placing the array on the various conformal surfaces. The phase shifters were manufactured by Hittite Microwave Corporation [95] (PN: HMC928LP5E) and the power divider, attenuators and amplifiers were manufactured by Mini-Circuits [96] (PNs: ZN8PD1-53-S+, ZX73-2500-S+ and ZX60-33LN-S+, respectively). Identical SMA cables were used to connect each patch to a port on the power divider. The attenuation and phase shift of the voltage variable attenuator and analog phase shifter were measured and are shown in Tables 8 and 9 in Appendix L and M respectively.

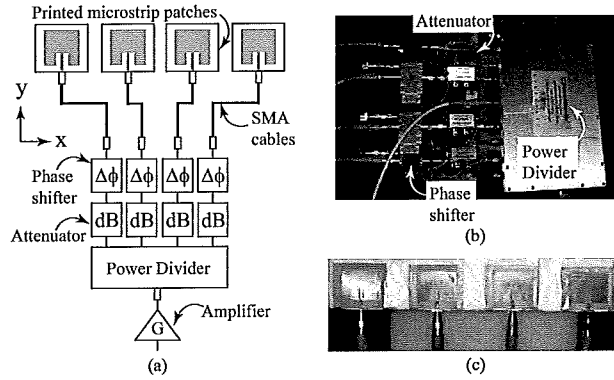


Figure 24. (a) Topology of the four-element beamforming array, (b) a photograph of the power divider, voltage controlled phase shifters and voltage controlled attenuators used for measurements and (c) a photograph of the microstrip patch elements used for attachment to conformal surfaces.

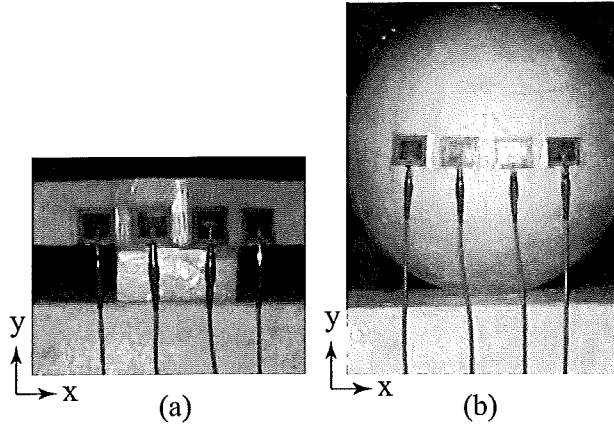


Figure 25. (a) Photograph of the four-element beamforming array being measured on the wedge-shaped surface with  $\theta_b = 30^\circ$  and (b) photograph of the four-element beamforming array being measured on the cylindrical shaped surface with  $r = 10$  cm.

Table 1. Summary of the beamformation patterns 1 and 2.

Variable	Pattern 1	Pattern 2
$\theta_{SOI}$	$0^\circ$	$40^\circ$
$\theta_{SNOI_1}$	$-30^\circ$	$-45^\circ$
$\theta_{SNOI_2}$	$30^\circ$	$-25^\circ$
$\theta_{SNOI_3}$	$40^\circ$	$10^\circ$

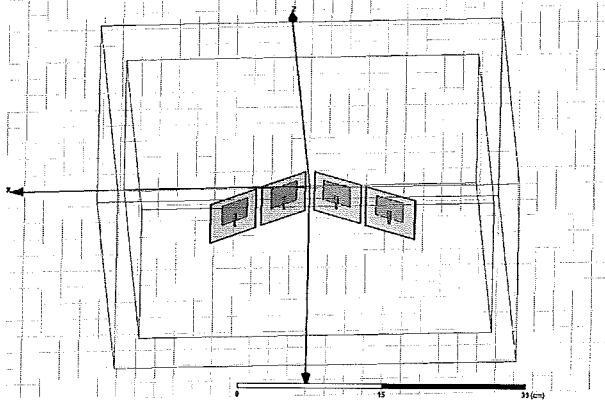


Figure 26. Picture of the four-element beamforming array in HFSS.

### 7.2. Beamforming results on the wedge with $\theta_b = 30^\circ$ .

The first measurements taken were for the four-element beamforming array on the wedge-shaped surface in Figure 17 for  $\theta_b = 30^\circ$  and the array weights were computed using (3.17). The inter-element spacing was  $0.5 \lambda$  and a picture of the array being measured on the surface with a 2-port network analyzer in a fully calibrated anechoic chamber is shown in Figure 25(a). The results from these measurements for both patterns summarized in Table 1 are shown in Figures 27 and 28. Next, the four-element beamforming array was simulated in HFSS as shown in Figure 26 and the weights computed using (3.17) were used to drive the array. The radiation pattern from these simulations can also be seen in Figures 27 and 28 at 2.47 GHz. Then, for a third comparison both patterns were computed analytically using the array factor expression in (3.5) with the weights determined using (3.17). These results are also shown in Figures 27 and 28. Finally, new weights that include the mutual coupling were computed using (5.9) and used in (3.5) to compute the radiation pattern analytically. These results are shown in Figures 27 and 28. Overall, agreement between measurements, simulations and analytical computations (with both sets of array weights) is shown. The array weights for the results in Figures 27 and 28 are

shown in Tables 2 and 3 in Appendix A.

### 7.3. Beamforming results on the wedge with $\theta_b = 45^\circ$ .

Next, measurements were taken for the four-element beamforming array on the wedge-shaped surface in Figure 17 for  $\theta_b = 45^\circ$ . The inter-element spacing was again  $0.5 \lambda$  and (3.17) was used to compute the new array weights. The results from these measurements for both patterns summarized in Table 1 are shown in Figures 29 and 30. Next, the four-element beamforming array was simulated in HFSS with the weights for  $\theta_b = 45^\circ$  and the radiation pattern can also be seen in Figures 29 and 30 at 2.47 GHz. Then, for a third comparison the expression in (3.5) was used to compute the analytical results shown in Figures 29 and 30. New weights that include the mutual coupling were also computed using (5.9) for the new value of  $\theta_b = 45^\circ$ . These weights were then used in (3.5) to compute the radiation pattern and these results are shown in Figures 29 and 30. As with the  $\theta_b = 30^\circ$  results, agreement between measurements, simulations and analytical computations is shown. The array weights for the results in Figures 29 and 30 are also shown in Tables 4 and 5 in Appendix A.

### 7.4. Beamforming results on the cylinder with $r = 10$ cm.

Finally, the same comparison between measurements, simulations and analytical computations was conducted for the four-element array on the cylindrical-shaped surface with  $r = 10$  cm. The array being measured in the full anechoic chamber is shown in Figure 25(b) and the results are shown in Figures 31 and 32. It should be mentioned that in order to measure the array on a cylindrical surface a sphere was used and the antenna elements were placed along the equator. This then resulted in an antenna shape similar to a cylindrical surface. Simulation results and analytical computations with and without the coupling are also shown in Figures 31 and 32 and overall agreement is shown. The array weights for the results in Figures 31 and 32 are shown in Tables 6 and 7 in Appendix A.

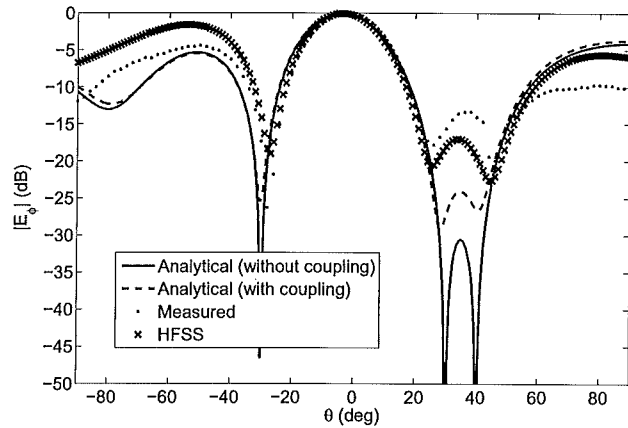


Figure 27. Pattern 1 beamforming results for the four-element array on the wedge-shaped surface with  $\theta_b = 30^\circ$ .

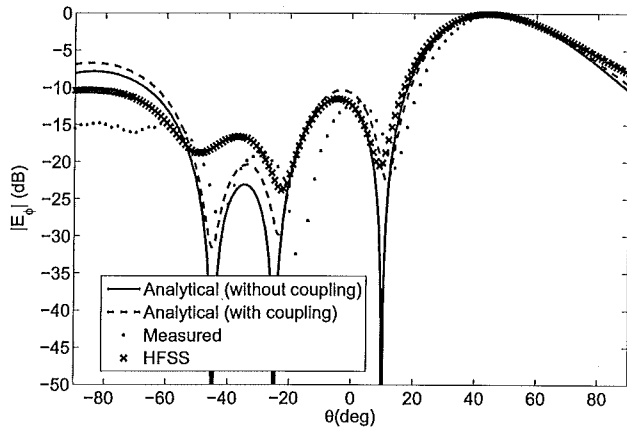


Figure 28. Pattern 2 beamforming results for the four-element array on the wedge-shaped surface with  $\theta_b = 30^\circ$ .

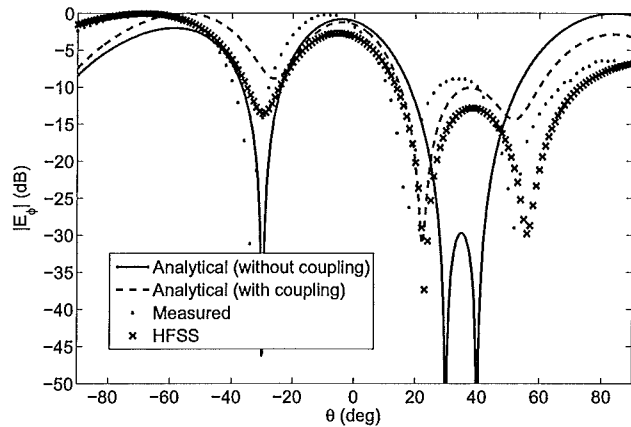


Figure 29. Pattern 1 beamforming results for the four-element array on the wedge-shaped surface with  $\theta_b = 45^\circ$ .

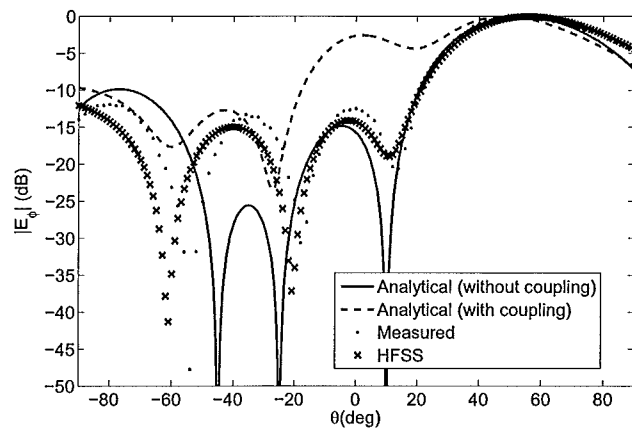


Figure 30. Pattern 2 beamforming results for the four-element array on the wedge-shaped surface with  $\theta_b = 45^\circ$ .

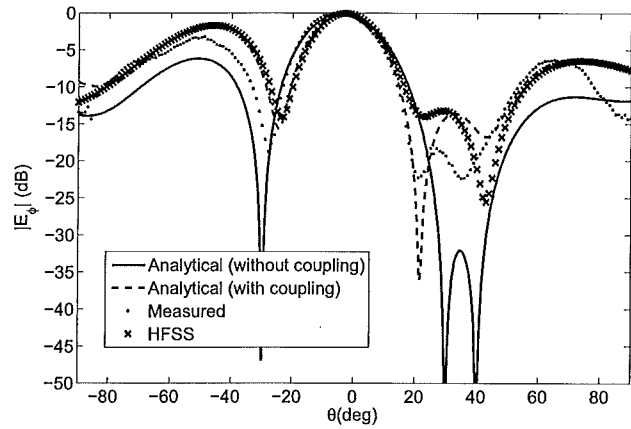


Figure 31. Pattern 1 beamforming results for the four-element array on the cylindrical-shaped surface with  $r = 10$  cm.

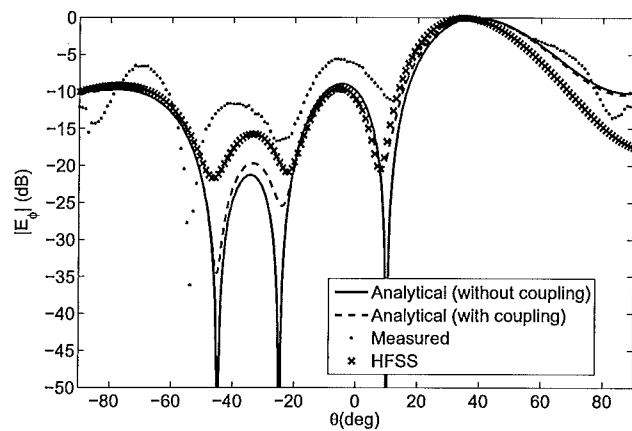


Figure 32. Pattern 2 beamforming results for the four-element array on the cylindrical-shaped surface with  $r = 10$  cm.

## 7.5. Discussion

For the results in Figures 27-32 the most agreement is between the measured results, the HFSS simulations and the analytical computations with the array weights including mutual coupling. This illustrates the improved accuracy of the weights computed using (5.9).

Also, when comparing the pattern 2 results in Figures 28 and 30, it is shown that more disagreement between the results around  $-60^\circ$  exist for the  $\theta_b = 45^\circ$  surface than for the  $\theta_b = 30^\circ$  surface. This is thought to be due to the more severe surface deformation that exists for the  $\theta_b = 45^\circ$  surface.

Overall though, the array weights computed using (3.23) and (5.9) have been shown to be accurate and the effects due to mutual coupling and surface deformations on the radiation pattern have been demonstrated. Then again, the weights computed using (5.9) can be used to model the coupling, and with proper optimization, an improved beamformation could be achieved in a general setting that includes the mutual coupling between elements on a changing conformal surface.

## CHAPTER 8. CONCLUSION

In this work, the beamforming of a conformal antenna on a changing conformal surface is investigated by relating the varying position of each antenna element in the array to the weighting coefficients (i.e, array weights) required to give a desired antenna beamformation. New matrices for computing the array weights that both do not include and include the mutual coupling between elements have been investigated. In particular, the beamforming of a  $1 \times 4$  array on a changing wedge- and cylindrical-shaped surface is studied using the projection method on a wavefront of a transmitted wave in a particular direction. To validate the theory, a  $1 \times 4$  prototype antenna with individual voltage-controlled phase shifters and attenuators is used to implement the computed weights of each individual antenna element for measurements in an anechoic chamber. Overall agreement between theory, simulations and measurements is shown throughout the work. Furthermore, the effects of mutual coupling and changing conformal surfaces on the behavior of the beamforming pattern and array weights is investigated and summarized.

## BIBLIOGRAPHY

- [1] David M. Pozar and Daniel H. Schaubert, *Microstrip Antennas: The analysis and Design of Microstrip Antennas and Arrays*, IEEE Press, Piscataway, NJ, 1995.
- [2] J. P. Daniel, "Directivity of linear microstrip arrays," *Electronics Letters*, pp. 897-899, vol. 23, no. 17, Aug. 1987.
- [3] W. L. Stutzman and G. A. Thiele, *Antenna Theory and Design*, 3rd ed., John Wiley and Sons, Inc., New York, NY, 2012.
- [4] R. C. Hansen, *Phased Array Antennas*, John Wiley and Sons, Inc., New York, NY, 1998.
- [5] J. Ramsay, "Highlights of antenna history," *IEEE Ant. Prop. Society Newsletter*, Vol. 6, pp. 8-20, Dec. 1981.
- [6] L. Josefsson and P. Persson, *Conformal Array Antenna Theory and Design*, John Wiley and Sons, Ltd., Hoboken, New Jersey, 2006.
- [7] Carl B. Dietrich, Jr., Warren L. Stutzman, Byung-Ki Kim and Kai Dietze, "Smart Antennas in Wireless Communications: Base-Station Diversity and Handset Beamforming," *IEEE Antennas and Propagation Magazine*, Vol. 42, No. 5, October 2000.
- [8] Panayiotis Ioannides and C. A. Balanis, "Uniform Circular Arrays for Smart Antennas," *IEEE Antennas and Propagation Magazine*, Vol. 47, No. 4, Aug. 2005.
- [9] Michael Chryssomallis, "Smart Antennas," *IEEE Antennas and Propagation Magazine*, Vol. 42, No. 3, June 2000.

- [10] V. Kalinichev, "Analysis of Beam-Steering and Directive Characteristics of Adaptive Antenna Arrays for Mobile Communications," *IEEE Antennas and Propagation Magazine*, Vol. 42, No. 3, June 2001.
- [11] <http://www.dtic.mil/cgi-bin/GetTRDoc?Location=U2/744630.pdf>
- [12] "Special Issue on Conformal Arrays," *IEEE Transactions on Antennas and Propagation*, Vol. AP-22, No.1, Jan. 1974.
- [13] E. Lier, D. Purdy and G. Kautz, US Patent 6163296, "Calibration and integrated beam control / conditioning system for phased-array antennas," Dec. 19, 2000.
- [14] E. Lier, D. Purdy, J. Ashe and G. Kautz, "An On-Board Integrated Beam Conditioning System for Active Phased Array Satellite Antennas," *2000 IEEE Intern. Conf. on Phased Array Systems and Technol.*, May 21-25 2000, Dana Point, CA , pp. 509 - 512.
- [15] D. Purdy, J. Ashe, E. Lier, US Patent: 2002/0171583 A1, "System and Method for Efficiently Characterizing the Elements in an Array Antenna," Nov. 21, 2002.
- [16] E. Lier, M. Zemlyansky, D. Purdy and D. Farina, "Phased array calibration and characterization based on orthogonal coding: Theory and experimental validation," *2010 IEEE Intern. Sympos. on Phased Array Systems and Technol. (ARRAY)*, pp. 271 - 278, Oct. 12 - 15, 2010.
- [17] H. Schippers, G. Spalluto and G. Vos, "Radiation analysis of conformal phased array antennas on distorted structures," *12th International Conference on Antennas and Propagation (ICAP 2003)*, Mar. 31 - Apr. 3, 2003, pp. 160-163.
- [18] H. Schippers, J. Verpoorte, P. Jorna, A. Hulzinga, A. Meijerink, C. Roeloffzen, R. G. Heideman, A. Leinse and M. Wintels, "Conformal phased array with beam

- forming on airborne satellite communication," *International ITG Workshop on Smart Antennas*, 26-27 Feb. 2008, pp. 343-350.
- [19] H. Schippers, P. Knott, T. Deloues, P. Lacomme and M. R. Scherbarth, "Vibrating antennas and compensation techniques research in NATO/RTO/SET 087/RTG 50", *IEEE Aerospace Conference*, Mar. 3 - 10, 2007, pp. 1-13.
- [20] Davies D.E.N., "Circular arrays: Their properties and potential applications," *IEEE Proceedings of 2nd International Conference on Anetnnas and Propagation,,*, pp. 1-10, April 1981.
- [21] Knudsen H.L., "Bidrag till teorien for antennsystemer med hel eller delvis rotationssymmetri", Ph.D. Thesis, Teknisk Forlag, Copenhagen (in Danish), 1953.
- [22] Knudsen H.L., "The field radiated by a ring quasi-array of an infinite number of tangential or radial dipoles," *Proceedings of IRE*, Vol. 41, No. 6, June 1953, pp. 781-789.
- [23] Dorey J., Garnier G., and Auvray G. "RIAS, Synthetic Impulse and Antenna Radar," *International Conference on Radar*, Vol. Paris, April 24-28, 1989.
- [24] "Phased Array Radars in France: Present and Future," *IEEE International Symposium on Phased Array Systems and Technology*, Oct. 15-18, 1996.
- [25] *Proc. of 1st Europ. Workshop on Conformal Antennas*, Karlsruhe, Germany, 29 October 1999.
- [26] *Proc. of 2nd Europ. Workshop on Conformal Antennas*, Hague, Netherlands, April 24-25, 2001.

- [27] *Proc. of 3rd Europ. Workshop on Conformal Antennas*, Bonn, Germany, Oct. 22-23, 2003.
- [28] *Proc. of 4th Europ. Workshop on Conformal Antennas*, Stockholm, Sweden, May. 23-24, 2005.
- [29] *Proc. of 5th Europ. Workshop on Conformal Antennas*, Bristol, UK, Sept. 10-11, 2007.
- [30] *Proc. of 7th Europ. Workshop on Conformal Antennas*, Zagreb, Croatia, Oct. 6-7, 2011.
- [31] K. Wincza and S. Gruszcynski, "Influence of Curvature Radius on Radiation Patterns in Multibeam Conformal Antennas," *36th European Microw. Conf.*, vol., no., pp. 1410-1413, Sept. 10 - 15, 2006.
- [32] K. Wincza, S. Gruszcynski and K. Sachse, "Conformal four-beam antenna arrays with reduced sidelobes," *Electronics Letters*, pp. 174-175, vol. 44, no. 3, Jan. 2008.
- [33] Benjamin D. Braaten, S. Roy, Irfanullah, S. Nariyal, M. A. Aziz, Neil F. Chamberlain, Michael T. Reich and Dimitris E. Anagnostou, "A self-adapting flexible (SELFLEX) antenna array for changing conformal surface applications," *IEEE Transactions on Antennas and Propagation*, Vol. 99, No. 1, October 2012.
- [34] I. Chiba, K. Hariu, S. Sato and S. Mano, "A projection method providing low sidelobe pattern in conformal array antennas," *Proc. IEEE Antennas Propag. Soc. Int. Symp. Dig.*, Jun. 26 - 30, 1989.
- [35] Irfanullah, S. Nariyal, S. Roy, M. M. Masud, B. Ijaz, A. Iftikhar, , S. A. Naqvi and B. D. Braaten, "A note on the fundamental maixmum gain limit

of the projection method for conformal phased array antennas," Accepted for publication in the *IEEE Proceedings of International Conference on Wireless Information Technology and Systems (IEEE ICWITS 2012)*, Maui, Hawaii, Nov. 2012.

- [36] S. Nariyal, Irfanullah, S. A. Naqvi, B. Ijaz, M. M. Masud, B. Booth, K. Asirvatham and B. D. Braaten, "On the Use of Amplitude Tapering for Pattern Correction of Conformal (Curved) Antennas," Submitted for review in the *7th European Conference on Antennas and Propagation (EuCAP 2013)*, Gothenburg, Sweden, Apr. 2013.
- [37] R. W. P. King, *The Theory of Linear Antennas with Charts and Table for Practical Applications*, Harvard University Press, Cambridge, MA, 1956.
- [38] G. A. Deschamps, "Microstrip Microwave Antennas," presented at the *3rd USAF Symposium on Antennas*, 1953.
- [39] K. Finkenzeller, *RFID Handbook: Fundamentals and Applications in Contactless Smart Cards and Identification*, John Wiley and Sons, West Sussex, England, 2003.
- [40] Rai E., Nishimoto, S., Katada, T., and Watanabe, H. "Historical Overview of Phased Array Antenna for Defence Applications in Japan," *IEEE International Symposium on Phased Array Systems and Technology*, Oct. 15-18, 1996, pp.217-221.
- [41] Kanno M., Hashimura, T., Katada, T., Sato, M., Fukutani, K., and Suzuki, A., "Digital Beamforming for Conformal Active Array Antenna," *IEEE International Symposium on Phased Array Systems and Technology*, Oct. 15-18, 1996, pp.37-40.

- [42] Steyskal H. "Pattern Synthesis for a Conformal Wing Array," *IEEE Aerospace Conference Proceedings*, Vol. 2, 2002, pp.819-824.
- [43] Constantine A. Balanis, "Antenna Theory: Analysis and Design," John Wiley and Sons, Ltd., Hoboken, New Jersey, 2005.
- [44] J. C. Liberti and T. S. Rappaport, "Smart Antennas for Wireless Communications: IS-95 and Third Generation CDMA Applications," Prentice Hall PTR, 1999.
- [45] T. S. Rappaport, *Smart Antennas: Adaptive Arrays, Algorithms, and Wireless Position Location*, New York, IEEE Press, 1998.
- [46] R.E. Munson, "Conformal microstrip antennas and microstrip phased arrays," *IEEE Transactions on Antennas and Propagation*, Vol. 22, Issue 1, January 1974, pp. 74-78.
- [47] T.G. Campbell, "An extremely thin omnidirectional microwave antenna array for spacecraft applications," NASA Tech. Note D-5539, Nov. 1969.
- [48] R.B. Waterhouse, S.D. Targonski and D.M. Kokotoff, "Design and performance of small printed antennas," *IEEE Transactions on Antennas and Propagation*, Vol. 46, No. 11, November 1998.
- [49] A. Shackelford, K.F. Lee, D. Chatterjee, Y.X. Guo, K.M. Luk and R. Chair, "Small-size wide-bandwidth microstrip patch antennas," *IEEE Antennas and Propagation Society International Symposium, 2001*, Vol. 1, July 8-13, 2001, pp. 86-89.
- [50] I.J. Bahl and P. Bhartia "Microstrip Antennas," Artech House, Inc. Dedham, MA, 1980, p.214-215.

- [51] William Palm III, "Introduction to MATLAB 6 for Engineers," 1<sup>st</sup> Ed., McGraw-Hill, New York, NY, 2001, p. 419-505.
- [52] www.agilent.com.
- [53] P.L. O'Donovan and A.W. Rudge, "Adaptive control of a flexible linear array," *Electron. Lett.*, vol.9, no.6, pp.121-122, Mar. 22, 1973.
- [54] D. J. Chung, S. K. Bhattacharya, G. E. Ponchak and J. Papapolymerou, "An 8x8 lightweight flexible multilayer antenna array," *Proc. IEEE Antennas Propag. Soc. Int. Symp. Dig.*, June 1-5, 2009, Charleston, SC.
- [55] R. L. Haupt, *Antenna Arrays: A Computational Approach*, John Wiley and Sons, Ltd., Hoboken, New Jersey, 2010.
- [56] R. A. Monzingo, R. L. Haupt and T. W. Miller, "Introduction to Adaptive Arrays," SciTech, 2011.
- [57] S. Nikolaou, G. E. Ponchak, J. Papapolymerou and M. M. Tentzeris, "Conformal double exponentially tapered slot antenna (DETSA) on LCP or UWB applications," *IEEE Trans. on Antennas Propag.*, pp. 1663 - 1669, vol. 54, no. 6, Jun. 2006.
- [58] J. - L. Guo and J. - Y. Li, "Pattern synthesis of conformal array antenna in the presence of platform using differential evolution algorithm," *IEEE Trans. on Antennas Propag.*, pp. 2615 - 2621, vol. 57, no. 9, Sep. 2009.
- [59] M. A. Aziz, S. Roy, L. A. Berge, Irfanullah and B. D. Braaten, "A conformal CPW folded slot antenna array printed on a Kapton substrate," Accepted for publication in the *2012 European Conf. on Antennas Propag. (EuCAP)*, Prague, Czech. Republic, Mar. 2012.

- [60] R. H. Roy, "An overview of Smart Antenna Technology: The Next Wave in Wireless Communications," *IEEE Aerospace Conference*, pp. 339-345, Vol. 3, May 1998.
- [61] H. Krim and M. Viberg, "Two Decades of Array Signal Processing Research: The Parametric Approach," *IEEE Signal Process. Magazine*, pp. 67-94, July 1996.
- [62] International Engineering Consortium, Smart Antenna Systems, [online tutorial]  
<http://www.iec.org/>
- [63] J. - S. Roh, Y. - S. Chi, J. - H. Lee, Y. Tak, S. Nam and T. J. Kang, "Embroidered wearable multiresonant folded dipole antenna for RF reception," *IEEE Antennas Wireless Propag. Lett.*, pp. 803 - 806, vol. 9, 2010.
- [64] P. Jorna, H. Schippers and J. Verpoorte, "Beam synthesis for conformal array antennas with efficient tapering," *Proc. of 5th Europ. Workshop on Conformal Antennas*, Bristol, Sept. 11-12, 2007.
- [65] P. Knott, "Deformation and vibration of conformal antenna arrays and compensation techniques," *Meeting proc. RTO-MP-AVT-141*, paper 19, pp. 1-12, 2006.
- [66] T. J. Seidel, W. S. T. Rowe and K. Ghorbani, "Passive compensation of beam shift in a bending array," *Prog. in Electrom. Research*, vol. 29, pp. 41-53, 2012.
- [67] Rogers Corporation, [online] [www.rogerscorp.com](http://www.rogerscorp.com).
- [68] Advanced Design System (ADS) by Agilent Technologies, [online] [www.agilent.com](http://www.agilent.com).
- [69] Federal Communications Commission, [online] [www.fcc.gov](http://www.fcc.gov).
- [70] Ansys Inc., Ansoft HFSS, Version 13.0.1, [online] [www.ansoft.com](http://www.ansoft.com)

- [71] C. A. Balanis, *Antenna Theory: Analysis and Design*, 3rd Ed., John Wiley and Sons, Hoboken, NJ, 2005, pp. 945-995.
- [72] A. J. Lockyer, K. H. Alt, D. P. Coughlin, M. D. Durham, J. N. Kudva, A. C. Goets and J. Tuss, "Design and developement of a conformal load-bearing smart skin antenna: overview of the AFRL smart skin structure technology demonstration (S3TD)", *Proc. SPIE 3674, Smart Structures and Materials 1999: Industrial and Commercial Applications of Smart Structures Technologies*, 410 Jul. 9, 1999,
- [73] S. Bellofiore, C. A. Balanis, J. Foutz and A. S. Spanias, "Smart-antenna systems for mobile communicaiton networks part 1: overview and antenna design," *IEEE Antennas and Propaga. Mag.*, vol. 44, no. 3, Apr. 15, 2003, pp. 145-154.
- [74] C. A. Balanis, "Smart antennas for future reconfigurable wireless communication networks," *IEEE Topical Conf. on Wireless Comm. Tech.*, Oct. 15-17, 2003, pp. 181-182.
- [75] A. J. Lockyer, K. H. Alt, R. W. Kinslow, H.-P. Kan, J. N. Kudva, J. Tuess and A. C. D. P. Coughlin, M. D. Durham, J. N. Kudva, A. C. Goets and J. Tuss, "Development of a structurally integrated conformal load-bearing multifunction antenna: overview of the Air Force Smart Skin Structures Technology Demonstration Program," *Proc. SPIE 2722, Smart Structures and Materials 1996: Smart Electronics and MEMS*, 55 May 20, 1996.
- [76] V. K. Varadan and V. V. Varadan, "Design and development of conformal smart spiral antenna," *Proc. SPIE 2722, Smart Structures and Materials 1996: Smart Electronics and MEMS* 46 May 20, 1996.

- [77] M. Beneditti, R. Azaro and A. Massa, "Experimental validation of full-adaptive smart antenna prototype," *Elec. Lett.*, vol. 44, no 11, May 22, 2008, pp. 661-662.
- [78] T. Ohira, "Electronically steerable passive array radiator antennas for low-cost analog adaptive beamforming," *2000 IEEE Int. Conf. on Phased Array Sys. and Tech.*, May 21-25, 2000, pp. 101-104.
- [79] A. J. Lockyer, K. H. Alt, R. W. Kinslow, H.-P. Kan, J. N. Kudva, J. Tuess and A. C. D. P. Coughlin, M. D. Durham, J. N. Kudva, A. C. Goets and J. Tuss, "Development of a structurally integrated conformal load-bearing multifunction antenna: overview of the Air Force Smart Skin Structures Technology Demonstration Program," *Proc. SPIE 2722, Smart Structures and Materials 1996: Smart Electronics and MEMS*, 55 May 20, 1996.
- [80] S. Choi and D. Shim, "A novel adaptive beamforming algorithm for a smart antenna system in a CDMA mobile communication environment," *IEEE Trans. on Vehicular Tech.*, vol. 49, no. 5, Aug. 2002, pp. 1793-1806.
- [81] H. Schippers, J. Verpoorte, P. Jorna, A. Hulzinga, A. Meijerink, C. Roeloffzen, R. G. Heideman, A. Leinse and M. Wintels, "Conformal phased array with beamforming on airborne satellite communication," *International ITG Workshop on Smart Antennas*, 26-27 Feb. 2008, pp. 343-350.
- [82] H. Schippers, G. Spalluto and G. Vos, "Radiation analysis of conformal phased array antennas on distorted structures," *12th International Conference on Antennas and Propagation (ICAP 2003)*, Mar. 31 - Apr. 3, 2003, pp. 160-163.
- [83] H. Schippers, P. Knott, T. Deloues, P. Lacomme and M. R. Scherbarth, "Vibrating antennas and compensation techniques research in NATO/RTO/SET 087/RTG 50", *IEEE Aerospace Conference*, Mar. 3 - 10, 2007, pp. 1-13.

- [84] P. Knott, "Deformation and vibration of conformal antenna arrays and compensation techniques," *Meeting proc. RTO-MP-AVT-141*, paper 19, pp. 1-12, 2006.
- [85] B. D. Braaten, M. A. Aziz, S. Roy, S. Nariyal, I. Irfanullah, N. F. Chamberlain, M. T. Reich and D. E. Anagnostou, "A Self-Adapting Flexible (SELFLEX) Antenna Array for Changing Conformal Surface Applications," *IEEE Trans. Antennas Propag.*, vol. 61, no. 2, Feb., 2013, pp. 655 - 665.
- [86] P. L. O'Donovan and A.W. Rudge, "Adaptive control of a flexible linear array," *Electron. Lett.*, vol.9, no.6, pp.121-122, Mar. 22, 1973.
- [87] J. - L. Guo and J. - Y. Li, "Pattern synthesis of conformal array antenna in the presence of platform using differential evolution algorithm," *EEE Trans. on Antennas Propag.*, pp. 2615 - 2621, vol. 57, no. 9, Sep. 2009.
- [88] Y. Wu, K. F. Warnick and C. Jin, "Design study of an L-band phased array feed for wide-field surveys and vibration compensation on FAST," *IEEE Trans. Antennas Propag.*, vol. 61, no. 6, Jun., 2013, pp. 3026 - 3033.
- [89] D. Purdy, J. Ashe, E. Lier, US Patent: 2002/0171583 A1, "System and Method for Efficiently Characterizing the Elements in an Array Antenna," Nov. 21, 2002.
- [90] P. Yang, F. Yang, Z.-P. Nie, B. Li, and X. Tang, "Robust adaptive beamformer using interpolation technique for conformal antenna array," *Progress In Electromagnetics Research B*, vol. 23, pp. 215-228, 2010.
- [91] T. J. Seidel, W. S. T. Rowe and K. Ghorbani, "Passive compensation of beam shift in a bending array," *Prog. in Electrom. Research*, vol. 29, pp. 41-53, 2012.
- [92] P. Salonen, Y. Rahmat-Samii, M. Schaffrath, and M. Kivikoski, "Effect of textile materials on wearable antenna performance: A case study of GPS antennas," in *Proc. IEEE Antennas Propag. Soc. Int. Symp.*, 2004, vol. 1, pp. 459-462.

- [93] I. J. Gupta and A. A. Ksieński, "Effect of mutual coupling on the performance of adaptive arrays," *IEEE Trans. on Antennas and Propaga.*, vol. 31, no. 5, Sep. 1983, pp. 785-791.
- [94] Ansys Inc., Ansoft HFSS, Version 13.0.1, [online] [www.ansoft.com](http://www.ansoft.com)
- [95] Hittite Microwave Corporation, [online] [www.hittite.com](http://www.hittite.com).
- [96] Mini-Circuits [Online]. Available: [www.minicircuits.com](http://www.minicircuits.com)

## APPENDIX A. ARRAY WEIGHTS FOR THE RESULTS IN FIGURES 27-32.

The following tables summarize the array weights for the results in Figures 27-32.

Table 2. Array weights of the conformal antenna on the wedge-shaped surface with  $\theta_b = 30^\circ$  without coupling using (4.17).

Pattern 1 weights	Pattern 2 weights
$w_{-2} = 0.9849\angle 128.76^\circ$	$w_{-2} = 0.3113\angle -72.72^\circ$
$w_{-1} = 0.2119\angle -75.85^\circ$	$w_{-1} = 0.5637\angle 135.57^\circ$
$w_1 = 1\angle 35.24^\circ$	$w_1 = 1\angle -2.34^\circ$
$w_2 = 0.5961\angle -174.73^\circ$	$w_2 = 0.8440\angle -78.45^\circ$

Table 3. Array weights of the conformal antenna on the wedge-shaped surface with  $\theta_b = 30^\circ$  with coupling using (6.9).

Pattern 1 weights	Pattern 2 weights
$w_{-2} = 0.9621\angle 88.34^\circ$	$w_{-2} = 0.3550\angle -112.26^\circ$
$w_{-1} = 0.2626\angle -108.76^\circ$	$w_{-1} = 0.6054\angle 91.65^\circ$
$w_1 = 1\angle -8.08^\circ$	$w_1 = 1\angle -39.52^\circ$
$w_2 = 0.6464\angle 146.62^\circ$	$w_2 = 0.8424\angle -124.08^\circ$

Table 4. Array weights of the conformal antenna on the wedge-shaped surface with  $\theta_b = 45^\circ$  without coupling using (4.17).

Pattern 1 weights	Pattern 2 weights
$w_{-2} = 1\angle -153.99^\circ$	$w_{-2} = 0.2619\angle -14.85^\circ$
$w_{-1} = 0.7462\angle -31.91^\circ$	$w_{-1} = 0.2619\angle 165.14^\circ$
$w_1 = 0.6266\angle 65.59^\circ$	$w_1 = 1\angle 39.57^\circ$
$w_2 = 0.5222\angle -107.08^\circ$	$w_2 = 0.8801\angle -16.86^\circ$

Table 5. Array weights of the conformal antenna on the wedge-shaped surface with  $\theta_b = 45^\circ$  with coupling using (6.9).

Pattern 1 weights	Pattern 2 weights
$w_{-2} = 1\angle -155.04^\circ$	$w_{-2} = 0.3440\angle -15.79^\circ$
$w_{-1} = 0.4090\angle -56.29^\circ$	$w_{-1} = 0.1426\angle 121.26^\circ$
$w_1 = 0.2436\angle 55.72^\circ$	$w_1 = 0.1754\angle 20.97^\circ$
$w_2 = 0.5353\angle -116.44^\circ$	$w_2 = 1\angle -28.94^\circ$

Table 6. Array weights of the conformal antenna on the cylindrical surface with  $r = 10$  cm without coupling using (4.17).

Pattern 1 weights	Pattern 2 weights
$w_{-2} = 0.9537\angle 48.27^\circ$	$w_{-2} = 0.5309\angle -133.55^\circ$
$w_{-1} = 0.2258\angle 38.35^\circ$	$w_{-1} = 0.8599\angle 83.89^\circ$
$w_1 = 1\angle -7.36^\circ$	$w_1 = 0.9131\angle -51.41^\circ$
$w_2 = 0.6003\angle 110.01^\circ$	$w_2 = 1\angle -136.09^\circ$

Table 7. Array weights of the conformal antenna on the cylindrical surface with  $r = 10$  cm with coupling using (6.9).

Pattern 1 weights	Pattern 2 weights
$w_{-2} = 0.9751\angle 5.39^\circ$	$w_{-2} = 0.5924\angle 168.29^\circ$
$w_{-1} = 0.2665\angle 102.15^\circ$	$w_{-1} = 0.9428\angle 29.34^\circ$
$w_1 = 1\angle -75.79^\circ$	$w_1 = 1\angle -102.68^\circ$
$w_2 = 0.9325\angle 61.92^\circ$	$w_2 = 0.8889\angle 169.59^\circ$

## APPENDIX B. ARRAY FACTOR OF THE TWO-ELEMENT ADAPTIVE ARRAY IN FIGURE 11.

The following MATLAB code plots the result in Figure 12.

```
% Two-element linear adaptive beamforming Matlab code
clc
close all;
clear all;
format long
f = 2.45e9;
c = 3e8;
lambda = c/f;
N=2;
d = .5*lambda; % Number of array elements
k = 2*pi/lambda;
theta_SOI = 0*(pi/180); % Spacing between elements
theta_SNOI = 30*(pi/180);
theta_SOI = 0*(pi/180);
theta_SNOI = 30*(pi/180);
N1 = exp((-j*k*d/2)*sin(theta_SOI));
N2 = exp((-j*k*d/2)*sin(theta_SNOI));
P1 = exp((j*k*d/2)*sin(theta_SOI));
P2 = exp((j*k*d/2)*sin(theta_SNOI));
c1 = 1;
c2 = 0;
A = [N1,N2;P1,P2];
C = [c1;c2]';
X = C/A;
w1 = X(1);
w2 = X(2);
theta = 0:.005:pi/2;
psi1 = (-j*k*d/2).*sin(theta);
psi2 = (j*k*d/2).*sin(theta);
AF = w1.*exp(psi1) + w2.*exp(psi2);
AF_uncorr = sum(AF,1);
% AF_corrected = sum(B_corr,2);
plot(theta*180/pi,20*log10(abs(AF_uncorr))./max(abs(AF_uncorr))), 'b', 'linewidth', 2;
%title('Linear Beamforming, SOI = 0 deg, SNOI = 30 deg');
% xlabel('theta(degrees)')
% xlabel('Observation angle (deg)')
ylabel('|AF(dB)|')
%axis([0 90 -50 0])
% hold on;
% plot(phi*180/pi,abs(AF_corrected)./max(abs(AF_corrected)), 'green', 'linewidth', 2);
% title('AF corrected');
% xlabel('phi(degrees)')
% ylabel('|AF corrected|')
grid on;
%%%%%%%%%%%%%
```

## APPENDIX C. FOUR-ELEMENT LINEAR ADAPTIVE BEAMFORMING.

The following MATLAB code plots the result in Figure 15.

```

patch_L =[

90 0.024144799      45 0.059491025      -1 0.079549623      -47 0.06966648
90 0.024144799      44 0.060579517      -2 0.079675862      -48 0.068674259
89 0.024202698      43 0.060974973      -3 0.079920744      -49 0.067274731
88 0.025460208      42 0.062181954      -4 0.080248813      -50 0.066246732
87 0.025842421      41 0.062499298      -5 0.080436976      -51 0.064659087
86 0.027003252      40 0.063711515      -6 0.080878403      -52 0.063814266
85 0.027086285      39 0.064249284      -7 0.081102171      -53 0.061993099
84 0.02827785      38 0.065476714      -8 0.081383502      -54 0.061131115
83 0.028604263      37 0.065858084      -9 0.081495407      -55 0.059305228
82 0.029686525      36 0.066973941      -10 0.081558238     -56 0.058723802
81 0.030022325      35 0.067451748      -11 0.081582968     -57 0.057232522
80 0.031326955      34 0.068270078      -12 0.080909581     -58 0.056433756
79 0.03160479      33 0.068873615      -13 0.08084502      -59 0.055095527
78 0.032650428      32 0.06983245      -14 0.080991533     -60 0.054279074
77 0.033100665      31 0.070235433      -15 0.080803691     -61 0.053109335
76 0.034192131      30 0.070705539      -16 0.080601674     -62 0.053059373
75 0.034437357      29 0.071099259      -17 0.080335719     -63 0.051562675
74 0.035580972      28 0.071792151      -18 0.079938881     -64 0.050502174
73 0.03593466      27 0.072064347      -19 0.080503846     -65 0.049172733
72 0.037321      26 0.072792515      -20 0.080525703     -66 0.048598564
71 0.037702915      25 0.073158474      -21 0.079994477     -67 0.047001807
70 0.038814349      24 0.073600734      -22 0.079575728     -68 0.046038091
69 0.039466396      23 0.074114877      -23 0.07935873     -69 0.044832706
68 0.040615662      22 0.074451753      -24 0.078987676     -70 0.043953753
67 0.040615662      21 0.074680142      -25 0.078824983     -71 0.042776597
66 0.042476821      20 0.074977095      -26 0.078505742     -72 0.041687643
65 0.042783566      19 0.075218798      -27 0.078491266     -73 0.040777002
64 0.044163537      18 0.075309892      -28 0.078120014     -74 0.03963423
63 0.044611412      17 0.075624082      -29 0.077997325     -75 0.038679914
62 0.046088218      16 0.075713093      -30 0.077385804     -76 0.037789898
61 0.046288318      15 0.075689451      -31 0.077311896     -77 0.036467342
60 0.047646567      14 0.075987287      -32 0.076928788     -78 0.035774145
59 0.04779875      13 0.07599516      -33 0.076902185     -79 0.034657647
58 0.04908691      12 0.076245802      -34 0.076584109     -80 0.033890048
57 0.049477331      11 0.07625589     -35 0.076328016     -81 0.032423642
56 0.050550611      10 0.076442222      -36 0.076082693     -82 0.031534522
55 0.050943974      9 0.076761236      -37 0.076115779     -83 0.030522441
54 0.052210827      8 0.0768153      -38 0.075605604     -84 0.029431902
53 0.052682467      7 0.077209686      -39 0.075518667     -85 0.028543507
52 0.053998819      6 0.077446193      -40 0.07481973     -86 0.027518828
51 0.054350309      5 0.077973986      -41 0.074784142     -87 0.026507558
50 0.055719146      4 0.077996139      -42 0.074027881     -88 0.025561485
49 0.05613478      3 0.078266176      -43 0.073523388     -89 0.024970803
48 0.057416637      2 0.078524608      -44 0.072886041     -90 0.024341084
47 0.057763169      1 0.078770171      -45 0.071966474
46 0.058954634      0 0.079278325      -46 0.070879909
];

```

```

flat_case2_meas = [
45 0.002958658      -1 0.011719287      -47 0.037833048
90 0.004176841      44 0.002823405      -2 0.011059824      -48 0.036904566
89 0.004428091      43 0.002771293      -3 0.010228608      -49 0.036519417
88 0.004925039      42 0.002779514      -4 0.009219035      -50 0.034214551
87 0.005230579      41 0.002938561      -5 0.008281623      -51 0.033011087
86 0.005451382      40 0.003217482      -6 0.007342474      -52 0.031462827
85 0.00571653       39 0.003959221      -7 0.006459517      -53 0.03062015
84 0.005974008      38 0.004151317      -8 0.006254719      -54 0.029297466
83 0.006476511      37 0.004726628      -9 0.006594921      -55 0.028272739
82 0.006528059      36 0.00467064     -10 0.007623901      -56 0.027004954
81 0.006713558      35 0.005465118      -11 0.009001702      -57 0.02610238
80 0.007042773      34 0.005601592      -12 0.010873614      -58 0.024999088
79 0.007065169      33 0.006424173      -13 0.013046768      -59 0.02404854
78 0.007059268      32 0.006373272      -14 0.015339251      -60 0.023016938
77 0.007406107      31 0.006588426      -15 0.017570484      -61 0.021717568
76 0.007371889      30 0.006971204      -16 0.020069086      -62 0.021118947
75 0.007693568      29 0.006985498      -17 0.022619093      -63 0.020017596
74 0.007569094      28 0.006610779      -18 0.024813856      -64 0.019038579
73 0.007500692      27 0.0066680981     -19 0.027323744      -65 0.018331378
72 0.007630044      26 0.006489406      -20 0.029548038      -66 0.017459813
71 0.007730213      25 0.005645648      -21 0.031611005      -67 0.016519591
70 0.007798932      24 0.005582324      -22 0.033862644      -68 0.015740348
69 0.007891736      23 0.005108217      -23 0.035837158      -69 0.01479844
68 0.00779716       22 0.00428802      -24 0.037267648      -70 0.014052392
67 0.007710387      21 0.003681107      -25 0.039581443      -71 0.0132248
66 0.007736525      20 0.002213897      -26 0.041000533      -72 0.012538362
65 0.007762983      19 0.002068933      -27 0.042601301      -73 0.01194036
64 0.007702506      18 0.001804576      -28 0.043525737      -74 0.011462586
63 0.007701099      17 0.0011109036     -29 0.044601749      -75 0.010692009
62 0.007413842      16 0.002314823      -30 0.044884835      -76 0.01010407
61 0.007311047      15 0.003080714      -31 0.046509278      -77 0.009644152
60 0.007601069      14 0.004397075      -32 0.046735652      -78 0.008964489
59 0.006943238      13 0.005246818      -33 0.046909374      -79 0.008487271
58 0.006790176      12 0.00641813      -34 0.047263319      -80 0.007924145
57 0.006601613      11 0.007561151      -35 0.046458055      -81 0.007568791
56 0.006457391      10 0.008655401      -36 0.046722483      -82 0.007302031
55 0.00605359       9 0.009554146      -37 0.046571156      -83 0.006777906
54 0.005802025      8 0.010558906      -38 0.04653094      -84 0.006512075
53 0.005363554      7 0.011190835      -39 0.0460037      -85 0.006248755
52 0.005089504      6 0.011948117      -40 0.045481931      -86 0.005870863
51 0.004783626      5 0.012271322      -41 0.044695678      -87 0.005584268
50 0.004428172      4 0.012666064      -42 0.043229388      -88 0.005326073
49 0.004044494      3 0.012854754      -43 0.042854284      -89 0.005191894
48 0.003725093      2 0.012824353      -44 0.040957671      -90 0.004866533
47 0.003537821      1 0.012731188      -45 0.040478147
46 0.003024429      0 0.012226641      -46 0.039339298
];

```

flat_case2_sim = [	-9.20E+01 -2.24E+01	-3.00E+00 -9.26E+00	8.60E+01 -2.07E+01
-1.80E+02 -1.91E+01	-9.10E+01 -2.81E+01	-2.00E+00 -9.39E+00	8.70E+01 -2.31E+01
-1.79E+02 -1.82E+01	-9.00E+01 -5.00E+01	-1.00E+00 -9.63E+00	8.80E+01 -2.66E+01
-1.78E+02 -1.75E+01	-8.90E+01 -2.80E+01	0.00E+00 -9.97E+00	8.90E+01 -3.27E+01
-1.77E+02 -1.69E+01	-8.80E+01 -2.20E+01	1.00E+00 -1.04E+01	9.00E+01 -5.00E+01
-1.76E+02 -1.64E+01	-8.70E+01 -1.86E+01	2.00E+00 -1.11E+01	9.10E+01 -3.22E+01
-1.75E+02 -1.61E+01	-8.60E+01 -1.62E+01	3.00E+00 -1.19E+01	9.20E+01 -2.65E+01
-1.74E+02 -1.59E+01	-8.50E+01 -1.46E+01	4.00E+00 -1.28E+01	9.30E+01 -2.33E+01
-1.73E+02 -1.57E+01	-8.40E+01 -1.33E+01	5.00E+00 -1.42E+01	9.40E+01 -2.12E+01
-1.72E+02 -1.56E+01	-8.30E+01 -1.23E+01	6.00E+00 -1.60E+01	9.50E+01 -1.97E+01
-1.71E+02 -1.56E+01	-8.20E+01 -1.15E+01	7.00E+00 -1.84E+01	9.60E+01 -1.86E+01
-1.70E+02 -1.57E+01	-8.10E+01 -1.09E+01	8.00E+00 -2.21E+01	9.70E+01 -1.78E+01
-1.69E+02 -1.59E+01	-8.00E+01 -1.04E+01	9.00E+00 -2.77E+01	9.80E+01 -1.71E+01
-1.68E+02 -1.62E+01	-7.90E+01 -9.95E+00	1.00E+01 -3.09E+01	9.90E+01 -1.66E+01
-1.67E+02 -1.65E+01	-7.80E+01 -9.62E+00	1.10E+01 -2.35E+01	1.00E+02 -1.62E+01
-1.66E+02 -1.69E+01	-7.70E+01 -9.36E+00	1.20E+01 -1.87E+01	1.01E+02 -1.59E+01
-1.65E+02 -1.74E+01	-7.60E+01 -9.15E+00	1.30E+01 -1.55E+01	1.02E+02 -1.58E+01
-1.64E+02 -1.80E+01	-7.50E+01 -8.99E+00	1.40E+01 -1.31E+01	1.03E+02 -1.54E+01
-1.63E+02 -1.87E+01	-7.40E+01 -8.88E+00	1.50E+01 -1.12E+01	1.04E+02 -1.52E+01
-1.62E+02 -1.95E+01	-7.30E+01 -8.80E+00	1.60E+01 -9.68E+00	1.05E+02 -1.51E+01
-1.61E+02 -2.04E+01	-7.20E+01 -8.76E+00	1.70E+01 -8.37E+00	1.06E+02 -1.49E+01
-1.60E+02 -2.14E+01	-7.10E+01 -8.75E+00	1.80E+01 -7.24E+00	1.07E+02 -1.48E+01
-1.59E+02 -2.26E+01	-7.00E+01 -8.78E+00	1.90E+01 -6.26E+00	1.08E+02 -1.47E+01
-1.58E+02 -2.39E+01	-6.90E+01 -8.83E+00	2.00E+01 -5.40E+00	1.09E+02 -1.46E+01
-1.57E+02 -2.53E+01	-6.80E+01 -8.91E+00	2.10E+01 -4.64E+00	1.10E+02 -1.46E+01
-1.56E+02 -2.67E+01	-6.70E+01 -9.03E+00	2.20E+01 -3.96E+00	1.11E+02 -1.45E+01
-1.55E+02 -2.78E+01	-6.60E+01 -9.18E+00	2.30E+01 -3.37E+00	1.12E+02 -1.45E+01
-1.54E+02 -2.83E+01	-6.50E+01 -9.35E+00	2.40E+01 -2.84E+00	1.13E+02 -1.44E+01
-1.53E+02 -2.80E+01	-6.40E+01 -9.57E+00	2.50E+01 -2.37E+00	1.14E+02 -1.44E+01
-1.52E+02 -2.71E+01	-6.30E+01 -9.81E+00	2.60E+01 -1.95E+00	1.15E+02 -1.43E+01
-1.51E+02 -2.60E+01	-6.20E+01 -1.01E+01	2.70E+01 -1.58E+00	1.16E+02 -1.43E+01
-1.50E+02 -2.49E+01	-6.10E+01 -1.04E+01	2.80E+01 -1.26E+00	1.17E+02 -1.43E+01
-1.49E+02 -2.38E+01	-6.00E+01 -1.08E+01	2.90E+01 -9.85E-01	1.18E+02 -1.42E+01
-1.48E+02 -2.29E+01	-5.90E+01 -1.12E+01	3.00E+01 -7.47E-01	1.19E+02 -1.42E+01
-1.47E+02 -2.21E+01	-5.80E+01 -1.17E+01	3.10E+01 -5.45E-01	1.20E+02 -1.42E+01
-1.46E+02 -2.15E+01	-5.70E+01 -1.22E+01	3.20E+01 -3.78E-01	1.21E+02 -1.41E+01
-1.45E+02 -2.09E+01	-5.60E+01 -1.28E+01	3.30E+01 -2.43E-01	1.22E+02 -1.41E+01
-1.44E+02 -2.05E+01	-5.50E+01 -1.35E+01	3.40E+01 -1.39E-01	1.23E+02 -1.40E+01
-1.43E+02 -2.01E+01	-5.40E+01 -1.42E+01	3.50E+01 -6.50E-02	1.24E+02 -1.40E+01
-1.42E+02 -1.98E+01	-5.30E+01 -1.51E+01	3.60E+01 -1.81E-02	1.25E+02 -1.39E+01
-1.41E+02 -1.96E+01	-5.20E+01 -1.61E+01	3.70E+01 2.52E-03	1.26E+02 -1.38E+01
-1.40E+02 -1.94E+01	-5.10E+01 -1.72E+01	3.80E+01 -1.77E-03	1.27E+02 -1.37E+01
-1.39E+02 -1.93E+01	-5.00E+01 -1.85E+01	3.90E+01 -2.99E-02	1.28E+02 -1.36E+01
-1.38E+02 -1.93E+01	-4.90E+01 -2.01E+01	4.00E+01 -8.07E-02	1.29E+02 -1.35E+01
-1.37E+02 -1.93E+01	-4.80E+01 -2.20E+01	4.10E+01 -1.53E-01	1.30E+02 -1.33E+01
-1.36E+02 -1.93E+01	-4.70E+01 -2.45E+01	4.20E+01 -2.46E-01	1.31E+02 -1.32E+01
-1.35E+02 -1.94E+01	-4.60E+01 -2.81E+01	4.30E+01 -3.59E-01	1.32E+02 -1.30E+01
-1.34E+02 -1.94E+01	-4.50E+01 -3.36E+01	4.40E+01 -4.91E-01	1.33E+02 -1.29E+01
-1.33E+02 -1.95E+01	-4.40E+01 -3.56E+01	4.50E+01 -6.41E-01	1.34E+02 -1.27E+01
-1.32E+02 -1.96E+01	-4.30E+01 -3.34E+01	4.60E+01 -8.09E-01	1.35E+02 -1.25E+01
-1.31E+02 -1.97E+01	-4.20E+01 -2.97E+01	4.70E+01 -9.94E-01	1.36E+02 -1.23E+01
-1.30E+02 -1.98E+01	-4.10E+01 -2.65E+01	4.80E+01 -1.19E+00	1.37E+02 -1.21E+01
-1.29E+02 -1.98E+01	-4.00E+01 -2.40E+01	4.90E+01 -1.41E+00	1.38E+02 -1.19E+01
-1.28E+02 -1.98E+01	-3.90E+01 -2.22E+01	5.00E+01 -1.64E+00	1.39E+02 -1.17E+01
-1.27E+02 -1.97E+01	-3.80E+01 -2.09E+01	5.10E+01 -1.88E+00	1.40E+02 -1.15E+01
-1.26E+02 -1.96E+01	-3.70E+01 -2.00E+01	5.20E+01 -2.14E+00	1.41E+02 -1.13E+01
-1.25E+02 -1.94E+01	-3.60E+01 -1.92E+01	5.30E+01 -2.41E+00	1.42E+02 -1.12E+01
-1.24E+02 -1.92E+01	-3.50E+01 -1.87E+01	5.40E+01 -2.69E+00	1.43E+02 -1.10E+01
-1.23E+02 -1.89E+01	-3.40E+01 -1.84E+01	5.50E+01 -2.99E+00	1.44E+02 -1.09E+01
-1.22E+02 -1.85E+01	-3.30E+01 -1.82E+01	5.60E+01 -3.29E+00	1.45E+02 -1.07E+01
-1.21E+02 -1.81E+01	-3.20E+01 -1.81E+01	5.70E+01 -3.61E+00	1.46E+02 -1.06E+01
-1.20E+02 -1.77E+01	-3.10E+01 -1.82E+01	5.80E+01 -3.93E+00	1.47E+02 -1.05E+01
-1.19E+02 -1.73E+01	-3.00E+01 -1.85E+01	5.90E+01 -4.26E+00	1.48E+02 -1.05E+01
-1.18E+02 -1.69E+01	-2.90E+01 -1.90E+01	6.00E+01 -4.61E+00	1.49E+02 -1.05E+01
-1.17E+02 -1.65E+01	-2.80E+01 -1.97E+01	6.10E+01 -4.96E+00	1.50E+02 -1.04E+01
-1.16E+02 -1.60E+01	-2.70E+01 -2.07E+01	6.20E+01 -5.31E+00	1.51E+02 -1.05E+01
-1.15E+02 -1.56E+01	-2.60E+01 -2.20E+01	6.30E+01 -5.68E+00	1.52E+02 -1.05E+01
-1.14E+02 -1.52E+01	-2.50E+01 -2.38E+01	6.40E+01 -6.06E+00	1.53E+02 -1.06E+01
-1.13E+02 -1.49E+01	-2.40E+01 -2.65E+01	6.50E+01 -6.44E+00	1.54E+02 -1.08E+01
-1.12E+02 -1.45E+01	-2.30E+01 -3.11E+01	6.60E+01 -6.82E+00	1.55E+02 -1.09E+01
-1.11E+02 -1.42E+01	-2.20E+01 -3.57E+01	6.70E+01 -7.22E+00	1.56E+02 -1.11E+01
-1.10E+02 -1.39E+01	-2.10E+01 -3.41E+01	6.80E+01 -7.62E+00	1.57E+02 -1.14E+01
-1.09E+02 -1.36E+01	-2.00E+01 -2.77E+01	6.90E+01 -8.03E+00	1.58E+02 -1.17E+01
-1.08E+02 -1.34E+01	-1.90E+01 -2.36E+01	7.00E+01 -8.45E+00	1.59E+02 -1.21E+01
-1.07E+02 -1.32E+01	-1.80E+01 -2.08E+01	7.10E+01 -8.88E+00	1.60E+02 -1.25E+01
-1.06E+02 -1.30E+01	-1.70E+01 -1.86E+01	7.20E+01 -9.32E+00	1.61E+02 -1.30E+01
-1.05E+02 -1.28E+01	-1.60E+01 -1.69E+01	7.30E+01 -9.77E+00	1.62E+02 -1.36E+01
-1.04E+02 -1.27E+01	-1.50E+01 -1.55E+01	7.40E+01 -1.02E+01	1.63E+02 -1.43E+01
-1.03E+02 -1.27E+01	-1.40E+01 -1.42E+01	7.50E+01 -1.07E+01	1.64E+02 -1.51E+01
-1.02E+02 -1.27E+01	-1.30E+01 -1.32E+01	7.60E+01 -1.12E+01	1.65E+02 -1.59E+01
-1.01E+02 -1.27E+01	-1.20E+01 -1.23E+01	7.70E+01 -1.18E+01	1.66E+02 -1.70E+01
-1.00E+02 -1.29E+01	-1.10E+01 -1.16E+01	7.80E+01 -1.23E+01	1.67E+02 -1.82E+01
-9.90E+01 -1.31E+01	-1.00E+01 -1.10E+01	7.90E+01 -1.29E+01	1.68E+02 -1.97E+01
-9.80E+01 -1.35E+01	-9.00E+00 -1.04E+01	8.00E+01 -1.36E+01	1.69E+02 -2.16E+01
-9.70E+01 -1.40E+01	-8.00E+00 -1.00E+01	8.10E+01 -1.44E+01	1.70E+02 -2.41E+01
-9.60E+01 -1.47E+01	-7.00E+00 -9.68E+00	8.20E+01 -1.52E+01	1.71E+02 -2.74E+01
-9.50E+01 -1.58E+01	-6.00E+00 -9.44E+00	8.30E+01 -1.62E+01	1.72E+02 -3.13E+01
-9.40E+01 -1.72E+01	-5.00E+00 -9.29E+00	8.40E+01 -1.74E+01	1.73E+02 -3.47E+01
-9.30E+01 -1.92E+01	-4.00E+00 -9.23E+00	8.50E+01 -1.88E+01	1.74E+02 -3.48E+01

```

1.76E+02 -3.00E+01           1.77E+02 -2.35E+01           1.79E+02 -2.02E+01       ];
1.76E+02 -2.60E+01           1.78E+02 -2.16E+01           1.80E+02 -1.91E+01

% patch_L = [ ] is the single patch pattern at 2.47 GHz from measurement. First column represents observation angles (from -90 to 90 degrees)
% and second column is the actual measurement data
% flat_case2_meas = [ ] is the measurement data of the four element linear array for case 2
% flat_case2_sim = [ ] is the simulation (ADS) data of the four element linear array for case 2
% Scanning of four element linear array using equations
close all;
clear all;
clc;
format long
N =4;
c = 3e8;
f = 2.47e9;
lambda = c/f;
d = lambda/2;
k = (2*pi)/lambda;
theta_b = 0*pi/180;
theta_s = 40*(pi/180); % Angle from x-axis = 90 deg or angle from z-axis = 0 deg
% Four elements antenna array
% Projections on wavefront
th0 = theta_s; %0*(pi/180);
th1 = -45*(pi/180); % -20*(pi/180); %receive angle
th2 = -25*(pi/180); %10*(pi/180); % first interferer angle
th3 = 10*(pi/180); %30*(pi/180); % second interferer angle
th4 = 25*(pi/180); %40*(pi/180); % third interferer angle
th_array = [th0 th1 th2 th3];

for m = 1:length(th_array)
    if th_array(m)<0
        th_pl(m) = theta_b-abs(th_array(m));
        th_pr(m) = -theta_b-abs(th_array(m));
    elseif th_array(m)>0
        th_pl(m) = theta_b+abs(th_array(m));
        th_pr(m) = -theta_b+abs(th_array(m));
    else
        %do nothing
    end
end
patch_L_norm = patch_L(:,2)/max(patch_L(:,2));
patch_L(:,2) = patch_L_norm; % Second column
patch_L(:,1) = filipud(patch_L(:,1)); % First column

% th_array = [th0 th1 th2 th3]*180/pi;
th_pl = th_pl*180/pi; % 40, -45, -25, 10
th_pr = th_pr*180/pi; % 40, -45, -25, 10

for n = 1:length(patch_L);
    if th_pl(1) == patch_L(n,1)
        el1 = patch_L(n,2);
        el2 = el1;
    else
        %do nothing
    end
end
for n = 1:length(patch_L);
    if th_pr(1) == patch_L(n,1)
        er3 = patch_L(n,2);
        er4 = er3;
    else
        %do nothing
    end
end
% Element pattern value at SOI = 40 deg
% el1 = 0.971750929679342;
% el2 = 0.971750929679342;
% er3 = 0.971750929679342;
% er4 = 0.971750929679342;
psi1_SOI = exp(-ij*k*(3*d/2)*sin(theta_b + th0))*el1; % Left element #1 on a wedge
psi2_SOI = exp(-ij*k*(d/2)*sin(theta_b + th0))*el2; % Left element #2 on a wedge
psi3_SOI = exp(-ij*k*(d/2)*sin(theta_b - th0))*er3; % Right element #3 on a wedge
psi4_SOI = exp(-ij*k*(3*d/2)*sin(theta_b - th0))*er4; % Right element #4 on a wedge
SOI = [psi1_SOI psi2_SOI psi3_SOI psi4_SOI]; % a

for n = 1:length(patch_L);
    if th_pl(2) == patch_L(n,1)
        el1 = patch_L(n,2);
        el2 = el1;
    else
        %do nothing
    end
end
for n = 1:length(patch_L);
    if th_pr(2) == patch_L(n,1)
        er3 = patch_L(n,2);
        er4 = er3;
    else
        %do nothing
    end
end

```

```

    end

% Element pattern value at SNOI = -45 deg
% el1 = 0.919028773260615;
% el2 = 0.919028773260615;
% er3 = 0.919028773260615;
% er4 = 0.919028773260615;
psi1_SNOI1 = exp(-ij*k*(3*d/2)*sin(theta_b + th1))*el1;
psi2_SNOI1 = exp(-ij*k*(d/2)*sin(theta_b + th1))*el2;
psi3_SNOI1 = exp(-ij*k*(d/2)*sin(theta_b - th1))*er3;
psi4_SNOI1 = exp(-ij*k*(3*d/2)*sin(theta_b - th1))*er4;
SNOI1 = [psi1_SNOI1 psi2_SNOI1 psi3_SNOI1 psi4_SNOI1.'];

for n = 1:length(patch_L);
    if th_pl(3) == patch_L(n,1)
        el1 = patch_L(n,2);
        el2 = el1;
    else
        %do nothing
    end
end
for n = 1:length(patch_L);
    if th_pr(3) == patch_L(n,1)
        er3 = patch_L(n,2);
        er4 = er3;
    else
        %do nothing
    end
end
% Element pattern value at SNOI = -45 deg
% el1 = 0.999696873004179;
% el2 = 0.999696873004179;
% er3 = 0.999696873004179;
% er4 = 0.999696873004179;
psi1_SNOI2 = exp(-ij*k*(3*d/2)*sin(theta_b + th2))*el1;
psi2_SNOI2 = exp(-ij*k*(d/2)*sin(theta_b + th2))*el2;
psi3_SNOI2 = exp(-ij*k*(d/2)*sin(theta_b - th2))*er3;
psi4_SNOI2 = exp(-ij*k*(3*d/2)*sin(theta_b - th2))*er4;
SNOI2 = [psi1_SNOI2 psi2_SNOI2 psi3_SNOI2 psi4_SNOI2.'];

tol = 0; % Not required for this case
for n = 1:length(patch_L);
    if th_pl(4)+tol == patch_L(n,1)
        el1 = patch_L(n,2);
        el2 = el1;
    else
        %do nothing
    end
end
for n = 1:length(patch_L);
    if th_pr(4)+tol == patch_L(n,1)
        er3 = patch_L(n,2);
        er4 = er3;
    else
        %do nothing
    end
end
% Element pattern value at SNOI = 10 deg
% el1 = 0.948553428455802;
% el2 = 0.948553428455802;
% er3 = 0.948553428455802;
% er4 = 0.948553428455802;
psi1_SNOI3 = exp(-ij*k*(3*d/2)*sin(theta_b + th3))*el1;
psi2_SNOI3 = exp(-ij*k*(d/2)*sin(theta_b + th3))*el2;
psi3_SNOI3 = exp(-ij*k*(d/2)*sin(theta_b - th3))*er3;
psi4_SNOI3 = exp(-ij*k*(3*d/2)*sin(theta_b - th3))*er4;
SNOI3 = [psi1_SNOI3 psi2_SNOI3 psi3_SNOI3 psi4_SNOI3.'];

% psai_SOI = exp(-ij*k*(3*d/2)*sin(theta_b + th0))*cos(th0 + theta_b); % Left element #1 on a wedge
% psi2_SOI = exp(-ij*k*(d/2)*sin(theta_b + th0))*cos(th0 + theta_b); % Left element #2 on a wedge
% psi3_SOI = exp(-ij*k*(d/2)*sin(theta_b - th0))*cos(th0 - theta_b); % Right element #3 on a wedge
% psi4_SOI = exp(-ij*k*(3*d/2)*sin(theta_b - th0))*cos(th0 - theta_b); % Right element #4 on a wedge
% SOI = [psai_SOI psi2_SOI psi3_SOI psi4_SOI.']; % a0
%
% psai_SNOI1 = exp(-ij*k*(3*d/2)*sin(theta_b + th1))*cos(th1 + theta_b);
% psi2_SNOI1 = exp(-ij*k*(d/2)*sin(theta_b + th1))*cos(th1 + theta_b);
% psi3_SNOI1 = exp(-ij*k*(d/2)*sin(theta_b - th1))*cos(th1 - theta_b);
% psi4_SNOI1 = exp(-ij*k*(3*d/2)*sin(theta_b - th1))*cos(th1 - theta_b);
% SNOI1 = [psai_SNOI1 psi2_SNOI1 psi3_SNOI1 psi4_SNOI1.']; % a1
%
% psai_SNOI2 = exp(-ij*k*(3*d/2)*sin(theta_b + th2))*cos(th2 + theta_b);
% psi2_SNOI2 = exp(-ij*k*(d/2)*sin(theta_b + th2))*cos(th2 + theta_b);
% psi3_SNOI2 = exp(-ij*k*(d/2)*sin(theta_b - th2))*cos(th2 - theta_b);
% psi4_SNOI2 = exp(-ij*k*(3*d/2)*sin(theta_b - th2))*cos(th2 - theta_b);
% SNOI2 = [psai_SNOI2 psi2_SNOI2 psi3_SNOI2 psi4_SNOI2.']; % a2
%
% psai_SNOI3 = exp(-ij*k*(3*d/2)*sin(theta_b + th3))*cos(th3 + theta_b);

```

```

% psi2_SNOI3 = exp(-ij*k*(d/2)*sin(theta_b + th3))*cos(th3 + theta_b);
% psi3_SNOI3 = exp(-ij*k*(d/2)*sin(theta_b - th3))*cos(th3 - theta_b);
% psi4_SNOI3 = exp(-ij*k*(3*d/2)*sin(theta_b - th3))*cos(th3 - theta_b);
% SNOI3 = [psi1_SNOI3 psi2_SNOI3 psi3_SNOI3 psi4_SNOI3]; % a3

A = [S01 SNOI1 SNOI2 SNOI3];
u = [1 0 0 0];
X0w1 = u\inv(A);
w = u/A;
w_mag_norm = abs(w)./max(abs(w));
w_mag_dB = 20*log10(w_mag_norm);
w_phase_deg = angle(w).*(180/pi);
% Array factor
theta = (pi/180)*(-90:1:90);
e_r = cos(theta - theta_b); % Element pattern for right 2 elements at theta = 45 deg from z-axis
e_l = cos(theta + theta_b); % Element pattern for left 2 elements at theta = -45 deg from z-axis
ui = sin(theta);
u2 = cos(theta);
x_n = [-3*d/2*cos(theta_b), -d/2*cos(theta_b), d/2*cos(theta_b), 3*d/2*cos(theta_b)];
z_n = [-3*d/2*sin(theta_b), d/2*sin(theta_b), d/2*sin(theta_b), 3*d/2*sin(theta_b)];

AP = w(1).*(patch_L_norm').*exp(j.*k.* (x_n(1).*u1 + z_n(1).*u2)) + ...
      w(2).* (patch_L_norm').*exp(j.*k.* (x_n(2).*u1 + z_n(2).*u2)) + ...
      w(3).* (patch_L_norm').*exp(j.*k.* (x_n(3).*u1 + z_n(3).*u2)) + ...
      w(4).* (patch_L_norm').*exp(j.*k.* (x_n(4).*u1 + z_n(4).*u2));

AP_norm = abs(AP)./max(abs(AP));
flat_case2_meas_norm = flat_case2_meas(:,2)./max(abs(flat_case2_meas(:,2)));
set(0,'DefaultAxesColorOrder',[0 0 0], ...
    'DefaultLineMarkerSize', 8, ...
    'DefaultAxesFontSize', 16, ...
    'DefaultTextFontSize', 16, ...
    'DefaultLineLineWidth', 2);
plot(theta*180/pi,20*log10(AP_norm),'k-');
hold on
plot(~flat_case2_meas(:,1),20*log10(flat_case2_meas_norm),'k.');
hold on
plot(flat_case2_sim(:,1),flat_case2_sim(:,2),'kx');
xlabel('theta (deg)');
ylabel('|E_{\phi}| (dB)')
axis([-90 90 -50 0])
legend('Analytical (without coupling)', 'Measured', 'ADS')

% th = -90:1:90;
% figure
% plot(th,20*log10(patch_L_norm))

```

## APPENDIX D. COMPLEX WEIGHTS FOR THE THREE-ELEMENT ARRAY ON THE WEDGE-SHAPED CONFORMAL SURFACE

The following MATLAB code plots the result in Figures 20-21.

```
% Effect of bend angles --- three elements antenna
close all;
clear all;
clc;
format short
N =3;
c = 3e8;
f = 2.47e9;
lambda = c/f;
d = lambda/2;
k = (2*pi)/lambda;
theta_b = (0:60)*pi/180;
theta_a = 40*(pi/180);
th0 = theta_a; %40*(pi/180); % SOI
th1 = -45*(pi/180); % -45*(pi/180); %receive angle
th2 = 10*(pi/180); %10*(pi/180); % first interferer angle
th22 = 10; % second interferer angle
th01 = 40;
th11 = -45;
th22 = 10;
theta_b1 = 0:60;
#####
% For SOI, SNOI = or > 0
for ii = 1:length(theta_b1)
if (th01 < theta_b1(ii))
psi1_SOI(ii) = exp(-ij.*k.*d).*sin(theta_b(ii) + th0).*cos(th0 + theta_b(ii));
psi2_SOI(ii) = exp(-ij.*k*(0).*sin(theta_b(ii) + th0)).*cos(th0);
psi3_SOI(ii) = exp(-ij.*k*(d).*sin(theta_b(ii) - th0)).*cos(th0 - theta_b(ii));
SOI1(:,ii) = [psi1_SOI(ii) psi2_SOI(ii) psi3_SOI(ii)].';
elseif (th01 > theta_b1(ii))
psi11_SOI(ii) = exp(-ij.*k.*(d).*sin(theta_b(ii) + th0)).*cos(th0 + theta_b(ii));
psi22_SOI(ii) = exp(-ij.*k*(0).*sin(theta_b(ii) + th0)).*cos(th0);
psi33_SOI(ii) = exp(1j.*k.*d).*sin(theta_b(ii) - abs(th0)).*cos(th0 - theta_b(ii));
SOI2(:,ii) = [psi11_SOI(ii) psi22_SOI(ii) psi33_SOI(ii)].';
else
end
end
end
SOI = [SOI2 SOI1(:,41:61,:)]; % a0
#####
% For SUI, SNOI < 0
for ii = 1:length(theta_b1)
if (abs(th1) <= theta_b1(ii))
psi1_SNOI1(ii) = exp(-ij.*k.*d).*sin(theta_b(ii) - abs(th1)).*cos(-abs(th1) + theta_b(ii));
psi2_SNOI1(ii) = exp(-ij.*k*(0).*sin(theta_b(ii) + abs(th1))).*cos(th1);
psi3_SNOI1(ii) = exp(-ij.*k*(d).*sin(theta_b(ii) + abs(th1))).*cos(-abs(th1) - theta_b(ii));
SNOI1_1(:,ii) = [psi1_SNOI1(ii) psi2_SNOI1(ii) psi3_SNOI1(ii)].';
elseif (abs(th1) > theta_b1(ii))
psi11_SNOI1(ii) = exp(1j.*k.*d).*sin(-theta_b(ii) + abs(th1)).*cos(-abs(th1) + theta_b(ii));
psi22_SNOI1(ii) = exp(-ij.*k*(0).*sin(theta_b(ii) + abs(th1))).*cos(th1);
psi33_SNOI1(ii) = exp(-ij.*k.*d).*sin(abs(th1) + theta_b(ii)).*cos(-abs(th1) - theta_b(ii));
SNOI1_2(:,ii) = [psi11_SNOI1(ii) psi22_SNOI1(ii) psi33_SNOI1(ii)].';
else
end
end
SNOI1 = [SNOI1_2 SNOI1_1(:,46:61,:)]; % a1
#####
% For SOI, SNOI = or > 0
for ii = 1:length(theta_b1)
if (th22 <= theta_b1(ii))
psi1_SOI2(ii) = exp(-ij.*k.*d).*sin(theta_b(ii) + th2).*cos(th2 + theta_b(ii));
psi2_SOI2(ii) = exp(-ij.*k*(0).*sin(theta_b(ii) + th2)).*cos(th2);
psi3_SOI2(ii) = exp(-ij.*k*(d).*sin(theta_b(ii) - th2)).*cos(th2 - theta_b(ii));
SNOI2_1(:,ii) = [psi1_SOI2(ii) psi2_SOI2(ii) psi3_SOI2(ii)].';
elseif (th22 > theta_b1(ii))
psi11_SOI2(ii) = exp(-ij.*k.*d).*sin(theta_b(ii) + th2).*cos(th2 + theta_b(ii));
psi22_SOI2(ii) = exp(-ij.*k*(0).*sin(theta_b(ii) + th2)).*cos(th2);
psi33_SOI2(ii) = exp(1j.*k.*d).*sin(theta_b(ii) - abs(th2)).*cos(theta_b(ii));
SNOI2_2(:,ii) = [psi11_SOI2(ii) psi22_SOI2(ii) psi33_SOI2(ii)].';
else
end
end
SNOI2 = [SNOI2_2 SNOI2_1(:,11:61,:)]; % a2
#####
u = [1 0 0];
```

```

for p = 1:length(theta_b1)
    A = [SOI(:,p) SHOI1(:,p) SHOI2(:,p)];
    w(:,p) = u/A; % For each bend angle the complex weights are stored in column vectors
    w_mag_norm(:,p) = abs(w(:,p))./max(abs(w(:,p)));
    w_mag_dB(:,p) = 20*log10(w_mag_norm(:,p));
    w_phase_deg(:,p) = angle(w(:,p)).*(180/pi);
end
set(0,'DefaultAxesColorOrder',[0 0 0], ...
    'DefaultLineMarkerSize', 8, ...
    'DefaultAxesFontSize', 16, ...
    'DefaultTextFontSize', 16, ...
    'DefaultLineLineWidth',2);
plot(theta_b1,w_mag_dB(1,:),'k-')
hold on
plot(theta_b1,w_mag_dB(2,:),'k--')
hold on
plot(theta_b1,w_mag_dB(3,:),'kx')
axis([0 60 -15 5])
xlabel('theta_b(deg)')
ylabel('Amplitude excitation(dB)')
legend('|w_{-1}|', '|w_0|', '|w_1|')
% Phase in degrees
figure
plot(theta_b1,w_phase_deg(1,:),'k-')
hold on
plot(theta_b1,w_phase_deg(2,:),'k--')
hold on
plot(theta_b1,w_phase_deg(3,:),'kx')
axis([0 60 -180 180])
xlabel('theta_b(deg)')
ylabel('Phase excitation(deg)')
legend('w^{\circ}_{-1}', 'w^{\circ}_0', 'w^{\circ}_1')

```

## APPENDIX E. COMPLEX WEIGHTS FOR THE THREE-ELEMENT ARRAY ON THE CYLINDRICAL-SHAPED CONFORMAL SURFACE

The following MATLAB code plots the result in Figures 22-23.

```
% Effect of various radius of curvature --- three elements antenna
close all;
clear all;
clc;
format short
H =3;
c = 3e8;
f = 2.47e9;
lambda = c/f;
d = lambda/2;
k = (2*pi)/lambda;
theta_s = 40*(pi/180);
th0 = theta_s; %40*(pi/180); %receive angle
th1 = -45*(pi/180); %45*(pi/180); % first interferer angle
th2 = 10*(pi/180); %10*(pi/180); % second interferer angle
r = (10:200).*1/100; % Radius of curvature varies from 10cm to 200cm
for ii = 1:length(r)
    theta1(ii) = d./r(ii);
    theta2(ii) = theta1(ii);
    phi1(ii) = pi/2 - theta1(ii);
    phi2(ii) = pi/2;
    phi3(ii) = phi1(ii);
    x_n1(ii) = -r(ii).*cos(phi3(ii));
    x_n2(ii) = 0;
    x_n3(ii) = -x_n1(ii);
    z_n1(ii) = r(ii).*sin(phi3(ii));
    z_n2(ii) = 0;
    z_n3(ii) = z_n1(ii);
    h_n1(ii) = sqrt((0-x_n1(ii))^2 + (r(ii)-z_n1(ii))^2);
    h_n2(ii) = 0;
    h_n3(ii) = h_n1(ii);
    phi_inv1(ii) = asin((r(ii)-z_n1(ii))./h_n1(ii));
    phi_inv2(ii) = 0;
    phi_inv3(ii) = phi_inv1(ii);
    phi_inv(ii,:) = [phi_inv1(ii) phi_inv2(ii) phi_inv3(ii)];
    theta_b = phi_inv; % First row contains 3 bend angles corresponding to r = 10cm,
%second row contains 3 bend angles corresponding to r = 11cm and so on; we have total 191 radii
end
%%%%%%%%%%%%%
% theta_s = 40 deg > theta_b
for ii = 1:length(r)
    if (th0 <= theta_b(ii,1))
        psi1_SOI(ii) = exp(-ij.*k.*h_n1(ii).*sin(theta_b(ii,1) + abs(th0))).*cos(pi/2-phi1(ii)+th0);
        psi2_SOI(ii) = exp(ij.*k.*h_n2(ii).*sin(theta_b(ii,2) + abs(th0))).*cos(th0);
        psi3_SOI(ii) = exp(-ij.*k.*h_n3(ii).*sin(theta_b(ii,3) - abs(th0))).*cos(pi/2-phi3(ii)-th0);
        SOI1(:,ii) = [psi1_SOI(ii) psi2_SOI(ii) psi3_SOI(ii).'];
    elseif (th0 > theta_b(ii,1))
        psi11_SOI(ii) = exp(-ij.*k.*h_n1(ii).*sin(theta_b(ii,1) + abs(th0))).*cos(pi/2-phi1(ii)+th0);
        psi22_SOI(ii) = exp(ij.*k.*h_n2(ii).*sin(theta_b(ii,2) + abs(th0))).*cos(th0);
        psi33_SOI(ii) = exp(ij.*k.*h_n3(ii).*sin(theta_b(ii,3) + abs(th0))).*cos(pi/2-phi3(ii)-th0);
        SOI2(:,ii) = [psi11_SOI(ii) psi22_SOI(ii) psi33_SOI(ii).'];
    else
    end
    end
    SOI = SOI2; % a0
% #####
% For |SNOI1| = 45 > theta_b
for ii = 1:length(r)
    if (abs(th1) <= theta_b(ii,1))
        ps11_SNOI1(ii) = exp(ij.*k.*h_n1(ii).*sin(theta_b(ii,1) - abs(th1))).*cos(pi/2-phi1(ii)+th1);
        ps12_SNOI1(ii) = exp(ij.*k.*h_n2(ii).*sin(theta_b(ii,2) + abs(th1))).*cos(th1);
        ps13_SNOI1(ii) = exp(-ij.*k.*h_n3(ii).*sin(theta_b(ii,3) + abs(th1))).*cos(pi/2-phi3(ii)-th1);
        SNOI1_1(:,ii) = [ps11_SNOI1(ii) ps12_SNOI1(ii) ps13_SNOI1(ii).'];
    elseif (abs(th1) > theta_b(ii,1))
        ps111_SNOI1(ii) = exp(ij.*k.*h_n1(ii).*sin(-theta_b(ii,1) + abs(th1))).*cos(pi/2-phi1(ii)+th1);
        ps122_SNOI1(ii) = exp(ij.*k.*h_n2(ii).*sin(theta_b(ii,2) + abs(th1))).*cos(th1);
        ps133_SNOI1(ii) = exp(-ij.*k.*h_n3(ii).*sin(theta_b(ii,3) + abs(th1))).*cos(pi/2-phi3(ii)-th1);
        SNOI1_2(:,ii) = [ps111_SNOI1(ii) ps122_SNOI1(ii) ps133_SNOI1(ii).'];
    else
    end
    end
    SNOI1 = SNOI1_2; % a1
% #####
% For SNOI2 = 10 < theta_b for r = 10 cm to 17 cm (8 rows)

```

```

for ii = 1:length(r)
    if (th2 <= theta_b(ii,1))
        psii1_SNOI2(ii) = exp(-ij.*k.*h_n1(ii).*sin(theta_b(ii,1) + abs(th2))).*cos(pi/2-phi1(ii)+th2);
        psii2_SNOI2(ii) = exp(ij.*k.*h_n2(ii).*sin(theta_b(ii,2) + abs(th2))).*cos(pi/2-phi2(ii)+th2);
        psii3_SNOI2(ii) = exp(-ij.*k.*h_n3(ii).*sin(theta_b(ii,3) - abs(th2))).*cos(pi/2-phi3(ii)-th2);
        SNOI2_1(:,ii) = [psii1_SNOI2(ii) psii2_SNOI2(ii) psii3_SNOI2(ii)].';
    elseif (th2 > theta_b(ii,1))
        psii1_SNOI2(ii) = exp(-ij.*k.*h_n1(ii).*sin(theta_b(ii,1) + abs(th2))).*cos(pi/2-phi1(ii)+th2);
        psii2_SNOI2(ii) = exp(ij.*k.*h_n2(ii).*sin(theta_b(ii,2) + abs(th2))).*cos(pi/2-phi2(ii)+th2);
        psii3_SNOI2(ii) = exp(-ij.*k.*h_n3(ii).*sin(theta_b(ii,3) - abs(th2))).*cos(pi/2-phi3(ii)-th2);
        SNOI2_1(:,ii) = [psii1_SNOI2(ii) psii2_SNOI2(ii) psii3_SNOI2(ii)].';
    else
        end
    end
    SNOI2 = [SNOI2_1 SNOI2_2(:,9:191,:)]; % a2
% #####%
u = [1 0 0];
r = 10:200;
for p = 1:length(r)
    A = [SOI(:,p) SNOI1(:,p) SNOI2(:,p)];
    w(:,p) = u/A; % For each radius of curvature the complex weights are stored in column vectors
    w_mag_norm(:,p) = abs(w(:,p))./max(abs(w(:,p)));
    w_mag_dB(:,p) = 20*log10(w_mag_norm(:,p));
    w_phase_deg(:,p) = angle(w(:,p)).*(180/pi);
end
set(0,'DefaultAxesColorOrder',[0 0 0], ...
    'DefaultLineMarkerSize', 8, ...
    'DefaultAxesFontSize', 16, ...
    'DefaultTextFontSize', 16, ...
    'DefaultLineWidth',2);
plot(r,w_mag_dB(:,1),'k-')
hold on
plot(r,w_mag_dB(2,:),'k--')
hold on
plot(r,w_mag_dB(3,:),'kx')
axis([10 200 -15 5])
xlabel('r(cm)')
ylabel('Amplitude excitation(dB)')
legend('|w_{-1}|', '|w_0|', '|w_1|')
% Phase in degrees
figure
plot(r,w_phase_deg(1,:),'k-')
hold on
plot(r,w_phase_deg(2,:),'k--')
hold on
plot(r,w_phase_deg(3,:),'kx')
axis([10 200 -180 180])
xlabel('r(cm)')
ylabel('Phase excitation(deg)')
legend('w^{\circ}_{-1}', 'w^{\circ}_0', 'w^{\circ}_1')

```

## APPENDIX F. PATTERN 1 BEAMFORMING RESULTS WITH $\theta_B = 30^\circ$ .

The following MATLAB code plots the result in Figure 27 for the four-element array on the wedge-shaped surface with  $\theta_b = 30^\circ$ .

```

corrected_case1_meas = [
46 0.015141212          -2 0.025519039          -50 0.004725773
44 0.014736793          -4 0.024029896          -52 0.005325033
90 0.006692691          -2 0.013725229          -6 0.022691967          -54 0.005720824
88 0.007080323          40 0.012895978          -8 0.020526933          -56 0.006349963
86 0.007819778          38 0.011460324          -10 0.018331675          -58 0.006861805
84 0.008373371          36 0.009798744          -12 0.0159553291         -60 0.00737798
82 0.009104818          34 0.008076701          -14 0.013460963          -62 0.007734741
80 0.009853097          32 0.005865916          -16 0.010942454          -64 0.00799933
78 0.010604021          30 0.003606596          -18 0.008517658          -66 0.008181294
76 0.010936999          28 0.0012849          -20 0.006436512          -68 0.008169831
74 0.011549337          26 0.002153772          -22 0.004832949          -70 0.008269471
72 0.012155138          24 0.004649697          -24 0.003640987          -72 0.00826517
70 0.0125841          22 0.007612913          -26 0.003410148          -74 0.008476529
68 0.013142217          20 0.010448968          -28 0.003863726          -76 0.00842451
66 0.013118707          18 0.013497526          -30 0.004389201          -78 0.0086779
64 0.013832338          16 0.016198968          -32 0.005051456          -80 0.008682349
62 0.014019421          14 0.01882764          -34 0.00555894          -82 0.008603541
60 0.014616701          12 0.021035553          -36 0.005688009          -84 0.008568125
58 0.014928607          10 0.023046018          -38 0.005711659          -86 0.008327717
56 0.015292193          8 0.024576311          -40 0.005252876          -88 0.008308542
54 0.015685211          6 0.025652349          -42 0.004897707          -90 0.008006422
52 0.015705626          4 0.026297819          -44 0.002845428
50 0.015956246          2 0.026375809          -46 0.002676564
48 0.015674528          0 0.026314212          -48 0.002688795

];
];

HFSS_case1 = [
-46 -21.97083271          -46 -2.193708998
-45 -22.54522392          -45 -0.136280144
-44 -22.51455999          2 -0.051121388
-43 -21.97126199          3 -0.005651171
-42 -21.15239973          4 0
-41 -20.732479173          5 -0.034528647
-40 -19.42797638          6 -0.109843691
-39 -18.69519262          7 -0.226820386
-38 -18.08662914          8 -0.386634319
-37 -17.60758505          9 -0.590803964
-36 -17.25817194          10 -0.841247113
-35 -17.0376506          11 -1.140355372
-34 -16.94631625          12 -1.491092673
-33 -16.98619946          13 -1.897126315
-32 -17.16104486          14 -2.363002821
-31 -17.47538711          15 -2.894386685
-30 -17.93187499          16 -3.498388752
-29 -18.52454103          17 -4.184024428
-28 -19.22308332          18 -4.962862204
-27 -19.94042093          19 -5.84995253
-26 -20.48549253          20 -6.865164015
-25 -20.56318086          21 -8.03507315
-24 -19.94866536          22 -9.395423741
-23 -18.71730073          23 -10.99327979
-22 -17.1578549          24 -12.88348287
-21 -15.52263885          25 -15.09247025
-20 -13.9456037          26 -17.43281007
-19 -12.47856373          27 -18.95736252
-18 -11.13718143          28 -18.32063149
-17 -9.907570532          29 -16.26530377
-16 -8.79085851          30 -14.08341923
-15 -7.773651145          31 -12.19112155
-14 -6.846384332          32 -10.60747615
-13 -6.000707742          33 -9.279985781
-12 -5.22941667          34 -8.15668442
-11 -4.526386833          35 -7.196854718
-10 -3.886435799          36 -6.36994717
-9 -3.305183688          37 -5.653025173
-8 -2.77892923          38 -5.028630059
-7 -2.304545201          39 -4.483240595
-6 -1.879392538          40 -4.006198759
-5 -1.501250903          41 -3.588961749
-4 -1.168263146          42 -3.224575823
-3 -0.878891369          43 -2.907300827
-2 -0.631882659          44 -2.632338025
-1 -0.426242966          45 -2.395629653
];
];

```

```

%close all;
clear all;
clc;
format short
N =4;
c = 3e8;
f = 2.47e9;
lambda = c/f;
d = lambda/2;
k = (2*pi)/lambda;
theta_b = 30*pi/180;
theta_s = 0*(pi/180);
% Four elements antenna array
% Projections on wavefront
th0 = theta_s; %0*(pi/180); %receive angle
th1 = -30*(pi/180); %-20*(pi/180); % first interferer angle
th2 = 30*(pi/180); %0*(pi/180); % second interferer angle
th3 = 40*(pi/180); %30*(pi/180); % third interferer angle
% For SOI, SNOI = 0
psi1_SOI = exp(-ij*k*(3*d/2)*sin(theta_b - abs(th0)))*cos(theta_b - abs(th0));
psi2_SOI = exp(-ij*k*(d/2)*sin(theta_b - abs(th0)))*cos(theta_b - abs(th0));
psi3_SOI = exp(-ij*k*(d/2)*sin(theta_b + abs(th0)))*cos(-abs(th0) - theta_b);
psi4_SOI = exp(-ij*k*(3*d/2)*sin(theta_b + abs(th0)))*cos(-abs(th0) - theta_b);
SOI = [psi1_SOI psi2_SOI psi3_SOI psi4_SOI].'; % a0
% For SOI, SNOI < 0
psi1_SNOI = exp(-ij*k*(3*d/2)*sin(theta_b - abs(th1)))*cos(theta_b - abs(th1));
psi2_SNOI = exp(-ij*k*(d/2)*sin(theta_b - abs(th1)))*cos(theta_b - abs(th1));
psi3_SNOI = exp(-ij*k*(d/2)*sin(theta_b + abs(th1)))*cos(-theta_b - abs(th1));
psi4_SNOI = exp(-ij*k*(3*d/2)*sin(theta_b + abs(th1)))*cos(-theta_b - abs(th1));
SNOI1 = [psi1_SNOI1 psi2_SNOI1 psi3_SNOI1 psi4_SNOI1].'; % a1
% For SOI, SNOI > 0
psi1_SNOI2 = exp(-ij*k*(3*d/2)*sin(theta_b + abs(th2)))*cos(theta_b + abs(th2));
psi2_SNOI2 = exp(-ij*k*(d/2)*sin(theta_b + abs(th2)))*cos(theta_b + abs(th2));
psi3_SNOI2 = exp(-ij*k*(d/2)*sin(theta_b - abs(th2)))*cos(-theta_b + abs(th2));
psi4_SNOI2 = exp(-ij*k*(3*d/2)*sin(theta_b - abs(th2)))*cos(-theta_b + abs(th2));
SNOI2 = [psi1_SNOI2 psi2_SNOI2 psi3_SNOI2 psi4_SNOI2].'; % a2
% For SOI, SNOI > 0
psi1_SNOI3 = exp(-ij*k*(3*d/2)*sin(theta_b + th3))*cos(abs(th3) + theta_b);
psi2_SNOI3 = exp(-ij*k*(d/2)*sin(theta_b + th3))*cos(abs(th3) + theta_b);
psi3_SNOI3 = exp(ij*k*(d/2)*sin(-theta_b + th3))*cos(abs(th3) - theta_b);
psi4_SNOI3 = exp(ij*k*(3*d/2)*sin(-theta_b + th3))*cos(abs(th3) - theta_b);
SNOI3 = [psi1_SNOI3 psi2_SNOI3 psi3_SNOI3 psi4_SNOI3].'; % a3
A = [SOI SNOI1 SNOI2 SNOI3];
u = [1 0 0 0];
%%%%%%%%%%%%%%%%%%%%%%%%%%%%%%%%%%%%%
u = u/A; % Weights with out including effect of mutual coupling
%%%%%%%%%%%%%%%%%%%%%%%%%%%%%%%%%%%%%
% Z parameters from HFSS
% Self Terms
Z11 = -7.045063-37.356893i;
% Mutual Terms
Z12 = -3.174079+2.976914i;
Z13 = -0.578495+0.547187i;
Z14 = 0.363317-0.010929i;
Z21 = Z12;
Z22 = Z12;
Z23 = 0.684065+0.205307i;
Z24 = -0.533723+0.461377i;
Z31 = Z13;
Z32 = Z23;
Z34 = -3.008657+3.121613i;
Z41 = Z14;
Z42 = Z24;
Z43 = Z34;
Z22 = Z11;
Z33 = Z11;
Z44 = Z11;
Z0 = 50;
Z = [Z11/Z0 Z12/Z0 Z13/Z0 Z14/Z0;Z21/Z0 Z22/Z0 Z23/Z0 Z24/Z0;Z31/Z0 Z32/Z0 Z33/Z0 Z34/Z0;Z41/Z0 Z42/Z0 Z43/Z0 Z44/Z0]; % Normalized Impedance Matrix
I = eye(4);
Zc = Z + I; %Normalized coupling matrix
Ac = Zc\A; %inv(Zc)*A;
wc = u/Ac;
% Weights with out mutual coupling
w_mag_norm = abs(w)./max(abs(w))
%w_mag_dB = 20*log10(w_mag_norm)
w_phase_deg = angle(w).*((180/pi))
% Weights including effect of mutual coupling
wc_mag_norm = abs(wc)./max(abs(wc))
%wc_mag_dB = 20*log10(wc_mag_norm)
wc_phase_deg = angle(wc).*((180/pi))
% Array factor
theta = (pi/180)*(-90:180:628:90);
e_r3 = cos(theta-theta_b); % Element pattern for right 2 elements at theta = 45 deg from z-axis
e_r4 = e_r3;
e_l1 = cos(theta+theta_b);
e_l2 = e_l1;
u1 = sin(theta);
u2 = cos(theta);
x_n = [-3*d/2*cos(theta_b),-d/2*cos(theta_b),d/2*cos(theta_b),3*d/2*cos(theta_b)];

```

```

z_n = -[3*d/2*sin(theta_b),d/2*sin(theta_b),d/2*sin(theta_b),3*d/2*sin(theta_b)];
figure
% No mutual coupling
AP = w(1).*e_11.*exp(j.*k.* (x_n(1).*u1 + z_n(1).*u2)) + ...
w(2).*e_12.*exp(j.*k.* (x_n(2).*u1 + z_n(2).*u2)) + ...
w(3).*e_13.*exp(j.*k.* (x_n(3).*u1 + z_n(3).*u2)) + ...
w(4).*e_14.*exp(j.*k.* (x_n(4).*u1 + z_n(4).*u2));
% Effects of mutual coupling
APc = wc(1).*e_11.*exp(j.*k.* (x_n(1).*u1 + z_n(1).*u2)) + ...
wc(2).*e_12.*exp(j.*k.* (x_n(2).*u1 + z_n(2).*u2)) + ...
wc(3).*e_13.*exp(j.*k.* (x_n(3).*u1 + z_n(3).*u2)) + ...
wc(4).*e_14.*exp(j.*k.* (x_n(4).*u1 + z_n(4).*u2));

AP_norm = abs(AP)./max(abs(AP));
APc_norm = abs(APc)./max(abs(APc));
corrected_norm_case1_mean = abs(corrected_case1_meas(:,2))./max((corrected_case1_meas(:,2)));
set(0,'DefaultAxesColorOrder',[0 0 0], ...
'DefaultLineMarkerSize', 8, ...
'DefaultAxesFontSize', 16, ...
'DefaultTextFontSize', 16, ...
'DefaultLineWidth',2);
plot(theta*180/pi,20*log10(AP_norm),'k-');
hold on
plot(theta*180/pi,20*log10(APc_norm),'k--');
hold on
plot(-corrected_case1_meas(:,1),20*log10(corrected_norm_case1_mean),'k.');
hold on
plot(-HFSS_case1(:,1),HFSS_case1(:,2),'kx');
xlabel('theta (deg)')
ylabel('|E_{phi}| (dB)')
axis([-90 90 -50 0])
legend('Analytical (without coupling)', 'Analytical (with coupling)', 'Measured', 'HFSS')

```

## APPENDIX G. PATTERN 2 BEAMFORMING RESULTS WITH $\theta_B = 30^\circ$ .

The following MATLAB code plots the result in Figure 28 for the four-element array on the wedge-shaped surface with  $\theta_b = 30^\circ$ .

```

corrected_case2_meas = [
    44 0.001157766   -4 0.006017846   -52 0.024469079
    42 0.0007837   -6 0.005531844   -54 0.023894853
    40 0.001302571   -8 0.00478087   -56 0.023225097
    38 0.00174356   -10 0.003888337   -58 0.022296355
    36 0.002254915   -12 0.002861724   -60 0.021420613
    34 0.002557885   -14 0.002288054   -62 0.020503092
    32 0.002722796   -16 0.00292005   -64 0.019305546
    30 0.002897831   -18 0.004322997   -66 0.018233178
    28 0.002892292   -20 0.006318996   -68 0.017502642
    26 0.002555009   -22 0.008365565   -70 0.016737769
    24 0.002392757   -24 0.010469019   -72 0.015929921
    22 0.001942776   -26 0.012672781   -74 0.015341722
    20 0.001165711   -28 0.014748917   -76 0.014746527
    18 0.000603597   -30 0.016527311   -78 0.014178994
    16 0.000326677   -32 0.018422544   -80 0.013317915
    14 0.001009476   -34 0.019996418   -82 0.01285356
    12 0.001921237   -36 0.021548117   -84 0.012027997
    10 0.002987791   -38 0.022778625   -86 0.011562143
    8 0.003765383   -40 0.023763395   -88 0.011094396
    6 0.004732502   -42 0.024377632   -90 0.010550721
    4 0.005396961   -44 0.024791144   ];
    2 0.005838472   -46 0.025069236
    0 0.006132657   -48 0.025065618
    -2 0.006338963   -50 0.024888825

HFSS_case2 = [
    -46 -0.022629242   0 -12.37960056   46 -18.34670297
    -45 -0.004194367   1 -12.01276087   47 -18.56777512
    -44 0   2 -11.74394681   48 -18.72762939
    -43 -0.010710838   3 -11.5656117   49 -18.80372198
    -42 -0.03703093   4 -11.47213876   50 -18.77860578
    -41 -0.079707043   5 -11.45953667   51 -18.64388046
    -40 -0.139532588   6 -11.52621109   52 -18.40226078
    -39 -0.217352273   7 -11.66780602   53 -18.08668455
    -38 -0.314067668   8 -11.88710544   54 -17.65691921
    -37 -0.430643892   9 -12.18398658   55 -17.19528632
    -36 -0.568117679   10 -12.56041688   56 -16.70309212
    -35 -0.727607122   11 -13.01948645   57 -16.19850311
    -34 -0.9001323459   12 -13.56546174   58 -16.69578035
    -33 -1.117585328   13 -14.20383126   59 -15.20540926
    -32 -1.350836076   14 -14.94127584   60 -14.73466006
    -31 -1.611664779   15 -15.78540708   61 -14.28826401
    -30 -1.901831915   16 -16.74391121   62 -13.86904226
    -29 -2.223300802   17 -17.82226112   63 -13.47842505
    -28 -2.578276357   18 -19.01811077   64 -13.11685364
    -27 -2.969253115   19 -20.30844866   65 -12.78407968
    -26 -3.399075178   20 -21.6232869   66 -12.47938324
    -25 -3.871011533   21 -22.80552148   67 -12.20172972
    -24 -4.388651385   22 -23.59824831   68 -11.94988219
    -23 -4.957025617   23 -23.76540391   69 -11.72248176
    -22 -5.580762247   24 -23.30920182   70 -11.51810528
    -21 -6.266285964   25 -22.46746869   71 -11.33530707
    -20 -7.021073096   26 -21.49546944   72 -11.17264904
    -19 -7.854172317   27 -20.54807133   73 -11.02872263
    -18 -8.776590844   28 -19.69363323   74 -10.90216447
    -17 -9.80170801   29 -18.95404313   75 -10.79166731
    -16 -10.9455607   30 -18.33074197   76 -10.69598715
    -15 -12.2264976   31 -17.81738181   77 -10.61394727
    -14 -13.66267982   32 -17.40532391   78 -10.54443959
    -13 -15.26294927   33 -17.0858548   79 -10.48642383
    -12 -16.99865498   34 -16.85097821   80 -10.43892478
    -11 -18.72960526   35 -16.69360253   81 -10.40102812
    -10 -20.08035399   36 -16.60747406   82 -10.3718751
    -9 -20.50567551   37 -16.58699907   83 -10.35065649
    -8 -19.87269208   38 -16.62700633   84 -10.3366063
    -7 -18.65680291   39 -16.72245965   85 -10.32899556
    -6 -17.33258792   40 -16.86810927   86 -10.32712662
    -5 -16.11511223   41 -17.05806191   87 -10.33032837
    -4 -15.06378637   42 -17.26524859   88 -10.3379526
    -3 -14.18017194   43 -17.54078293   89 -10.3493718
    -2 -13.44940526   44 -17.81324131   90 -10.36397864
    -1 -12.85431185   45 -18.08797579   ];

```

```

#####
%close all;
clear all;
clc;
format short
N =4;
c = 3e8;
f = 2.47e9;
lambda = c/f;
d = lambda/2;
k = (2*pi)/lambda;
theta_b = 30*(pi/180);
theta_s = 40*(pi/180); % Angle from x-axis = 90 deg or angle from z-axis = 0 deg
% Four elements antenna array
% Projections on wavefront
th0 = theta_s; %0*(pi/180); %receive angle
th1 = -45*(pi/180); %20*(pi/180); % first interferer angle
th2 = -25*(pi/180); %10*(pi/180); % second interferer angle
th3 = 10*(pi/180); %30*(pi/180); % third interferer angle

% For SOI, SNOI = or > 0
psi1_SOI = exp(-ij*k*(3*d/2)*sin(theta_b + th0))*cos(th0 + theta_b);
psi2_SOI = exp(-ij*k*(d/2)*sin(theta_b + th0))*cos(th0 + theta_b);
psi3_SOI = exp(1j*k*(d/2)*sin(-theta_b + th0))*cos(th0 - theta_b);
psi4_SOI = exp(1j*k*(3*d/2)*sin(-theta_b + th0))*cos(th0 - theta_b);
SOI = [psi1_SOI psi2_SOI psi3_SOI psi4_SOI].'; % a0
% For SNOI, SNOI < 0
psi1_SNOI1 = exp(1j*k*(3*d/2)*sin(-theta_b + abs(th1)))*cos(theta_b - abs(th1));
psi2_SNOI1 = exp(1j*k*(d/2)*sin(-theta_b + abs(th1)))*cos(theta_b - abs(th1));
psi3_SNOI1 = exp(-ij*k*(d/2)*sin(theta_b + abs(th1)))*cos(-theta_b - abs(th1));
psi4_SNOI1 = exp(-ij*k*(3*d/2)*sin(theta_b + abs(th1)))*cos(-theta_b - abs(th1));
SNOI1 = [psi1_SNOI1 psi2_SNOI1 psi3_SNOI1 psi4_SNOI1].'; % a1
% For SOI, SNOI < 0
psi1_SNOI2 = exp(-ij*k*(3*d/2)*sin(theta_b - abs(th2)))*cos(theta_b - abs(th2));
psi2_SNOI2 = exp(-ij*k*(d/2)*sin(theta_b - abs(th2)))*cos(theta_b - abs(th2));
psi3_SNOI2 = exp(-ij*k*(d/2)*sin(theta_b + abs(th2)))*cos(-theta_b - abs(th2));
psi4_SNOI2 = exp(-ij*k*(3*d/2)*sin(theta_b + abs(th2)))*cos(-theta_b - abs(th2));
SNOI2 = [psi1_SNOI2 psi2_SNOI2 psi3_SNOI2 psi4_SNOI2].'; % a2
% For SOI, SNOI = or > 0
psi1_SNOI3 = exp(-ij*k*(3*d/2)*sin(theta_b + th3))*cos(th3 + theta_b);
psi2_SNOI3 = exp(-ij*k*(d/2)*sin(theta_b + th3))*cos(th3 + theta_b);
psi3_SNOI3 = exp(-ij*k*(d/2)*sin(theta_b - th3))*cos(th3 - theta_b);
psi4_SNOI3 = exp(-ij*k*(3*d/2)*sin(theta_b - th3))*cos(th3 - theta_b);
SNOI3 = [psi1_SNOI3 psi2_SNOI3 psi3_SNOI3 psi4_SNOI3].'; % a3

A = [SOI SNOI1 SNOI2 SNOI3];
u = [1 0 0 0];
%%%%%%%%%%%%%%%
w = u/A; % Weights with out including effect of mutual coupling
%%%%%%%%%%%%%%%
% Z parameters from HFSS
% Self Terms
Z11 = -7.045083-37.356893i;
% Mutual Terms
Z12 = -3.174079+2.976914i;
Z13 = -0.578495+0.547187i;
Z14 = 0.363317-0.010929i;
Z21 = Z12;
Z23 = 0.684065+0.205307i;
Z24 = -0.533723+0.461377i;
Z31 = Z13;
Z32 = Z23;
Z34 = -3.008657+3.121613i;
Z41 = Z14;
Z42 = Z24;
Z43 = Z34;
Z22 = Z11;
Z33 = Z11;
Z44 = Z11;
Z0 = 50;
Z = [Z11/20 Z12/20 Z13/20 Z14/20;Z21/20 Z22/20 Z23/20 Z24/20;Z31/20 Z32/20 Z33/20 Z34/20;Z41/20 Z42/20 Z43/20 Z44/20]; % Normalized Impedance Matrix
I = eye(4);
Zc = Z + I; %Normalized coupling matrix
Ac = Zc\A; %inv(Zc)*A;
wc = u\Ac;
w_mag_norm = abs(w)/max(abs(w));
%w_mag_dB = 20*log10(w_mag_norm)
w_phase_deg = angle(w).*((180/pi))
wc_mag_norm = abs(wc)/max(abs(wc));
%wc_mag_dB = 20*log10(wc_mag_norm)
wc_phase_deg = angle(wc).*((180/pi))
% Array factor
theta = (pi/180)*(-90:180/628:90);
%theta = (pi/180)*(-90:2:90);
e_r3 = cos(theta-theta_b); % Element pattern for right 2 elements at theta = 45 deg from z-axis
e_r4 = e_r3;
e_l1 = cos(theta+theta_b); % Element pattern for left 2 elements at theta = -45 deg from z-axis
e_l2 = e_l1;
u1 = sin(theta);

```

```

u2 = cos(theta);
% v = [1,1,1,1];

x_n = [-3*d/2*cos(theta_b),-d/2*cos(theta_b),d/2*cos(theta_b),3*d/2*cos(theta_b)];
z_n = -[3*d/2*sin(theta_b),d/2*sin(theta_b),3*d/2*sin(theta_b),0];

figure
% No mutual coupling
AP = v(1).*e_11.*exp(j.*k.*(x_n(1).*u1 + z_n(1).*u2)) + ...
v(2).*e_12.*exp(j.*k.*(x_n(2).*u1 + z_n(2).*u2)) + ...
v(3).*e_13.*exp(j.*k.*x_n(3).*u1 + z_n(3).*u2) + ...
v(4).*e_14.*exp(j.*k.*x_n(4).*u1 + z_n(4).*u2));
% Effects of mutual coupling
APc = wc(1).*e_11.*exp(j.*k.*x_n(1).*u1 + z_n(1).*u2)) + ...
wc(2).*e_12.*exp(j.*k.*x_n(2).*u1 + z_n(2).*u2)) + ...
wc(3).*e_13.*exp(j.*k.*x_n(3).*u1 + z_n(3).*u2)) + ...
wc(4).*e_14.*exp(j.*k.*x_n(4).*u1 + z_n(4).*u2));

AP_norm = abs(AP)./max(abs(AP));
APc_norm = abs(APc)./max(abs(APc));
corrected_norm_case2_meas = abs(corrected_case2_meas(:,2))./max((corrected_case2_meas(:,2)));
set(0,'DefaultAxesColorOrder',[0 0 0], ...
'DefaultLineMarkerSize', 8, ...
'DefaultAxesFontSize', 16, ...
'DefaultTextFontSize', 16, ...
'DefaultLineLineWidth', 2);
plot(theta*180/pi,20*log10(AP_norm),'k-');
hold on
plot(theta*180/pi,20*log10(APc_norm),'k--');
hold on
plot(-corrected_case2_meas(:,1),20*log10(corrected_norm_case2_meas),'k.');
hold on
plot(-HFSS_case2(:,1),HFSS_case2(:,2),'kx');
xlabel('theta(deg)')
ylabel('E_{phi} (dB)')
axis([-90 90 -50 0])
legend('Analytical (without coupling)', 'Analytical (with coupling)', 'Measured', 'HFSS')

```

## APPENDIX H. PATTERN 1 BEAMFORMING RESULTS WITH $\theta_B = 45^\circ$ .

The following MATLAB code plots the result in Figure 29 for the four-element array on the wedge-shaped surface with  $\theta_b = 45^\circ$ .

```

corrected_case1_meas = [
46 0.013259581      -2 0.015566668      -50 0.001364653
90 0.015910452      44 0.011353368      -4 0.013698969      -52 0.000741468
88 0.016811439      42 0.009269644      -6 0.011659929      -54 0.001717006
86 0.017241097      40 0.007317156      -8 0.009566591      -56 0.002839978
84 0.017790437      38 0.005192306      -10 0.007325754      -58 0.003568427
82 0.018417578      36 0.002879459      -12 0.005386197      -60 0.004370457
80 0.018876269      34 0.000578943      -14 0.003243998      -62 0.005097717
78 0.019265906      32 0.001798237      -16 0.001399905      -64 0.005684456
76 0.019614756      30 0.004099249      -18 0.001019148      -66 0.006331598
74 0.019538757      28 0.006534775      -20 0.0024917      -68 0.007116319
72 0.020068021      26 0.008890837      -22 0.003978367      -70 0.007322464
70 0.020496742      24 0.010919162      -24 0.005150232      -72 0.008189359
68 0.020551686      22 0.012959365      -26 0.006024717      -74 0.008813356
66 0.020643516      20 0.014868889      -28 0.006815874      -76 0.009144497
64 0.020829283      18 0.016499958      -30 0.007217144      -78 0.009794232
62 0.02020186192     16 0.018088668      -32 0.007511271      -80 0.00970523
60 0.020297114      14 0.019200106      -34 0.007498713      -82 0.00990223
58 0.019616228      12 0.020048644      -36 0.007516696      -84 0.010024559
56 0.019277051      10 0.020415133      -38 0.007209161      -86 0.00942773
54 0.018153763      8 0.020298281      -40 0.006857587      -88 0.009087614
52 0.017498869      6 0.020166464      -42 0.005641956      -90 0.008701712
50 0.0160668692     4 0.019032016      -44 0.00459156      ];
2 0.018327811      -46 0.003559439
48 0.014951028      -48 0.002362186
];

```

```

HFSS_case1 = [
-46 -14.82938882      0 -3.141598539      46 -3.297667507
-45 -14.30232707      1 -2.978327171      47 -2.938319745
-90 -6.767111408      -44 -13.86415979      2 -2.849412727      48 -2.608966458
-89 -6.847054958      -43 -13.506400015      3 -2.754221398      49 -2.307327354
-88 -6.936622134      -42 -13.22297758      4 -2.692321891      50 -2.031359626
-87 -7.036336925      -41 -13.00979101      5 -2.663473533      51 -1.779230802
-86 -7.146774334      -40 -12.86442669      6 -2.667619178      52 -1.549293922
-85 -7.268567594      -39 -12.78599611      7 -2.704892481      53 -1.340065318
-84 -7.402418251      -38 -12.77507079      8 -2.775569265      54 -1.150204912
-83 -7.549109459      -37 -12.83370675      9 -2.88017289      55 -0.978498838
-82 -7.709522781      -36 -12.96556558      10 -3.019383567      56 -0.82384414
-81 -7.884658756      -35 -13.17615157      11 -3.194101659      57 -0.685235352
-80 -8.075661458      -34 -13.473236      12 -3.405459451      58 -0.561752724
-79 -8.283847323      -33 -13.86747453      13 -3.654819722      59 -0.452551981
-78 -8.510738563      -32 -14.37349001      14 -3.943845043      60 -0.356855456
-77 -8.758101695      -31 -15.01156352      15 -4.274478939      61 -0.273944493
-76 -9.027992033      -30 -15.81053082      16 -4.64899342      62 -0.203153032
-75 -9.322805501      -29 -16.81294204      17 -5.070002377      63 -0.143862273
-74 -9.645339943      -28 -18.08493974      18 -5.540460588      64 -0.095496305
-73 -9.98869251      -27 -19.73706355      19 -6.063621304      65 -0.057518612
-72 -10.38723538      -26 -21.97419633      20 -6.642909622      66 -0.029429307
-71 -10.81496576      -25 -25.23968102      21 -7.281630695      67 -0.010762971
-70 -11.287427733      -24 -30.72963213      22 -7.982360718      68 -0.001086958
-69 -11.81103382      -23 -37.2902122      23 -8.745739218      69 0
-68 -12.39353159      -22 -28.91390822      24 -9.568160642      70 -0.007130984
-67 -13.0440254      -21 -23.58128411      25 -10.43754795      71 -0.022137768
-66 -13.7754446      -20 -20.13116383      26 -11.32617469      72 -0.044705905
-65 -14.60162612      -19 -17.58994843      27 -12.18029475      73 -0.0745472
-64 -15.54237066      -18 -15.58057654      28 -12.91059627      74 -0.111398027
-63 -16.62352623      -17 -13.92229606      29 -13.3975146      75 -0.155017376
-62 -17.88041463      -16 -12.51054992      30 -13.53100527      76 -0.205184639
-61 -19.36245736      -15 -11.29775392      31 -13.27433224      77 -0.261697151
-60 -21.13925375      -14 -10.23039993      32 -12.69030492      78 -0.324367572
-59 -23.30225929      -13 -9.285364775      33 -11.89750181      79 -0.393021174
-58 -25.91730188      -12 -8.44278152      34 -11.00871879      80 -0.467493148
-57 -28.66101192      -11 -7.687892249      35 -10.10220293      81 -0.54762603
-56 -29.70706437      -10 -7.009445967      36 -9.22267336      82 -0.633267374
-55 -27.80706282      -9 -6.398683298      37 -8.391996492      83 -0.724267757
-54 -25.12526494      -8 -5.848667942      38 -7.618766319      84 -0.820479221
-53 -22.80129239      -7 -5.353832091      39 -6.904548128      85 -0.921754214
-52 -20.91942716      -6 -4.909658701      40 -6.247454469      86 -1.02794507
-51 -19.39050582      -5 -4.451245158      41 -5.644071487      87 -1.138904043
-50 -18.13148271      -4 -4.159182313      42 -5.090456116      88 -1.25448387
-49 -17.08227235      -3 -3.847341249      43 -4.5826327      89 -1.374538798
-48 -16.20071638      -2 -3.57487051      44 -4.116825773      90 -1.498956005
-47 -15.45693549      -1 -3.340080523      45 -3.689556114      ];

```

```

%close all
clear all;
clc;
format short
N =4;
c = 3e8;
f = 2.4e9;
lambda = c/f;
d = lambda/2;
k = (2*pi)/lambda;
theta_b = 45*(pi/180);
theta_s = 0*(pi/180);
% Four elements antenna array
% Projections on wavefront
th0 = theta_s; %0*(pi/180); %receive angle
th1 = -30*(pi/180); %20*(pi/180); % first interferer angle
th2 = 30*(pi/180); %10*(pi/180); % second interferer angle
th3 = 40*(pi/180); %30*(pi/180); % third interferer angle
% For SOI, SNOI = 0
psi1_SOI = exp(-ij*k*(3*d/2)*sin(theta_b - abs(th0)))*cos(theta_b - abs(th0));
psi2_SOI = exp(-ij*k*(d/2)*sin(theta_b - abs(th0)))*cos(theta_b - abs(th0));
psi3_SOI = exp(-ij*k*(d/2)*sin(theta_b + abs(th0)))*cos(-abs(th0) - theta_b);
psi4_SOI = exp(-ij*k*(3*d/2)*sin(theta_b + abs(th0)))*cos(-abs(th0) - theta_b);
SOI = [psi1_SOI psi2_SOI psi3_SOI psi4_SOI].'; % a0
% For SOI, SNOI < 0
psi1_SNOI1 = exp(-ij*k*(3*d/2)*sin(theta_b - abs(th1)))*cos(theta_b - abs(th1));
psi2_SNOI1 = exp(-ij*k*(d/2)*sin(theta_b - abs(th1)))*cos(theta_b - abs(th1));
psi3_SNOI1 = exp(-ij*k*(d/2)*sin(theta_b + abs(th1)))*cos(-theta_b - abs(th1));
psi4_SNOI1 = exp(-ij*k*(3*d/2)*sin(theta_b + abs(th1)))*cos(-theta_b - abs(th1));
SNOI1 = [psi1_SNOI1 psi2_SNOI1 psi3_SNOI1 psi4_SNOI1].'; % a1
% For SOI, SNOI > 0
psi1_SNOI2 = exp(-ij*k*(3*d/2)*sin(theta_b + abs(th2)))*cos(theta_b + abs(th2));
psi2_SNOI2 = exp(-ij*k*(d/2)*sin(theta_b + abs(th2)))*cos(theta_b + abs(th2));
psi3_SNOI2 = exp(-ij*k*(d/2)*sin(theta_b - abs(th2)))*cos(-theta_b + abs(th2));
psi4_SNOI2 = exp(-ij*k*(3*d/2)*sin(theta_b - abs(th2)))*cos(-theta_b + abs(th2));
SNOI2 = [psi1_SNOI2 psi2_SNOI2 psi3_SNOI2 psi4_SNOI2].'; % a2
% For SOI, SNOI > 0
psi1_SNOI3 = exp(-ij*k*(3*d/2)*sin(theta_b + th3)))*cos(abs(th3) + theta_b);
psi2_SNOI3 = exp(-ij*k*(d/2)*sin(theta_b + th3))*cos(abs(th3) + theta_b);
psi3_SNOI3 = exp(-ij*k*(d/2)*sin(theta_b - th3))*cos(abs(th3) - theta_b);
psi4_SNOI3 = exp(-ij*k*(3*d/2)*sin(theta_b - th3))*cos(abs(th3) - theta_b);
SNOI3 = [psi1_SNOI3 psi2_SNOI3 psi3_SNOI3 psi4_SNOI3].'; % a3
A = [SOI SNOI1 SNOI2 SNOI3];
u = [1 0 0 0];
%%%%%%%%%%%%%%%
v = u/A; % Weights with out including effect of mutual coupling
%%%%%%%%%%%%%%
% Z parameters from HFSS
% Self Terms
Z11 = 36.34+0.759i;
Z22 = -27.1-27.878i;
Z33 = -38.51-7.43i;
Z44 = 32.9-15.17i;
% Mutual Terms
Z12 = -3.58+2.31i;
Z13 = 0.1-0.1i;
Z14 = 0.73+0.0084i;
Z21 = Z12;
Z23 = -0.914-0.0624i;
Z24 = 0.172-0.1474i;
Z31 = Z13;
Z32 = Z23;
Z34 = -3.416+2.44i;
Z41 = Z14;
Z42 = 0.172-0.1474i;
Z43 = Z34;
Z0 = 80;
Z = [Z11/Z0 Z12/Z0 Z13/Z0 Z14/Z0;Z21/Z0 Z22/Z0 Z23/Z0 Z24/Z0;Z31/Z0 Z32/Z0 Z33/Z0 Z34/Z0;Z41/Z0 Z42/Z0 Z43/Z0 Z44/Z0]; % Normalized Impedance Matrix
I = eye(4);
Zc = Z + I; %Normalized coupling matrix
Ac = Zc\A; %inv(Zc)*A;
wc = u/Ac;
w_mag_norm = abs(w)/max(abs(w))
%w_mag_dB = 20*log10(w_mag_norm)
v_phase_deg = angle(w).*((180/pi))
wc_mag_norm = abs(wc)/max(abs(wc))
%wc_mag_dB = 20*log10(wc_mag_norm)
wc_phase_deg = angle(wc).*((180/pi))
% Array factor
theta = (pi/180)*(-90:180/628:90);
%theta = (pi/180)*(-90:2:90);
e_r3 = cos(theta-theta_b);
e_r4 = e_r3;
e_l1 = cos(theta+theta_b);
e_l2 = e_l1;
u1 = sin(theta);
u2 = cos(theta);
% w = [1,1,1,1];

```

```

x_n = [-3*d/2*cos(theta_b), -d/2*cos(theta_b), d/2*cos(theta_b), 3*d/2*cos(theta_b)];
z_n = [3*d/2*sin(theta_b), d/2*sin(theta_b), d/2*sin(theta_b), 3*d/2*sin(theta_b)];

figure
% No mutual coupling
AP = w(1).*e_11.*exp(j.*k.*(x_n(1).*u1 + z_n(1).*u2)) + ...
w(2).*e_12.*exp(j.*k.*x_n(2).*u1 + z_n(2).*u2))+ ...
w(3).*e_33.*exp(j.*k.*x_n(3).*u1 + z_n(3).*u2))+ ...
w(4).*e_44.*exp(j.*k.*x_n(4).*u1 + z_n(4).*u2));

% Effects of mutual coupling
APc = wc(1).*e_11.*exp(j.*k.*x_n(1).*u1 + z_n(1).*u2)) + ...
wc(2).*e_12.*exp(j.*k.*x_n(2).*u1 + z_n(2).*u2))+ ...
wc(3).*e_33.*exp(j.*k.*x_n(3).*u1 + z_n(3).*u2))+ ...
wc(4).*e_44.*exp(j.*k.*x_n(4).*u1 + z_n(4).*u2));

AP_norm = abs(AP)./max(abs(AP));
APc_norm = abs(APc)./max(abs(APc));
corrected_norm_case1_meas = abs(corrected_case1_meas(:,2))./max((corrected_case1_meas(:,2)));
set(0,'DefaultAxesColorOrder',[0 0 0], ...
'DefaultLineMarkerSize', 8, ...
'DefaultAxesFontSize', 16, ...
'DefaultTextFontSize', 16, ...
'DefaultLineWidth', 2);
plot(theta*180/pi,20*log10(AP_norm),'k-');
hold on
plot(theta*180/pi,20*log10(APc_norm),'k--');
hold on
plot(-corrected_case1_meas(:,1),20*log10(corrected_norm_case1_meas),'k.');
hold on
plot(-HFSS_case1(:,1),HFSS_case1(:,2),'kx');
xlabel('theta (deg)')
ylabel('|E_{\phi}| (dB)')
axis([-90 90 -50 0])
legend('Analytical (without coupling)', 'Analytical (with coupling)', 'Measured', 'HFSS')

```

## APPENDIX I. PATTERN 2 BEAMFORMING RESULTS WITH $\theta_B = 45^\circ$ .

The following MATLAB code plots the result in Figure 30 for the four-element array on the wedge-shaped surface with  $\theta_b = 45^\circ$ .

```

corrected_case2_meas = [
46 0.002786193      -2 0.005482761      -50 0.023829366
44 0.003349728      -4 0.005115543      -52 0.02396324
42 0.004098128      -6 0.004742322      -54 0.023931291
88 0.004815412      -8 0.004724013      -56 0.023689098
88 0.005253683      -10 0.002871193      -58 0.023579108
86 0.00561818       -12 0.002307958      -60 0.02269134
84 0.005974044      -14 0.002245786      -62 0.022719732
82 0.006010661      -16 0.003081866      -64 0.022020643
80 0.006091816      -18 0.004463861      -66 0.021703812
78 0.005966971      -20 0.004211242      -68 0.021298287
76 0.0059567896     -22 0.00355502       -70 0.020755615
74 0.005582013      -24 0.003047901      -72 0.019747973
72 0.005247097      -26 0.0031982      -74 0.019252185
70 0.004623481      -28 0.01149471      -76 0.019038138
68 0.004084263      -30 0.013153445      -78 0.018484792
66 0.003606683      -32 0.014968161      -80 0.017875189
64 0.0027635      -34 0.016580897      -82 0.016794444
62 0.002254038      -36 0.017853163      -84 0.016196381
60 0.001681229      -38 0.018905985      -86 0.015379247
58 0.001260649      -40 0.020509638      -88 0.014573826
56 0.000613164      -42 0.021474022      -90 0.013875409
54 9.86E-05          -44 0.022309126
52 0.000616547      -46 0.022808765
50 0.001339845      -48 0.023598137
48 0.002093044      -48 0.023677654

HFSS_case2 = [
-46 -0.631415174      0 -14.26468244      46 -15.76674462
-45 -0.652148158      1 -14.12467881      47 -16.09688866
-90 -4.117298532      2 -14.05383689      48 -16.49051394
-89 -4.201997224      3 -14.037121212      49 -16.95395179
-88 -3.989844757      4 -1.102630625      50 -17.49532699
-87 -3.780965654      5 -1.284393346      51 -18.12514479
-86 -3.576494385      6 -1.483135231      52 -18.85719686
-85 -3.373575307      7 -1.699625043      53 -19.70999789
-84 -3.175362668      8 -1.834680872      54 -20.70915069
-83 -2.98102745      9 -2.189178627      55 -21.89143362
-82 -2.790723855      10 -2.464062715      56 -23.31232101
-81 -2.60465662      11 -2.760358999      57 -25.06098027
-80 -2.423014028      12 -3.079190081      58 -27.2934495
-79 -2.246001474      13 -3.421792977      59 -30.31606827
-78 -2.073834654      14 -3.789539234      60 -34.81193018
-77 -1.906739237      15 -4.183957554      61 -41.24423854
-76 -1.744950278      16 -4.606758951      62 -37.81802691
-75 -1.588711302      17 -5.058794411      63 -32.26085769
-74 -1.438273047      18 -5.845434793      64 -28.701007
-73 -1.293891839      19 -6.05590228      65 -26.17964129
-72 -1.15582764      20 -6.624001684      66 -24.25305172
-71 -1.0243418      21 -7.222798128      67 -22.70852281
-70 -0.899894612      22 -7.865703991      68 -21.42981691
-69 -0.782142781      23 -8.556471342      69 -20.34674037
-68 -0.67193693      24 -9.2991335      70 -19.41363858
-67 -0.569319331      25 -10.09784427      71 -18.59909541
-66 -0.474521994      26 -10.95652269      72 -17.88052667
-65 -0.3877653      27 -11.87811927      73 -17.24113034
-64 -0.309257322      28 -12.86318027      74 -16.66806331
-63 -0.239193961      29 -13.90713029      75 -16.15129735
-62 -0.177759982      30 -14.99537455      76 -15.68287084
-61 -0.125130994      31 -16.09523404      77 -15.25638088
-60 -0.081476361      32 -17.14511733      78 -14.86662665
-59 -0.046962973      33 -18.04703927      79 -14.50935101
-58 -0.021759739      34 -18.67939485      80 -14.18104767
-57 -0.006042623      35 -18.94631719      81 -13.87881362
-56 0      36 -18.83847076      82 -13.60023366
-55 -0.003838055      37 -18.44031313      83 -13.34328857
-54 -0.017785981      38 -17.87472152      84 -13.10628113
-53 -0.042100692      39 -17.2475457      85 -12.88777633
-52 -0.077070853      40 -16.62847611      86 -12.68655299
-51 -0.123020031      41 -14.93283444      87 -12.50156483
-50 -0.180308881      42 -14.99872263      88 -12.33190949
-49 -0.249336347      43 -15.11351371      89 -12.17680433
-48 -0.330539949      44 -15.27834639      90 -12.03556789
-47 -0.424395313      45 -15.49515638      1;
];

```

```

%close all;
clear all;
clc;
format short
N =4;
c = 3e8;
f = 2.4e9;
lambda = c/f;
d = lambda/2;
k = (2*pi)/lambda;
theta_b = 45*(pi/180);
theta_s = 40*(pi/180); % Angle from x-axis = 90 deg or angle from z-axis = 0 deg
% Four elements antenna array
% Projections on wavefront
th0 = theta_s; %0*(pi/180); %receive angle
th1 = -45*(pi/180); %-20*(pi/180); % first interferer angle
th2 = -25*(pi/180); %10*(pi/180); % second interferer angle
th3 = 10*(pi/180); %30*(pi/180); % third interferer angle

% For SDI, SNOI = or > 0
psi1_SOI = exp(-1j*k*(3*d/2)*sin(theta_b + th0))*cos(th0 + theta_b);
psi2_SOI = exp(-1j*k*(d/2)*sin(theta_b + th0))*cos(th0 + theta_b);
psi3_SOI = exp(-1j*k*(d/2)*sin(theta_b - th0))*cos(th0 - theta_b);
psi4_SOI = exp(-1j*k*(3*d/2)*sin(theta_b - th0))*cos(th0 - theta_b);
SOI = [psi1_SOI psi2_SOI psi3_SOI psi4_SOI].';
% For SDI, SNOI < 0
psi1_SNOI1 = exp(-1j*k*(3*d/2)*sin(theta_b - abs(th1)))*cos(theta_b - abs(th1));
psi2_SNOI1 = exp(-1j*k*(d/2)*sin(theta_b - abs(th1)))*cos(theta_b - abs(th1));
psi3_SNOI1 = exp(-1j*k*(d/2)*sin(theta_b + abs(th1)))*cos(-theta_b - abs(th1));
psi4_SNOI1 = exp(-1j*k*(3*d/2)*sin(theta_b + abs(th1)))*cos(-theta_b - abs(th1));
SNOI1 = [psi1_SNOI1 psi2_SNOI1 psi3_SNOI1 psi4_SNOI1].'; % a1
% For SDI, SNOI < 0
psi1_SNOI2 = exp(-1j*k*(3*d/2)*sin(theta_b - abs(th2)))*cos(theta_b - abs(th2));
psi2_SNOI2 = exp(-1j*k*(d/2)*sin(theta_b - abs(th2)))*cos(theta_b - abs(th2));
psi3_SNOI2 = exp(-1j*k*(d/2)*sin(theta_b + abs(th2)))*cos(-theta_b - abs(th2));
psi4_SNOI2 = exp(-1j*k*(3*d/2)*sin(theta_b + abs(th2)))*cos(-theta_b - abs(th2));
SNOI2 = [psi1_SNOI2 psi2_SNOI2 psi3_SNOI2 psi4_SNOI2].'; % a2
% For SDI, SNOI = or > 0
psi1_SNOI3 = exp(-1j*k*(3*d/2)*sin(theta_b + th3))*cos(th3 + theta_b);
psi2_SNOI3 = exp(-1j*k*(d/2)*sin(theta_b + th3))*cos(th3 + theta_b);
psi3_SNOI3 = exp(-1j*k*(d/2)*sin(theta_b - th3))*cos(th3 - theta_b);
psi4_SNOI3 = exp(-1j*k*(3*d/2)*sin(theta_b - th3))*cos(th3 - theta_b);
SNOI3 = [psi1_SNOI3 psi2_SNOI3 psi3_SNOI3 psi4_SNOI3].'; % a3
A = [SOI SNOI1 SNOI2 SNOI3];
u = [1 0 0 0];
w = u/A; % Weights with out including effect of mutual coupling
%%%%%%%%%%%%%%%%%%%%%%%%%%%%%%%%%%%%%%%
% Z parameters from HFSS
% Self Terms
Z11 = 36.34+0.759i;
Z22 = -27.1-27.878i;
Z33 = -38.51-7.43i;
Z44 = 32.9-15.17i;
% Mutual Terms
Z12 = -3.58+2.31i;
Z13 = 0.1-0.1i;
Z14 = 0.73+0.0084i;
Z21 = Z12;
Z23 = -0.914-0.062i;
Z24 = 0.172-0.147i;
Z31 = Z13;
Z32 = Z23;
Z34 = -3.416+2.44i;
Z41 = Z14;
Z42 = 0.172-0.147i;
Z43 = Z34;
Z0 = 50;
Z = [Z11/Z0 Z12/Z0 Z13/Z0 Z14/Z0;Z21/Z0 Z22/Z0 Z23/Z0 Z24/Z0;Z31/Z0 Z32/Z0 Z33/Z0 Z34/Z0;Z41/Z0 Z42/Z0 Z43/Z0 Z44/Z0]; % Normalized Impedance Matrix
I = eye(4);
Zc = Z + I; %Normalized coupling matrix
Ac = Zc\A; %inv(Zc)*A;
%Ac = inv(Zc)*A;
wc = u/Ac;
w_mag_norm = abs(w)/max(abs(w))
%w_mag_db = 20*log10(w_mag_norm)
w_phase_deg = angle(w).*180/pi
wc_mag_norm = abs(wc)/max(abs(wc))
%wc_mag_db = 20*log10(wc_mag_norm)
wc_phase_deg = angle(wc).*180/pi
% Array factor
theta = (pi/180)*(-90:180:628:90);
%theta = (pi/180)*(-90:2:90);
e_r3 = cos(theta-theta_b);
e_r4 = e_r3;
e_l1 = cos(theta+theta_b);
% Element pattern for right 2 elements at theta = 45 deg from z-axis
% Element pattern for left 2 elements at theta = -45 deg from z-axis

```

```

e_12 = e_11;
u1 = sin(theta);
u2 = cos(theta);
% w = [1,1,1,1];

x_n = [-3*d/2*cos(theta_b),-d/2*cos(theta_b),d/2*cos(theta_b),3*d/2*cos(theta_b)];
z_n = -[3*d/2*sin(theta_b),d/2*sin(theta_b),d/2*sin(theta_b),3*d/2*sin(theta_b)];

figure
% No mutual coupling
AP = w(1).*e_11.*exp(j.*k.*(x_n(1).*u1 + z_n(1).*u2)) + ...
w(2).*e_12.*exp(j.*k.*((x_n(2).*u1 + z_n(2).*u2))+ ...
w(3).*e_13.*exp(j.*k.*((x_n(3).*u1 + z_n(3).*u2))+ ...
w(4).*e_14.*exp(j.*k.*((x_n(4).*u1 + z_n(4).*u2)));

% Effects of mutual coupling
APc = wc(1).*e_11.*exp(j.*k.*((x_n(1).*u1 + z_n(1).*u2)) + ...
wc(2).*e_12.*exp(j.*k.*((x_n(2).*u1 + z_n(2).*u2))+ ...
wc(3).*e_13.*exp(j.*k.*((x_n(3).*u1 + z_n(3).*u2))+ ...
wc(4).*e_14.*exp(j.*k.*((x_n(4).*u1 + z_n(4).*u2)));

AP_norm = abs(AP)./max(abs(AP));
APc_norm = abs(APc)./max(abs(APc));
corrected_norm_case2_meas = abs(corrected_case2_meas(:,2))./max((corrected_case2_meas(:,2)));
set(0,'DefaultAxesColorOrder',[0 0 0], ...
'DefaultLineMarkerSize', 8, ...
'DefaultAxesFontSize', 16, ...
'DefaultTextFontSize', 16, ...
'DefaultLineLineWidth',2);
plot(theta*180/pi,20*log10(AP_norm),'k-');
hold on
plot(theta*180/pi,20*log10(APc_norm),'k--');
hold on
plot(-corrected_case2_meas(:,1),20*log10(corrected_norm_case2_meas),'k.');
hold on
plot(-HFSS_case2(:,1),HFSS_case2(:,2),'kx');
xlabel('theta(deg)')
ylabel('|E_{phi}| (dB)')
axis([-90 90 -50 0])
legend('Analytical (without coupling)',
```

## APPENDIX J. PATTERN 1 BEAMFORMING RESULTS WITH $R = 10$ CM.

The following MATLAB code plots the result in Figure 31 for the four-element array on the cylindrical-shaped surface with  $r = 10$  cm.

```

HFSS_case1 = [
-90 -7.699761969          0 -20.16005841          46 -1.637549228
-89 -7.564023248          -45 -22.24951431          45 -0.092078148
-88 -7.434390267          -44 -24.32903914          47 -1.654620102
-87 -7.310064465          -43 -26.49448879          48 -1.696408
-86 -7.194050404          -42 -24.82262163          49 -1.761401322
-85 -7.083737911          -41 -23.00344403          50 -1.848211282
-84 -6.980323733          -40 -21.06609096          51 -1.955552791
-83 -6.884103455          -39 -19.36958709          52 -0.242859375
-82 -6.795415307          -38 -17.95525401          53 -2.227113464
-81 -6.714642048          -37 -16.79072565          54 -2.389145993
-80 -6.642212958          -36 -15.83698042          55 -2.567314397
-79 -6.578605991          -35 -15.06186288          56 -2.760649331
-78 -6.524350141          -34 -14.44104081          57 -2.968215546
-77 -6.480028094          -33 -13.95650586          58 -3.189104903
-76 -6.446279242          -32 -13.524350328         59 -3.422430203
-75 -6.423803147          -31 -13.3460824          60 -3.667319763
-74 -6.413363567          -30 -13.20179985         61 -3.922912623
-73 -6.41579317          -29 -13.15438343         62 -4.188354348
-72 -6.4319991          -28 -13.19510085         63 -4.462793341
-71 -6.462986958          -27 -13.31191438         64 -4.745377655
-70 -6.509781831          -26 -13.48628237         65 -5.035262241
-69 -6.573611491          -25 -13.6888766           66 -5.315566337
-68 -6.655744089          -24 -13.87496951         67 -5.633423047
-67 -6.757588855          -23 -13.98240368         68 -5.939748482
-66 -6.88069557          -22 -13.9379636           69 -6.250325439
-65 -7.026775183          -21 -13.67716455         70 -6.563577601
-64 -7.197725176          -20 -13.17142386         71 -6.87823148
-63 -7.39566097          -19 -12.44240142         72 -7.195143115
-62 -7.622955065          -18 -11.5498446          73 -7.511608391
-61 -7.882286212          -17 -10.56456556          74 -7.827280869
-60 -8.176701667          -16 -9.547536975         75 -8.141215161
-59 -8.509696778          -15 -8.541392021         76 -8.452460935
-58 -8.885317754          -14 -7.573633042         77 -8.760065915
-57 -9.308295847          -13 -6.659224041         78 -9.063079609
-56 -9.784224668          -12 -5.805670381         79 -9.360557809
-55 -10.31979745          -11 -5.015892174         80 -9.651567894
-54 -10.92312866          -10 -4.2902119           81 -9.935194949
-53 -11.60419522          -9 -3.627573663         82 -10.21054869
-52 -12.37644774          -8 -3.026265914         83 -10.47677114
-51 -13.25265984          -7 -2.484339792         84 -10.73304501
-50 -14.25609237          -6 -1.999846042         85 -10.97860263
-49 -15.41199742          -5 -1.570956733         86 -11.21273473
-48 -16.76416708          -4 -1.196079808         87 -11.43480076
-47 -18.32380708          -3 -0.873804252         88 -11.64423711
-        -2 -0.603006768         89 -11.84056632
-        -1 -0.382814463         90 -12.02340496
-        0 -1.646852471         1;

Meas_case1 = [
64 0.010934366          37 0.009523169          10 0.020469282
63 0.011133205          36 0.008775441          9 0.020555565
62 0.011294904          35 0.0081411          8 0.02100079
61 0.011622956          34 0.007368806          7 0.021161929
60 0.011960145          33 0.006526734          6 0.021129188
59 0.012478186          32 0.005590426          5 0.021180038
58 0.012750105          31 0.004585323          4 0.021060374
57 0.012994605          30 0.003675491          3 0.020827805
56 0.013315627          29 0.0029626126         2 0.020466958
55 0.013626754          28 0.002460204          1 0.02022434
54 0.013973309          27 0.002772513          0 0.019801271
53 0.014317978          26 0.003194645         -1 0.019182594
52 0.014463817          25 0.004469649         -2 0.01854999
51 0.014329399          24 0.005630082         -3 0.018083733
50 0.014455198          23 0.00686139          -4 0.017308695
49 0.01465662          22 0.008172521         -5 0.016569023
48 0.014038663          21 0.009604312         -6 0.015420659
47 0.013910302          20 0.010871003         -7 0.014747736
46 0.013495861          19 0.012287593         -8 0.01363605
45 0.012968986          18 0.013409727         -9 0.012685019
44 0.012795708          17 0.014632399         -10 0.011430154
43 0.012587023          16 0.015709705         -11 0.010535332
42 0.012087275          15 0.016744665         -12 0.009340008
41 0.011862028          14 0.017705689         -13 0.008265292
40 0.011228422          13 0.018622878         -14 0.00685573
39 0.01059415           12 0.019176216         -15 0.005911287
38 0.009910818          11 0.019773593         -16 0.00463212
];

```

```

-17 0.003643911      -36 0.001629223      -55 0.007497103      -74 0.008804995
-18 0.002808856      -37 0.00169876      -56 0.007891968      -75 0.008280619
-19 0.002162698      -38 0.001854049      -57 0.008464659      -76 0.007792759
-20 0.001802117      -39 0.002061851      -58 0.008916704      -77 0.007228552
-21 0.001636443      -40 0.00223112      -59 0.009224472      -78 0.006702811
-22 0.001682192      -41 0.002375037      -60 0.009712913      -79 0.006214599
-23 0.001799374      -42 0.002565751      -61 0.009840812      -80 0.005866145
-24 0.00295019      -43 0.002783723      -62 0.010075482      -81 0.005689734
-25 0.002586932      -44 0.003093205      -63 0.010125484      -82 0.005323478
-26 0.002380521      -45 0.003357823      -64 0.010154113      -83 0.005123008
-27 0.002675293      -46 0.003542157      -65 0.010264028      -84 0.004743729
-28 0.002479216      -47 0.004051943      -66 0.010151358      -85 0.004396232
-29 0.00241215      -48 0.004240798      -67 0.010009696      -86 0.004417535
-30 0.0023115      -49 0.004804199      -68 0.010140778      -87 0.004243534
-31 0.002053073      -50 0.00529016      -69 0.009877523      -88 0.004394516
-32 0.0019886      -51 0.005696588      -70 0.009765531      -89 0.004095377
-33 0.001791012      -52 0.006169244      -71 0.009617377      -90 0.004152222
-34 0.001680781      -53 0.006061265      -72 0.0093022      ];
-35 0.001624608      -54 0.007174793      -73 0.009099893

```

```

%close all;
clear all;
clc;
format short
N =4;
c = 3e8;
f = 2.4e9;
lambda = c/f;
d = lambda/2;
k = (2*pi)/lambda;
theta_s = 0*(pi/180); % Angle from x-axis = 90 deg or angle from z-axis = 0 deg
% Four elements antenna array
% Projections on wavefront
th0 = theta_s; %0*(pi/180);
th1 = -30*(pi/180); % -20*(pi/180); % first interferer angle
th2 = 30*(pi/180); %10*(pi/180); % second interferer angle
th3 = 40*(pi/180); %30*(pi/180); % third interferer angle

% Elements locations on curved conformal surface
%%%%%%%%%%%%%
r = 0.2032; % For 8 inches radius sphere
theta1 = d/r;
theta2 = d/(2*r);
phi1 = pi/2 - (theta1 + theta2);
phi2 = phi1 + theta1;
phi3 = phi2;
phi4 = phi1;
phi_n = [phi1;phi2;phi3;phi4];
for m = 1:N/2
    x_n(m) = -r*cos(phi_n(m));
end
for m = (N/2+1):N
    x_n(:,m) = r*cos(phi_n(m)); % x_n = [-0.0896 -0.0311 0.0311 0.0896]
end
for m = 1:N
    z_n(m) = r*sin(phi_n(m)); % z_n = [0.1578 0.1788 0.1788 0.1578]
end
%%%%%%%%%%%%%
for m = 1: N
    h_n(m) = sqrt((0-x_n(m))^2 + (r-z_n(m))^2); % h_n = [0.0927 0.0312 0.0312 0.0927]
    phi_inv(m) = asin((r-z_n(m))/h_n(m));
end
theta_b = phi_inv;
theta_b_degrees = theta_b*180/pi
% For theta_s = 0, the wave front hits all elements with negative phase delays with respect to origin
psi1_SOI = exp(-ij*k*h_n(1)*sin(theta_b(1) + abs(th0)))*cos(pi/2-phi_n(1)+th0);
psi2_SOI = exp(-ij*k*h_n(2)*sin(theta_b(2) + abs(th0)))*cos(pi/2-phi_n(2)+th0);
psi3_SOI = exp(-ij*k*h_n(3)*sin(theta_b(3) + abs(th0)))*cos(pi/2-phi_n(3)-th0);
psi4_SOI = exp(-ij*k*h_n(4)*sin(theta_b(4) + abs(th0)))*cos(pi/2-phi_n(4)-th0);
SOI = [psi1_SOI psi2_SOI psi3_SOI psi4_SOI]; % a0
% For theta_s = theta_SOI = -30 < 0 and > theta_b, the wave front hits left elements 1,2
% first and right elements 3,4 later with respect to origin
psi1_SNOI1 = exp(ij*k*h_n(1)*sin(-theta_b(1) + abs(th1)))*cos(pi/2-phi_n(1)+th1);
psi2_SNOI1 = exp(ij*k*h_n(2)*sin(-theta_b(2) + abs(th1)))*cos(pi/2-phi_n(2)+th1);
psi3_SNOI1 = exp(-ij*k*h_n(3)*sin(theta_b(3) + abs(th1)))*cos(pi/2-phi_n(3)-th1);
psi4_SNOI1 = exp(-ij*k*h_n(4)*sin(theta_b(4) + abs(th1)))*cos(pi/2-phi_n(4)-th1);
SNOI1 = [psi1_SNOI1 psi2_SNOI1 psi3_SNOI1 psi4_SNOI1]; % a1
% For SOI, SNOI = 30 > theta_b, the wave front hits right elements 3,4 first and left elements 1,2 later with respect to origin
psi1_SNOI2 = exp(-ij*k*h_n(1)*sin(theta_b(1) + abs(th2)))*cos(pi/2-phi_n(1)+th2);
psi2_SNOI2 = exp(-ij*k*h_n(2)*sin(theta_b(2) + abs(th2)))*cos(pi/2-phi_n(2)+th2);
psi3_SNOI2 = exp(ij*k*h_n(3)*sin(theta_b(3) + abs(th2)))*cos(pi/2-phi_n(3)-th2);
psi4_SNOI2 = exp(ij*k*h_n(4)*sin(theta_b(4) + abs(th2)))*cos(pi/2-phi_n(4)-th2);
SNOI2 = [psi1_SNOI2 psi2_SNOI2 psi3_SNOI2 psi4_SNOI2]; % a2
% For SNOI = 40 > theta_b
psi1_SNOI3 = exp(-ij*k*h_n(1)*sin(theta_b(1) + abs(th3)))*cos(pi/2-phi_n(1)+th3);
psi2_SNOI3 = exp(-ij*k*h_n(2)*sin(theta_b(2) + abs(th3)))*cos(pi/2-phi_n(2)+th3);
psi3_SNOI3 = exp(ij*k*h_n(3)*sin(theta_b(3) + abs(th3)))*cos(pi/2-phi_n(3)-th3);
psi4_SNOI3 = exp(ij*k*h_n(4)*sin(theta_b(4) + abs(th3)))*cos(pi/2-phi_n(4)-th3);
SNOI3 = [psi1_SNOI3 psi2_SNOI3 psi3_SNOI3 psi4_SNOI3]; % a3

```

```

A = [S01 S011 S012 S013];
u = [1 0 0 0];
w = u/A;
#####
% Z parameters from HFSS at f = 2.4729 GHz
% Self Terms
Z11 = -37.87-16.15i;
% Mutual Terms
Z12 = 0.45+3.94i;
Z13 = -1.355+1.923i;
Z14 = 0.8+0.186i;
Z21 = Z12;
Z22 = -2.63+3.77i;
Z24 = -1.26+1.82i;
Z31 = Z13;
Z32 = Z23;
Z34 = 0.844+3.856i;
Z41 = Z14;
Z42 = Z24;
Z43 = Z34;
Z22 = Z11;
Z33 = Z11;
Z44 = Z11;
Z0 = 50;
Z = [Z11/20 Z12/20 Z13/20 Z14/20;Z21/20 Z22/20 Z23/20 Z24/20;Z31/20 Z32/20 Z33/20 Z34/20;Z41/20 Z42/20 Z43/20 Z44/20]; % Normalized Impedance Matrix
I = eye(4);
Zc = Z + I ; %Normalized coupling impedance matrix
Ac = Zc\A; %inv(Zc)*A;
wc = u/Ac;
w_mag_norm = abs(w)./max(abs(w));
% w_mag_db = 20*log10(w_mag_norm);
w_phase_deg = angle(w).*(180/pi);
wc_mag_norm = abs(wc)./max(abs(wc));
% wc_mag_db = 20*log10(wc_mag_norm);
wc_phase_deg = angle(wc).*(180/pi);
% Array factor
theta = (pi/180)*(-90:180/628:90);
e_11 = cos(pi/2 - phi_n(1)+theta);
e_12 = cos(pi/2 - phi_n(2)+theta);
e_r3 = cos(pi/2 - phi_n(3)-theta);
e_r4 = cos(pi/2 - phi_n(4)-theta);
u1 = sin(theta);
u2 = cos(theta);
figure
% No mutual coupling
AP = w(1).*e_11.*exp(j.*k.*(x_n(1).*u1 + z_n(1).*u2)) + ...
w(2).*e_12.*exp(j.*k.*x_n(2).*u1 + z_n(2).*u2))+ ...
w(3).*e_r3.*exp(j.*k.*x_n(3).*u1 + z_n(3).*u2))+ ...
w(4).*e_r4.*exp(j.*k.*x_n(4).*u1 + z_n(4).*u2));
% Effects of mutual coupling
APc = wc(1).*e_11.*exp(j.*k.*x_n(1).*u1 + z_n(1).*u2)) + ...
wc(2).*e_12.*exp(j.*k.*x_n(2).*u1 + z_n(2).*u2))+ ...
wc(3).*e_r3.*exp(j.*k.*x_n(3).*u1 + z_n(3).*u2))+ ...
wc(4).*e_r4.*exp(j.*k.*x_n(4).*u1 + z_n(4).*u2));
AP_norm = abs(AP)./max(abs(AP));
APc_norm = abs(APc)./max(abs(APc));
set(0,'DefaultAxesColorOrder',[0 0 0], ...
'DefaultLineMarkerSize', 8, ...
'DefaultAxesFontSize', 16, ...
'DefaultTextFontSize', 16, ...
'DefaultLineLineWidth',2);
plot(theta*180/pi,20*log10(AP_norm),'k-');
hold on
plot(theta*180/pi,20*log10(APc_norm),'k--');
hold on
Meas_case1_norm = abs(Meas_case1(:,2))./max((Meas_case1(:,2)));
plot(-Meas_case1(:,1),20*log10(Meas_case1_norm),'k.');
hold on
plot(-HFSS_case1(:,1),HFSS_case1(:,2),'kx');
xlabel('theta(deg)')
ylabel('|E_{phi}| (dB)')
axis([-90 90 -50 0])
legend('Analytical (without coupling)', 'Analytical (with coupling)', 'Measured', 'HFSS')
%plot(theta*180/pi,e_12)
%plot(x_n,z_n,'o')

```

## APPENDIX K. PATTERN 2 BEAMFORMING RESULTS WITH $R = 10$ CM.

The following MATLAB code plots the result in Figure 32 for the four-element array on the cylindrical-shaped surface with  $r = 10$  cm.

```

HFSS_case2 = [
-90 -17.49781058 -46 -1.381433494 0 -10.98236111 46 -21.56083753
-89 -17.33444117 -45 -1.156893696 1 -10.45311972 47 -21.61200935
-88 -17.14637871 -44 -0.949928009 2 -10.05581138 48 -21.25937609
-87 -16.93335302 -43 -0.761206738 3 -9.775915025 49 -20.57410708
-86 -16.69541578 -42 -0.591428246 4 -9.602765962 50 -19.68761629
-85 -16.43294503 -41 -0.441322934 5 -9.528650585 51 -18.72076021
-84 -16.14663485 -40 -0.311657632 6 -9.548175123 52 -17.75401281
-83 -15.83747151 -39 -0.203240513 7 -9.657833869 53 -16.83113673
-82 -15.50669831 -38 -0.116926654 8 -9.855720415 54 -15.97202665
-81 -15.15577243 -37 -0.053624409 9 -10.14134134 55 -15.18327613
-80 -14.78631715 -36 -0.014302777 10 -10.51550074 56 -14.46473563
-79 -14.40007326 -35 0 11 -10.98022666 57 -13.81311291
-78 -13.99885239 -34 -0.011833677 12 -11.53870172 58 -13.2238557
-77 -13.58449489 -33 -0.051012758 13 -12.19513372 59 -12.69208804
-76 -13.15883351 -32 -0.118851859 14 -12.984439797 60 -12.21305619
-75 -12.72366394 -31 -0.216788477 15 -13.82147498 61 -11.78232279
-74 -12.28072208 -30 -0.346403834 16 -14.7992807 62 -11.39583475
-73 -11.83166779 -29 -0.509446308 17 -15.88509338 63 -11.04992971
-72 -11.37807435 -28 -0.707872676 18 -17.06204947 64 -10.74131432
-71 -10.9214228 -27 -0.943866838 19 -18.28300509 65 -10.46703141
-70 -10.4631001 -26 -1.21990821 20 -19.445330502 66 -10.22442453
-69 -9.004400407 -25 -1.538822774 21 -20.3726575 67 -10.01110374
-68 -9.546528749 -24 -1.903862883 22 -20.86792861 68 -9.824914538
-67 -9.090605473 -23 -2.318807492 23 -20.80065659 69 -9.663910366
-66 -8.637672823 -22 -2.78809281 24 -20.2995676 70 -9.526328711
-65 -8.188701158 -21 -3.31698473 25 -21.56295133 71 -9.41057053
-64 -7.744595766 -20 -3.918093873 26 -18.76696444 72 -9.31518259
-63 -7.306203592 -19 -4.580265583 27 -18.01562651 73 -9.238842338
-62 -6.874319793 -18 -5.331853568 28 -17.356868967 74 -9.180344903
-61 -6.449694006 -17 -6.178469862 29 -16.8082058 75 -9.138591897
-60 -6.03303628 -16 -7.135236483 30 -16.37297967 76 -9.112581693
-59 -5.625022643 -15 -8.221646257 31 -16.04877505 77 -9.10140094
-58 -5.2263003 -14 -9.463070918 32 -15.83138932 78 -9.104217068
-57 -4.837492467 -13 -10.89241994 33 -15.71661756 79 -9.120271608
-56 -4.45920888 -12 -12.55054264 34 -15.70100441 80 -9.148874155
-55 -4.092020031 -11 -14.47888224 35 -15.78211198 81 -9.189396843
-54 -3.73652103 -10 -16.67697975 36 -15.95854443 82 -9.241269201
-53 -3.393275376 -9 -18.92745642 37 -16.22980928 83 -9.303973309
-52 -3.062848419 -8 -20.39121356 38 -16.59599157 84 -9.377039132
-51 -2.745804699 -7 -20.02468666 39 -17.05711279 85 -9.460039976
-50 -2.442711145 -6 -18.36981915 40 -17.61189413 86 -9.552687971
-49 -2.154140182 -5 -16.52829906 41 -18.25539024 87 -9.65432951
-48 -1.880672784 -4 -14.91775856 42 -18.97457386 88 -9.764940572
-47 -1.622901497 -3 -13.59299958 43 -19.74058882 89 -9.884121837
-46 -1.381433494 -2 -12.52188705 44 -20.49698876 90 -10.01159352
-45 -1.156893696 -1 -11.6631694 45 -21.14775103 ];
```

```

Meas_case2 = [
90 0.005379713 65 0.00877458 38 0.005635435 11 0.009731563
89 0.005327968 64 0.008377722 37 0.0058525267 10 0.010115502
88 0.005229077 63 0.00780107 36 0.005384371 9 0.010694668
87 0.005620271 62 0.007018703 35 0.005489622 8 0.011037761
86 0.004187664 61 0.0068564339 34 0.005140715 7 0.01130935
85 0.004173925 60 0.005564076 33 0.004820596 6 0.011366059
84 0.004268526 59 0.004663742 32 0.004814068 5 0.011288745
83 0.004502444 58 0.003885959 31 0.004636606 4 0.011265297
82 0.004915263 57 0.00281597 30 0.004247092 3 0.010898233
81 0.005444111 56 0.002056156 29 0.004140805 2 0.01085648
80 0.005821133 55 0.000888529 28 0.00367055 1 0.010706383
79 0.006578969 54 0.00033664 27 0.00329899 0 0.010485171
78 0.007222913 53 0.001061667 26 0.003169944 -1 0.010220418
77 0.007649016 52 0.001633635 25 0.003191874 -2 0.009974416
76 0.008149314 51 0.002647827 24 0.003240534 -3 0.009091267
75 0.008780653 50 0.003131348 23 0.003303634 -4 0.008728578
74 0.009357899 49 0.003814634 22 0.00334314 -5 0.008304698
73 0.00961975 48 0.004050629 21 0.003550584 -6 0.007848829
72 0.010212752 47 0.004504728 20 0.004130215 -7 0.007431185
71 0.010096747 46 0.004839674 19 0.004491379 -8 0.007120622
70 0.010118154 45 0.005103696 18 0.004941333 -9 0.006503809
69 0.010137471 44 0.005279312 17 0.0057629901 -10 0.006239231
68 0.010149732 43 0.005468995 16 0.006463127 -11 0.006087989
67 0.009660603 42 0.005661991 15 0.007095413 -12 0.005943051
66 0.009282193 41 0.005665414 14 0.007747393 -13 0.006098258
39 0.005648166 40 0.005652798 13 0.008638175 -14 0.006505539
38 0.005648166 39 0.009117954 -15 0.007286123
];
```

```

-16 0.007926386          -35 0.021264382          -54 0.016960113          -73 0.010371605
-17 0.009091223          -36 0.021447327          -55 0.0165132           -74 0.009855391
-18 0.010082952          -37 0.021565867          -56 0.015905832          -75 0.009127716
-19 0.011415235          -38 0.021659893          -57 0.015645732          -76 0.008233972
-20 0.012397931          -39 0.021461342          -58 0.01564153           -77 0.007344748
-21 0.013622857          -40 0.021452016          -59 0.015158958          -78 0.006732662
-22 0.014566106          -41 0.021348282          -60 0.014851089          -79 0.006115747
-23 0.015178976          -42 0.021152173          -61 0.014535192          -80 0.005596771
-24 0.016071535          -43 0.020945004          -62 0.014276737          -81 0.005158186
-25 0.016912983          -44 0.020704854          -63 0.0141666           -82 0.00488069
-26 0.017465902          -45 0.020405004          -64 0.013969016          -83 0.004560371
-27 0.0183507          -46 0.020162176          -65 0.013565928          -84 0.004626517
-28 0.018851073          -47 0.01994065          -66 0.013105516          -85 0.004740726
-29 0.019351066          -48 0.019234673          -67 0.012967344          -86 0.004847864
-30 0.0198118691         -49 0.018858956          -68 0.012549181          -87 0.005299266
-31 0.020324242         -50 0.018638814          -69 0.01206181           -88 0.005603867
-32 0.020789691         -51 0.018242237          -70 0.011726477          -89 0.005443955
-33 0.021085197         -52 0.017771216          -71 0.011447511          -90 0.005751116
-34 0.021159414         -53 0.017272996          -72 0.010723701          ];

%close all;
clear all;
clc;
format short
N = 4;
c = 3e8;
f = 2.4e9;
lambda = c/f;
d = lambda/2;
k = (2*pi)/lambda;
theta_s = 40*(pi/180); % Angle from x-axis = 90 deg or angle from z-axis = 0 deg
% Four elements antenna array
% Projections on wavefront
th0 = theta_s; %0*(pi/180);
th1 = -45*(pi/180); %20*(pi/180); %receive angle
th2 = -25*(pi/180); %10*(pi/180); % first interferer angle
th3 = 10*(pi/180); %30*(pi/180); % second interferer angle
th4 = 30*(pi/180); %30*(pi/180); % third interferer angle

% Elements locations on curved conformal surface
%%%%%%%%%%%%%%%%%%%%%%%%%%%%%%%%%%%%%
r = 0.2032; % For 8 inches = 0.2032 m radius sphere
theta1 = d/r;
theta2 = d/(2*r);
phi1 = pi/2 - (theta1 + theta2);
phi2 = phi1 + theta1;
phi3 = phi2;
phi4 = phi1;
phi_n = [phi1;phi2;phi3;phi4];
for m = 1:N/2
    x_n(m) = -r*cos(phi_n(m));
end
for m = (N/2+1):N
    x_n(:,m) = r*cos(phi_n(m)); % x_n = [-0.0896 -0.0311 0.0311 0.0896]
end
for m = 1:N
    z_n(m) = r*sin(phi_n(m)); % z_n = [0.1578 0.1788 0.1788 0.1578]
end
%%%%%%%%%%%%%%%%%%%%%%%%%%%%%%%%%%%%%
for m = 1:N
    h_n(m) = sqrt((0-x_n(m))^2 + (r-z_n(m))^2); % h_n = [0.0927 0.0312 0.0312 0.0927]
    phi_inv(m) = asin((r-z_n(m))/h_n(m));
end
theta_b = phi_inv;
theta_b_degrees = theta_b*180/pi % theta_b = [13.2172 4.4057 4.4057 13.2172]

% For theta_s = 40 > 0, theta_b, the wave front hits right elements 3,4 first and left elements 1,2 later with respect to origin
psi1_SOI = exp(-ij*k*h_n(1)*sin(theta_b(1) + abs(th0)))*cos(pi/2-phi_n(1)+th0);
psi2_SOI = exp(-ij*k*h_n(2)*sin(theta_b(2) + abs(th0)))*cos(pi/2-phi_n(2)+th0);
psi3_SOI = exp(ij*k*h_n(3)*sin(-theta_b(3) + abs(th0)))*cos(pi/2-phi_n(3)-th0);
psi4_SOI = exp(ij*k*h_n(4)*sin(-theta_b(4) + abs(th0)))*cos(pi/2-phi_n(4)-th0);
SOI = [psi1_SOI psi2_SOI psi3_SOI psi4_SOI]; % a0
% For theta_s = theta_SOI = -45 < 0 and > theta_b, the wave front hits left elements 1,2 first and right elements 3,4 later with respect to origin
psi1_SNOI = exp(ij*k*h_n(1)*sin(-theta_b(1) + abs(th1)))*cos(pi/2-phi_n(1)+th1);
psi2_SNOI = exp(ij*k*h_n(2)*sin(-theta_b(2) + abs(th1)))*cos(pi/2-phi_n(2)+th1);
psi3_SNOI = exp(-ij*k*h_n(3)*sin(theta_b(3) + abs(th1)))*cos(pi/2-phi_n(3)-th1);
psi4_SNOI = exp(-ij*k*h_n(4)*sin(theta_b(4) + abs(th1)))*cos(pi/2-phi_n(4)-th1);
SNOI1 = [psi1_SNOI1 psi2_SNOI1 psi3_SNOI1 psi4_SNOI1]; % a1
% For SNI1, SNOI1 < 0
psi1_SNOI2 = exp(ij*k*h_n(1)*sin(-theta_b(1) + abs(th2)))*cos(pi/2-phi_n(1)+th2);
psi2_SNOI2 = exp(ij*k*h_n(2)*sin(-theta_b(2) + abs(th2)))*cos(pi/2-phi_n(2)+th2);
psi3_SNOI2 = exp(-ij*k*h_n(3)*sin(theta_b(3) + abs(th2)))*cos(pi/2-phi_n(3)-th2);
psi4_SNOI2 = exp(-ij*k*h_n(4)*sin(theta_b(4) + abs(th2)))*cos(pi/2-phi_n(4)-th2);
SNOI2 = [psi1_SNOI2 psi2_SNOI2 psi3_SNOI2 psi4_SNOI2]; % a2
% For SNOI1 = 10 > 0
psi1_SNOI3 = exp(-ij*k*h_n(1)*sin(theta_b(1) + abs(th3)))*cos(pi/2-phi_n(1)+th3);
psi2_SNOI3 = exp(-ij*k*h_n(2)*sin(theta_b(2) + abs(th3)))*cos(pi/2-phi_n(2)+th3);
psi3_SNOI3 = exp(ij*k*h_n(3)*sin(-theta_b(3) + abs(th3)))*cos(pi/2-phi_n(3)-th3);
psi4_SNOI3 = exp(-ij*k*h_n(4)*sin(theta_b(4) - abs(th3)))*cos(pi/2-phi_n(4)-th3);

```

```

SNOI3 = [psi1_SNOI3 psi2_SNOI3 psi3_SNOI3 psi4_SNOI3].'; % a3

A = [SOI SNOI1 SNOI2 SNOI3];
u = [1 0 0 0];
w = u/A; % Weights with out including effect of mutual coupling

%%%%%%%%%%%%%%%
% Z parameters from HFSS at f = 2.4729 GHz
% Self Terms
Z11 = -30.95-25.57i ;
% Z22 = -37.87-16.15i;
% Z33 = -41.18-5.66i;
% Z44 = -5.11-39.33i;
% Mutual Terms
Z12 = 0.45+3.94i;
Z13 = -1.355+1.923i;
Z14 = 0.8+0.186i;
Z21 = Z12;
Z23 = -2.63+3.77i;
Z24 = -1.25+1.82i;
Z31 = Z13;
Z32 = Z23;
Z34 = 0.844+3.856i;
Z41 = Z14;
Z42 = Z24;
Z43 = Z34;
Z22 = Z11;
Z33 = Z11;
Z44 = Z11;
Z0 = 50;
Z = [Z11/Z0 Z12/Z0 Z13/Z0 Z14/Z0;Z21/Z0 Z22/Z0 Z23/Z0 Z24/Z0;Z31/Z0 Z32/Z0 Z33/Z0 Z34/Z0;Z41/Z0 Z42/Z0 Z43/Z0 Z44/Z0]; % Normalized Impedance Matrix
I = eye(4);
Zc = Z + I ; %Normalized coupling impedance matrix
Ac = Zc\A; %inv(Zc)*A;
wc = u/Ac;
%w = Z*w; %inv(Z)*w.';

w_mag_norm = abs(w)./max(abs(w));
%w_mag_dB = 20*log10(w_mag_norm);
w_phase_deg = angle(w).*180/pi;
wc_mag_norm = abs(wc)./max(abs(wc));
%wc_mag_dB = 20*log10(wc_mag_norm);
wc_phase_deg = angle(wc).*180/pi;
% Array factor
theta = (pi/180)*(-90:180/628:90);
%theta = (pi/180)*(-90:2:90);
e_11 = cos(pi/2 - phi_n(1)+theta);
e_12 = cos(pi/2 - phi_n(2)+theta);
e_r3 = cos(pi/2 - phi_n(3)-theta);
e_r4 = cos(pi/2 - phi_n(4)-theta);

u1 = sin(theta);
u2 = cos(theta);

%w = [1,1,1,1];
% No mutual coupling
figure
AP = w(1).*e_11.*exp(ii.*k.*((x_n(1).*u1 + z_n(1).*u2)) + ...
w(2).*e_12.*exp(ii.*k.*((x_n(2).*u1 + z_n(2).*u2)) + ...
w(3).*e_r3.*exp(ii.*k.*((x_n(3).*u1 + z_n(3).*u2)) + ...
w(4).*e_r4.*exp(ii.*k.*((x_n(4).*u1 + z_n(4).*u2)) + ...

% Effects of mutual coupling
APc = wc(1).*e_11.*exp(ii.*k.*((x_n(1).*u1 + z_n(1).*u2)) + ...
wc(2).*e_12.*exp(ii.*k.*((x_n(2).*u1 + z_n(2).*u2)) + ...
wc(3).*e_r3.*exp(ii.*k.*((x_n(3).*u1 + z_n(3).*u2)) + ...
wc(4).*e_r4.*exp(ii.*k.*((x_n(4).*u1 + z_n(4).*u2)) + ...

AP_norm = abs(AP)./max(abs(AP));
APc_norm = abs(APc)./max(abs(APc));
set(0,'DefaultAxesColorOrder',[0 0 0], ...
'DefaultLineMarkerSize', 8, ...
'DefaultAxesFontSize', 16, ...
'DefaultTextFontSize', 16, ...
'DefaultLineLineWidth',2);
plot(theta*180/pi,20*log10(AP_norm),'k-');
hold on
plot(theta*180/pi,20*log10(APc_norm),'k--');
hold on
Meas_case2_norm = abs(Meas_case2(:,2))./max((Meas_case2(:,2)));
plot(-Meas_case2(:,1),20*log10(Meas_case2_norm),'k.');
hold on
plot(-HFSS_case2(:,1),HFSS_case2(:,2),'kx');

xlabel('\theta(deg)')
ylabel('|\mathbf{E}(\phi)| (dB)')
axis([-90 90 -50 0])
legend('Analytical (without coupling)', 'Analytical (with coupling)', 'Measured', 'HFSS')
%plot(theta*180/pi,e_12)
%plot(x_n,z_n,'o')


```

## APPENDIX L. MEASURED ATTENUATION OF THE VOLTAGE VARIABLE ATTENUATOR.

The following table is the measured attenuation of voltage variable attenuator (PN: ZX73-2500-S+) manufactured by Mini-Circuits [96].

Table 8. Measured attenuation of voltage variable attenuator.

Control voltage (V)	Attenuation (dB)
0.0	-34.9
0.1	-34.9
0.2	-34.9
0.3	-34.9
0.4	-34.9
0.5	-34.9
0.6	-34.9
0.7	-34.9
0.8	-34.9
0.9	-34.5
1.0	-34.1
1.1	-29.7
1.2	-27.8
1.3	-24.9
1.4	-22.4
1.5	-22.0
1.6	-19.9
1.7	-18.3
1.8	-17.7
1.9	-16.7
2.0	-16.0
2.1	-15.5
2.2	-14.9
2.3	-14.0
2.4	-13.7
2.5	-13.5
2.6	-12.8
2.7	-12.6
2.8	-12.3

Control voltage (V)	Attenuation (dB)
2.9	-11.9
3.0	-11.5
3.1	-11.2
3.2	-10.9
3.3	-10.7
3.4	-10.4
3.5	-10.3
3.6	-9.9
3.7	-9.7
3.8	-9.5
3.9	-9.3
4.0	-9.1
4.1	-8.8
4.2	-8.7
4.3	-8.6
4.4	-8.2
4.5	-8.1
4.6	-7.9
4.7	-7.7
4.8	-7.6
4.9	-7.3
5.0	-7.1
5.1	-6.9
5.2	-6.8
5.3	-6.6
5.4	-6.4
5.5	-6.3
5.6	-6.1
5.7	-5.9
5.8	-5.7
5.9	-5.6
6.0	-5.4
6.1	-5.3
6.2	-5.2
6.3	-5.1
6.4	-5.0
6.5	-5.0
6.6	-4.9
6.7	-4.9
6.8	-4.8
6.9	-4.8
7.0	-4.8

Control voltage (V)	Attenuation (dB)
7.1	-4.7
7.2	-4.7
7.3	-4.7
7.4	-4.7
7.5	-4.6
7.6	-4.6
7.7	-4.6
7.8	-4.6
7.9	-4.6
8.0	-4.5
8.1	-4.5
8.2	-4.5
8.3	-4.5
8.4	-4.5
8.5	-4.4
8.6	-4.4
8.7	-4.4
8.8	-4.4
8.9	-4.4
9.0	-4.3
9.1	-4.3
9.2	-4.3
9.3	-4.3
9.4	-4.3
9.5	-4.3
9.6	-4.3
9.7	-4.3
9.8	-4.3
9.9	-4.3
10.0	-4.2
10.1	-4.2
10.2	-4.2
10.3	-4.2
10.4	-4.2
10.5	-4.2
10.6	-4.2
10.7	-4.2
10.8	-4.2
10.9	-4.1
11.0	-4.1
11.1	-4.1
11.2	-4.1

Control voltage (V)	Attenuation (dB)
11.3	-4.1
11.4	-4.1
11.5	-4.1
11.6	-4.1
11.7	-4.1
11.8	-4.1
11.9	-4.1
12.0	-4.0
12.1	-4.0
12.2	-4.0
12.3	-4.0
12.4	-4.0
12.5	-4.0
12.6	-4.0
12.7	-4.0
12.8	-4.0
12.9	-4.0
13.0	-4.0
13.1	-4.0
13.2	-3.9
13.3	-3.9
13.4	-3.9
13.5	-3.9
13.6	-3.9
13.7	-3.9
13.8	-3.9
13.9	-3.9
14.0	-3.9
14.1	-3.9
14.2	-3.9
14.3	-3.9
14.4	-3.9
14.5	-3.9
14.6	-3.9
14.7	-3.9
14.8	-3.8
14.9	-3.8
15.0	-3.8
15.1	-3.8
15.2	-3.8
15.3	-3.8
15.4	-3.8

Control voltage (V)	Attenuation (dB)
15.5	-3.8
15.6	-3.8
15.7	-3.8
15.8	-3.8
15.9	-3.8
16.0	-3.8
16.1	-3.8
16.2	-3.8
16.3	-3.8
16.4	-3.8
16.5	-3.8
16.6	-3.8
16.7	-3.8
16.8	-3.8
16.9	-3.8
17.0	-3.8

## APPENDIX M. MEASURED PHASE SHIFT OF THE ANALOG PHASE SHIFTER.

The following table is the measured phase shift of analog phase shifter (PN: HMC928LP5E) manufactured by Hittite Microwave Corporation [95].

Table 9. Measured phase shift of analog phase shifter.

Control voltage (V)	Phase shift (degrees)
0.0	-82.9
0.1	-71.5
0.2	-66.4
0.3	-54.0
0.4	-48.0
0.5	-39.2
0.6	-32.8
0.7	-25.5
0.8	-16.6
0.9	-13.0
1.0	-5.3
1.1	0.0
1.2	7.0
1.3	14.2
1.4	17.3
1.5	23.0
1.6	29.6
1.7	35.2
1.8	37.6
1.9	43.7
2.0	48.9
2.1	53.5
2.2	59.3
2.3	63.1
2.4	67.7
2.5	70.6
2.6	75.8
2.7	79.7
2.8	83.8

Control voltage (V)	Phase shift (degrees)
2.9	87.0
3.0	94.8
3.1	98.7
3.2	101.8
3.3	105.9
3.4	109.0
3.5	115.4
3.6	119.1
3.7	122.8
3.8	126.8
3.9	130.5
4.0	135.6
4.1	139.7
4.2	143.0
4.3	146.7
4.4	149.6
4.5	153.2
4.6	158.0
4.7	161.2
4.8	165.4
4.9	169.6
5.0	174.0
5.1	178.3
5.2	-178.2
5.3	-176.0
5.4	-172.5
5.5	-167.0
5.6	-163.4
5.7	-161.9
5.8	-159.0
5.9	-155.9
6.0	-152.5
6.1	-148.3
6.2	-143.5
6.3	-140.8
6.4	-138.0
6.5	-133.5
6.6	-130.8
6.7	-127.3
6.8	-125.7
6.9	-123.4
7.0	-118.0

Control voltage (V)	Phase shift (degrees)
7.1	-115.7
7.2	-112.7
7.3	-110.0
7.4	-106.8
7.5	-103.2
7.6	-101.6
7.7	-98.4
7.8	-95.9
7.9	-92.2
8.0	-88.5
8.1	-86.0
8.2	-83.5
8.3	-81.9
8.4	-78.1
8.5	-77.0
8.6	-72.9
8.7	-70.8
8.8	-67.9
8.9	-64.2
9.0	-63.1
9.1	-60.7
9.2	-57.8
9.3	-55.2
9.4	-52.3
9.5	-48.7
9.6	-47.0
9.7	-44.4
9.8	-41.2
9.9	-39.4
10.0	-35.5
10.1	-33.4
10.2	-31.0
10.3	-28.3
10.4	-26.5
10.5	-23.3
10.6	-21.3
10.7	-18.6
10.8	-16.8
10.9	-15.2
11.0	-11.4
11.1	-8.9

Control voltage (V)	Phase shift (degrees)
11.2	-7.4
11.3	-5.8
11.4	-3.8
11.5	-1.9
11.6	0.0
11.7	2.0
11.8	3.1
11.9	5.0
12.0	5.8
12.1	7.9
12.2	9.2
12.3	10.3
12.4	11.1
12.5	12.6
12.6	13.6
12.7	14.2
12.8	14.7
12.9	15.8
13.0	16.4